Aerosol Retrieval and Assimilation phase 2

(ARIA-2)

final report

G.H.L. Verver, J.S. Henzing, M. Schaap, P.J.H. Builtjes, P.F.J. van Velthoven, R.M. Schoemaker and G. de Leeuw

Authors: Verder, G.H.L.
         Henzing, J.S.
         Schaap, M.
         Builtjes, P.J.H.
         Velthoven, P.F.J. van
         Schoemaker, R.M.
         Leeuw, G. de

● ● ● ●

Aerosol Retrieval and Assimilation phase 2 (ARIA-2)

Final Report

G.H.L. Verver,
J.S. Henzing,
M. Schaap,
P.J.H. Builtjes,
P.F.J. van Velthoven
R.M. Schoemaker
G. de Leeuw

P.O. Box 35

2600 AA Delft

The Netherlands

Kluyverweg 1

2629 HS Delft

The Netherlands

Tel. +31 (0)15 278 80 25

Fax +31 (0)15 262 30 96

Email info@nivr.nl

www.nivr.nl

NATIONAL USER SUPPORT PROGRAMME (NUSP) 2001-2005

http://www.ao-go.nivr.nl

The National User Support Programme 2001-2005 (NUSP) is executed by the Netherlands Agency for Aerospace Programmes (NIVR) and the SRON Netherlands Institute for Space Research. The NUSP is financed from the national space budget. The NUSP subsidy arrangement contributes to the development of new applications and policy-supporting research, institutional use and use by private companies.

The objectives of the NUSP are:

- To support those in the Netherlands, who are users of information from existing and future European and non-European earth observation systems in the development of new applications for scientific research, industrial and policy research and operational use;

- To stimulate the (inter)national service market based on space-based derived operational geo-information products by means of strengthening the position of the Dutch private service sector;

- To assist in the development of a national Geo-spatial data and information infrastructure, in association with European and non-European infrastructures, based on Dutch user needs;

- To supply information to the general public on national and international space-based geo-information applications, new developments and scientific research results

Aerosol Retrieval and Assimilation phase 2 (ARIA-2)

Final Report

G.H.L. Verver, J.S. Henzing, P.F.J. van Velthoven

Royal Netherlands Meteorological Institute (KNMI) (http://www.knmi.nl)

M. Schaap, P.J.H. Builtjes

TNO Environment and geosciences (www.tno.nl)

R. M. Schoemaker, G. de Leeuw

TNO Defence, Security and Safety (www.tno.nl)

Content

Executive Summary

There are large uncertainties involved in the estimation of the distribution of atmospheric aerosol. This distribution has to be known in order to assess effects on the climate as well as for the air quality. However, atmospheric aerosols are difficult to model since there are many parameters to characterize it: size distribution, number density, chemical composition, the ability to take up water, the single scattering albedo, etcetera. Moreover, the short atmospheric lifetime and the inhomogeneous distribution of sources results in highly variable distributions. In order to estimate atmospheric concentrations satellite observations can be used to constrain the modelled distribution. A working prototype of such a system has been developed during the first phase of ARIA (ARIA-1), where aerosol optical depths (AOD) were derived from the observations of the ATSR-2 instrument on the ERS-2 satellite, which were subsequently assimilated in a global atmospheric transport/chemistry model TM3. The system was tested for the Indian Ocean and surrounding during the INDOEX measurement campaign. In the second phase (ARIA-2) described in this report, the global assimilation system using the TM transport chemistry model is updated, and tested for Europe. In addition a regional assimilation system using the LOTOS-EUROS model with higher spatial resolution is applied over Europe. The objective of this second phase was (1) to demonstrate a pre-operational assimilation system to produce the geographical distribution of aerosols obtained from assimilation of satellite observed optical depths in a global 3D aerosol chemistry model, and (2) to demonstrate the operation of a tool to estimate regional emissions of aerosol based on the assimilation of retrieved optical depths into a regional high resolution aerosol chemistry model. Secondary objectives were (1) to adapt aerosol chemistry models for assimilation of aerosol optical depth data, (2) to derive PM 2.5 concentrations at ground level, based on the analyzed aerosol mass obtained by the high-resolution regional model, and (3) to evaluate of the retrieval and assimilation products against independent observations.

We have shown that the data assimilation technique can be successfully applied to assimilate aerosol optical depth fields over Europe and the INDOEX region. Both models, LOTOS-EUROS and TM4, are adjusted towards the retrieved AOD values as a result of the assimilation. Experiments with the regional LOTOS-EUROS system revealed a close resemblance with retrieved AOD when it is assumed that the retrieval is very accurate. Unfortunately this is not the status of the present day AOD data, e.g. due to cloud contamination or unknown mixtures that contribute to the AOD. Assimilation of observational data into the global TM4 model effectively acts as a source of aerosols, and improves the agreement with independent surface observations of AOD. After the introduction of size resolved sea salt aerosol in TM4 it is shown that significant part of the AOD over the Atlantic Ocean and in the INDOEX region is determined by this type of aerosol.
European surface concentrations of NH4, NO3 and SO4 are reasonably represented by both models without assimilation. Surface SO2 concentrations are overestimated by both models, but most severely by TM4.

The free running models both systematically underestimate the AOD values significantly. As a consequence of this large systematic deviation the assimilation scheme induces a large and unrealistic change in the emissions in LOTOS-EUROS and strong discontinuities in the distribution of aerosols in space and time in TM4. The LOTOS-EUROS assimilation system uses emissions to close the complete gap between measured and observed data. Hence, the estimated emission changes do not yield realistic values, although after assimilation the AOD's are in better agreement with independent surface observations.

The high corrections indicate that we need to improve the modelling of the total aerosol mass and the calculation of aerosol optical depth from the aerosol components in both models. To improve the assimilation systems for future applications it is suggested that the models are constrained by ground based measurements of (several) aerosol components. This avoids the introduction of additional errors due to the uncertain optical parameters and uncertain humidity effects on aerosol size distribution, which makes the current AOD assimilation less effective. Since aerosols and humidity are both very variable parameters of the atmosphere, increasing the spatial resolution may also improve the agreement with observations.

ABSTRACT

The objective of the ARIA-1 project was to create a working prototype of a system to estimate the global distribution of aerosol by the assimilation of satellite retrieved aerosol optical depths (AOD) in the global atmospheric transport/chemistry model TM3. In the second phase (ARIA-2) described in this report, the global assimilation system is updated, and tested both for Europe and the INDOEX region. In addition a regional assimilation system using the LOTOS-EUROS model with higher spatial resolution is applied over Europe, yielding estimates of aerosol emission and PM 2.5 concentration. It is shown that as a result of the assimilation both models are adjusted towards the retrieved AOD values. Assimilation of observational data into the global TM4 model effectively acts as a source of aerosols, improving the agreement with independent surface observations of AOD. However, the free running models both systematically underestimate the AOD values significantly. As a consequence the assimilation schemes induce in LOTOS-EUROS a large and unrealistic change in the emissions and in TM4 strong discontinuities in the distribution of aerosols in space and time. These results indicate the need to improve the modelling of the total aerosol mass and the subsequent calculation of aerosol optical depths. Moreover it shown that more accurate retrieved AOD data are needed to improve emission estimates by the LOTOS-EUROS assimilation system. It is also suggested to constrain the models in the future by ground based measurements, and to further increase the spatial resolution.

1. INTRODUCTION

1.1 PROBLEM DESCRIPTON

One of the major challenges in climate research is the assessment of the climate forcing by aerosols on global and regional scales. Aerosols scatter and absorb solar and infrared radiation. Depending on aerosol type this direct radiative forcing may be positive or negative. Aerosols indirectly affect radiative forcing because they can act as cloud condensation nuclei and influence cloud albedo and lifetime. The latest estimate by IPCC (2001) of the global direct radiative forcing by aerosols is -0.5 W/m^2. Their indirect forcing is also negative and quite uncertain, in between 0 and -2 W/m^2. The radiative forcing by long-lived greenhouse gases is positive and quantitatively well known. The radiative forcing by the anthropogenic increase in greenhouse gases since 1750 is estimated at 2.43 W/m^2 by IPCC (2001). Hence, the total radiative forcing by anthropogenic aerosols is of the same order of magnitude as the forcing by the anthropogenic greenhouse gases, but of opposite sign and it has a much larger level of uncertainty. Furthermore, aerosols show large spatial gradients, resulting in regional forcings which can be substantially larger than the global average.

Estimates of radiative forcing by aerosols in IPCC (2001) are mostly based on global transport models with quite simplified aerosol chemistry. Only very few observations exist that can be used to evaluate and improve such models. The most extensive observations have been made during recent international measurement campaigns such as ACE-1, ACE-2, TARFOX, INDEX and ACE-ASIA, where a variety of ground-based and airborne instruments were deployed. Results from these campaigns show the large differences in aerosol properties from one region to another. Therefore, results from such campaigns cannot be extrapolated to the global scale. Global ground-based measurement networks, such as AERONET (sun-photometers), provide only point measurements that are still sparsely distributed over the globe. A combination of global satellite observations and global modeling seems the only alternative. An evaluation of aerosol models with (satellite based) aerosol observations is also needed to gain confidence in predictions about future climate change made with these models for climate assessments such as IPCC.

Aerosols are also an important environmental factor because of their health effect on human beings. In particular high concentrations of small particles, PM2.5 (mass of articles with an effective diameter smaller than 2.5μm), can be a hazard for human health when inhaled. This is an air quality issue that requires the determination of surface concentrations of aerosols. The current EU standard is based on PM10, however it is the general opinion that the EU will also adopt a PM2.5 standard in the near future. The feasibility of determining this information using satellite remote sensing data has been studied by Builtjes et al. (2001).

Satellite observations of aerosol
Several present day aerosol products derived from global satellite observations, such as the TOMS, GOME and SCIAMACHY absorbing aerosol index (Hsu et al., 1999; De Graaf et al., 2004, 2005), are not directly related *quantitatively* to the aerosol properties of interest. The absorbing aerosol indices only provide information on absorbing aerosols, whereas most of the anthropogenic aerosols are non-absorbing, resulting in negative climate forcing. In the derivation of these products no use is made of aerosol chemistry-transport models, which could give a priori information about the aerosol type and the profile to expect at the pixels observed by the satellite instrument. Current retrieval algorithms utilize an aerosol model, sometimes based on expected aerosol composition for the area and/or meteorological situation. Alternatively, aerosol climatologies of the geographical occurrences of various aerosol types and their vertical extent can be used as input. The latter operational approach is followed for the OMI aerosol retrieval product, for which the algorithm has been developed in a co-operation between KNMI, TNO-FEL and NASA (Torres et al., 2002). Aerosol products from the NOAA AVHRR series are available only over sea and provide only the aerosol optical depth, no aerosol speciation. Algorithms have been developed for application with ATSR-2 and AATSR (the ATSR-2 successor on ENVISAT) both over land and over sea, and due to the small pixel size of these instruments the future products will be very well suited for air pollution applications. Since validated SCIAMACHY and AATSR observations are not yet available it was decided to use existing ATSR-2 data for the demonstration of the system within this project.

Modelling aerosol transport and chemistry
Up to five years ago aerosol cycles were only crudely or not all represented in global climate and chemistry

models. A WCRP workshop in 1995 revealed a factor of 3 variation in global annual mean sulphate burden between several global chemistry-transport models (Rasch et al., 2000). In recent years sophisticated parameterisations for various types of aerosols have been developed. For many models a module for sulphate aerosol chemistry is now available. It has long been thought that above industrialised regions, such as Europe and the USA, the aerosol optical depth is mainly determined by ammonium salts of sulphate and nitrate. Recently, it was found that at northern mid-latitudes there may also be a relatively important contribution from other aerosol types (Jeuken et al., 2001; Ten Brink et al., 2001) such as organic aerosols (Russell et al.,1999; Robles-Gonzalez et al., 2001) and black carbon (Cooke et al., 1999). In the tropics and subtropics mineral dust and carbonaceous aerosols from biomass burning often constitute the dominant aerosol type. Few models yet contain all these different types of aerosol, although they have all been simulated in one model or another.

On the regional, European scale a number of models are available at the moment which incorporate aerosols, with a focus on air quality. They treat primary aerosols/fine particles, secondary inorganic aerosols, and some of them both biogenic and anthropogenic secondary organic aerosols. Recently, a model intercomparison study has been performed (Van Loon et al, 2004). Next to the uncertainty in the treatment of secondary organic aerosols, a large uncertainty exists concerning the emissions of primary aerosols and aerosol-precursors.

Satellite data assimilation
Data assimilation is a technique that allows optimal use of observations of atmospheric compounds in a chemistry-transport model to derive global three-dimensional distributions of atmospheric species. The field of chemical data assimilation is in rapid development, however it is still strongly focussed on gaseous species, such as ozone. Data assimilation focussing on ozone has been developed in a previous BCRS-projects by Van Loon et al. (1999) and Jeuken (1999). The assimilation of aerosol optical depth is described in the final reports of the BCRS project Aerosol Air Quality Satellite Data (Builtjes et al., 2001) and Aerosol Retrieval and Assimilation (Verver, 2002). During the Indian Ocean experiment in 1999 satellite retrieved aerosol optical thickness was assimilated in a chemistry-transport model by Collins et al. (2001). It was shown to be a promising approach for the calculation of aerosol distributions and radiative forcing.

An overview of the current situation with respect to satellite data assimilation techniques has recently be made in the framework of the EU-project DAEDALUS (Van Velthoven et al, 2004)

1.2   OBJECTIVES OF THE PROJECT

In this project we aim at developing 2 products utilizing satellite observations of aerosols:

Primary objective:
-To demonstrate a pre-operational assimilation system to produce the geographical distribution of aerosols obtained from assimilation of satellite observed optical depths in a global 3D aerosol chemistry model.
-To demonstrate the operation of a tool to estimate regional emissions of aerosol based on the assimilation of retrieved optical depths into a regional high resolution aerosol chemistry model.

Secondary objectives:
-Adaptation of aerosol chemistry models (both high resolution regional scale, down to 5x5 km, as well as more coarse resolution on global scale), for assimilation of aerosol optical depth data.
-Derivation of PM 2.5 concentrations at ground level, based on the analyzed aerosol mass obtained by the high-resolution regional model.
-Evaluation of the retrieval and assimilation products against independent observations.

1.3   INVOLVEMENT OF USERS

In the course of the project consultation of potential users of the new aerosol products took place, in order to ensure that the products will satisfy the different requirements. The use of the ARIA results is foreseen in several applications: i.e. the assessments of health risks in relation to human exposure to aerosols and UV radiation; the estimation of present day radiative forcing by aerosols (the direct effect); the attribution of

climate change to different aerosol types and sources; the estimation of the indirect climate effect of aerosols; forecasting visibility for aircraft traffic and other applications.

A consultation meeting of the ARIA advisory Group (AG), composed of 4 scientists employed in different working fields (see appendix 1), took place in October 2004. It was concluded that forecasts of aerosol concentration could be useful for the assessment of health risks caused by the exposure to air pollution and UV radiation. Although the direct results of ARIA are analysed fields of atmospheric aerosol, the tools needed to prepare forecasts are developed within the project.

The advisory group acknowledges the need for better estimates of the distribution of different aerosol types, as aimed for in this project, and better estimates of aerosol emission sources and sinks.

2. APPROACH

2.1 INTRODUCTION

In figure 2.1 the setup of the aerosol retrieval and assimilation system as implemented in ARIA-2 is shown. The retrieval of aerosol information from the ATSR-2 radiances is not part of this project. However, to assimilate these observations, information is needed on the errors and assumptions involved in the retrieval. Therefore the retrieval method and products are described in section 2.4 of this report. For the global model the observations are aggregated into 'super'-observations, i.e. they are averaged over one (model) grid cell which is then treated as one single observation. This reduces the computational costs considerably, which is a requirement when in the future much larger datasets with global coverage are assimilated, possibly in near real-time.

The global TM4 model that is used to produce the aerosol forecast as well as the Optimal Interpolation (OI) assimilation scheme is described in section 2.2.The regional aerosol model LOTOS-EUROS is described in section 2.3, including the applied Ensemble Kalman Filter Data-assimilation method.In section 2.4 the retrieved AOD-data which have been used in this project for data-assimilation are described. Section 2.5 gives a short overview of the European surface observations for the year 2000 which have been used to evaluate the results of TM4 and LOTOS-EUROS over Europe. Synthesis and evaluation of the approach is given in session 2.6
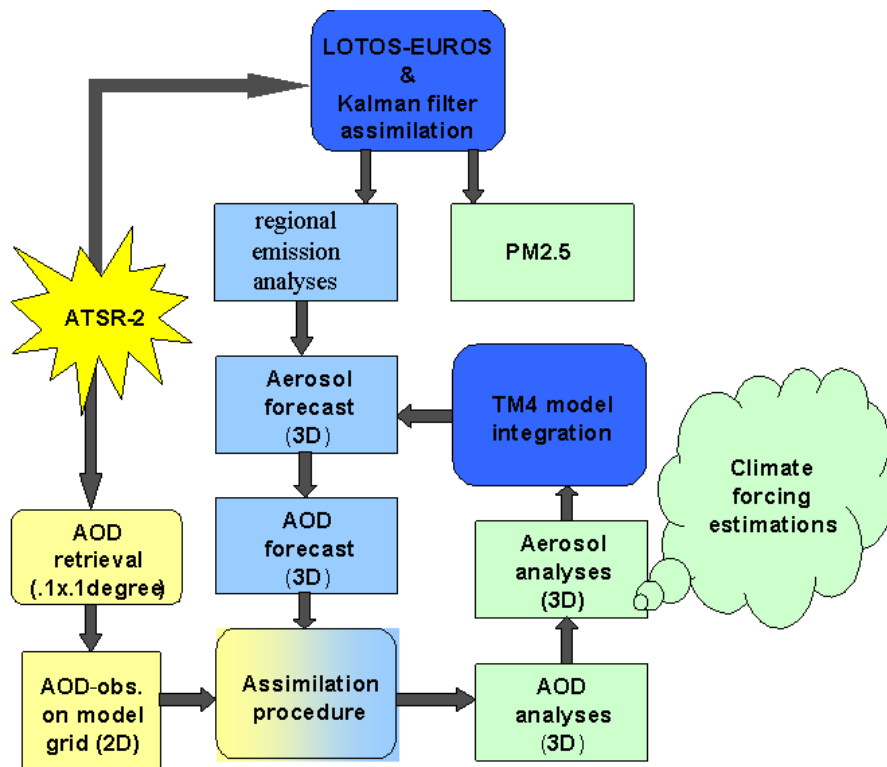
Figure 2.1 Setup of the aerosol retrieval and assimilation system as implemented in ARIA-2.

2.2 GLOBAL AEROSOL MODELLING AND ASSIMILATION

2.2.1 The global TM4 model

The three dimensional, global, off-line aerosol model TM4 (Heimann, 1995; Dentener et al., 1999; Meijer et al., 2000) is used, driven by archived meteorological output from the ECMWF weather forecast model. The model version 4 used in this study contains sulfate, nitrate, ammonium, and 4 different types of carbonaceous aerosol. As part of this project 12 sea salt aerosol tracers are added (see section 3.2). Parameterizations are used to calculate convective mass fluxes (Tiedtke, 1989) and vertical diffusion (Holtslag and Boville, 1993; Vogelezang and Holtslag, 1996; Beljaars and Viterbo, 1999). Large scale advection of aerosol tracers is performed using the slopes scheme of Russell and Lerner (1981). We use a horizontal resolution of 6° longitude and 4° latitude. In the vertical the total number of hybrid σ-pressure levels (Simmons and Burridge, 1981) has been reduced from 60 (ECMWF) to 25 (TM4).

Chemistry

TM4 describes full tropospheric chemistry of HO_x-NO_x-SO_x-CO-CH_4 and Non Methane Hydro Carbons (NMHC's) using a modified version of the CBM-4 scheme (Houweling et al., 1998). To calculate photolysis rates we use the scheme of Krol and Van Weele (1997). The sulfur cycle (Jeuken, 2000; Metzger et al., 2002b) is fully coupled to the photochemistry code. In our model version all oxidants are explicitly calculated as well as heterogeneous reaction rates of N_2O_5 on preexisting aerosol surface resulting in the formation of HNO_3 (Dentener and Crutzen, 1993). Gas and cloud phase reactions of SO_2, DMS, NH_3, SO_4^{2-} and NH_4^+ are incorporated (Dentener and Crutzen, 1994). For a complete list of all other gas phase reactions the reader is referred to Houweling et al. (1998). In total 55 atmospheric constituents are considered, of which 21 gaseous and 19 aerosol tracers are transported. 110 gas phase reactions and 24 photolysis reactions are taken in account.

Emissions

Sulfate aerosol is mainly produced from gas-phase and aqueous-phase oxidation of SO_2 and DMS. Only a very small fraction of the sulfur emissions is directly emitted as sulfate (2% in our model). Ammonium and nitrate aerosol is formed when low volatile precursor gases condensate. The gas-particle partitioning of the sulfate-ammonium-nitrate system, which depends on the amount of precursor gases but also strongly on the ambient relative humidity and temperature, is accounted for by a simplified thermodynamic equilibrium model (EQSAM, Metzger et al., 2002a). The main assumption of this model is that aerosols are internally mixed and obey thermodynamic gas-aerosol equilibrium. For global modeling this assumption is adequate as the time required for gas-aerosol equilibration is much shorter than the model timestep (Metzger et al., 2002a). To increase the computational efficiency of EQSAM the total number of equilibrium reactions is minimized by making use of concentration domains that contain fewer species than the entire set of possible aerosol compositions (Nenes et al., 1998, Metzger et al., 2002a). Critical for the aerosol composition is the amount of NH_3 plus NH_4^+ (total ammonia). The mole ratio of total ammonia to total sulfate, which defines the domains, determines the sulfate state, i.e. non-neutralized H_2SO_4 or neutralized HSO_4^- or SO_4^{2-}. Only for a surplus of total ammonia, ammonium nitrate salts will be formed. The actual gas-aerosol partitioning only occurs for the ammonium nitrate salts; the other ammonium salts and sulfuric acid are treated as nonvolatile and they remain in the aerosol phase.

Four types of carbonaceous aerosol are considered. We differentiate between organic carbon (OC) and black carbon (BC). Both OC and BC can be hydrophobic or hydrophilic. Hydrophobic aerosol will neither be activated as cloud condensation nuclei, nor will it be scavenged by precipitation. BC is predominantly emitted as hydrophobic aerosol, but a small fraction of the emissions may be hydrophilic (Cachier, 1998). We assume that 80% of the BC emissions are hydrophobic and 20% is hydrophilic as is common in other models. OC is emitted in equal proportions of hydrophobic and hydrophilic aerosol in accordance with Cooke et al. (1999). The sources of BC and OC sub-micron aerosol particles were taken form the work of Cooke et al. (1999). They provide global-scale emissions of carbonaceous aerosol from fossil fuel usage with a horizontal resolution of 1°×1°. The quantity of carbonaceous aerosol emitted by fossil fuel combustion is proportional to the quantity of fuel consumed and the emission factor for the combustion process. The quantity of fuel

consumed is reasonably well known (e.g. United Nations, 1993). The distinction between BC and OC emission factors for the Cooke et al. (1999) emission data, is based on fuel type (e.g. diesel, kerosene, coal, gas), consuming sector (domestic, transport, and industry), and level of development of the country. The emissions are equally spread over the year.

Sea salt emissions were added to the TM4 model as part of this project, as described in the section on TM Model Developments (3.2)

Optimal Interpolation Assimilation of Aerosol Optical Depth
Observational data from satellite instruments are irregularly distributed in space and time. This is because the satellite passes over only at discrete times and retrievals can only be made in cloud-free situations. By data assimilation continuous fields in space and time can be calculated (Jeuken et al., 1999; Collins et al., 2001). In the first phase of ARIA (Verver et al., 2002) a scheme for assimilation of aerosol optical depths was developed for the TM3 model. As a first step the assimilation of observed aerosol optical depth at one wavelength was implemented. The assimilation scheme is a simplified version of the GOME ozone assimilation scheme (Eskes et al., 2002), and is outlined below. During this project this scheme was ported to version 4 of the global model (TM4).

The assimilation scheme is based on the Kalman filter equations (Kalman and Bucy, 1961) and has been used for ozone in TM3 (Jeuken et al., 1999; Eskes et al, 2003). The scheme adjusts modeled aerosol fields to match observed quantities in a manner consistent with uncertainties in the model and retrieval. In our application the 'observations' are column-integrated aerosol optical depths retrieved from satellite-observed radiances denoted τ^o. Running the model yields forecasts of aerosol optical depth, τ^f. The core of the assimilation scheme is the analysis of the aerosol optical depth field given by:

$$\tau_k{}^a = \tau_k{}^f + \mathbf{P}\mathbf{H}^T\left(\mathbf{H}\mathbf{P}\mathbf{H}^T + \mathbf{R}\right)^{-1}\left(\tau^o - \mathbf{H}\tau_k{}^f\right) \quad , \tag{2.1}$$

where $\mathbf{H}$ is the observation operator; $\mathbf{R}$ is the observation error covariance matrix, $\mathbf{P}$ is the forecast error covariance matrix, and T denotes the transpose of the matrix. To reduce computation time, high-resolution optical depth retrievals are averaged to the TM grid. This avoids the spatial interpolation of model values to the location of the individual satellite pixels online and the observation operator $\mathbf{H}$ becomes a simple diagonal matrix representing the summation over the vertical layers. The error covariance matrices determine the relative weighting of the model forecast and the observations. A large forecast error ($\mathbf{P}$) and relatively small error in the observation ($\mathbf{R}$) will result in strong adjustment towards the observation. Vice versa, highly uncertain observational data, but trustworthy modeled fields, will result in a small impact of the observations on the analyses. For the observations we define a diagonal error covariance matrix $\mathbf{R}$, implying that the observational errors are uncorrelated in space. The diagonal elements are the observation errors in the averaged observations (super-observations) that are estimated in Section 3.4.1. The forecast error covariance matrix $\mathbf{P}$, which is kept constant in time, is prescribed by (Eskes et al., 2003):

$$P_{ij} = \sigma_\tau{}^2 f_{\text{vert}} f_{\text{hor}} \quad , \tag{2.2}$$

where $\sigma_\tau{}^2$ is the forecast error variance in the total optical depth, that is estimated in section 3.4.1. The vertical distribution of the error correlation is accounted for by the function f_{vert} that scales the error variance with the vertical distribution of τ_k. The horizontal forecast error correlation is represented by the function f_{hor} derived by Thiebaux (1976) based on the assumption that the errors can be represented as a second-order regressive process:

$$f_{\text{hor}}(d_x) = \left(1 + \frac{d_x}{l_x}\right)\exp\left(-\frac{d_x}{l_x}\right) \quad , \tag{2.3}$$

with d_x the horizontal distance between two model grids, and l_x the horizontal correlation length-scale for errors in the model fields. In the current version of the assimilation module l_x is set to 200 km.

Finally, when equation (2.1) is solved and an optimal distribution of $\tau_k{}^a$ is obtained, the mass of each aerosol tracer is adjusted. As we do not have additional information as to which aerosol specie is responsible for the mismatch between observed and modeled aerosol optical depth, we choose to adjust each aerosol type proportional to its mass M in gridcel k:

$$M_{sk}^a = M_{sk}^f \frac{\tau_k{}^a}{\tau_k{}^f} \tag{2.4}$$

As discussed in the final report of the first phase of ARIA, further refinement of this assimilation scheme is needed before it can be used operationally (Verver et al., 2002). Therefore in ARIA-2 observational and model error covariances will be estimated by analyses of the model results and retrieved AOD observations. The sensitivity of the assimilation system for different parameter settings (e.g. horizontal and vertical correlation lengths for the errors, fractional errors, error variances) needed to be assessed to determine the optimal settings. The results of the changes made to the assimilation scheme during ARIA-2 are presented in section 3.4.

2.3   REGIONAL AEROSOL MODELLING AND ASSIMILATION.

In the first phase of ARIA it was speculated that the discrepancy between modelled and retrieved optical depths was at least partly caused by carbonaceous aerosol emissions that are not well known. This is especially true for the natural primary emissions of black and organic carbon where the uncertainty is roughly a factor 2 (IPCC, 2001), caused mainly by the uncertain spatial and temporal distribution of biomass burning. The formation of secondary carbonaceous aerosol by the oxidation of hydrocarbons is also hard to quantify. The hydrocarbon emissions and the fractional yield of aerosol are both very uncertain, resulting in secondary production estimates that span a range of a factor of 5 (IPCC, 2001). Emissions of dust have been experimentally determined but these data are difficult to generalise for other regions and seasons (IPCC, 2001).
Sea salt contributes 44% to the global aerosol optical depth. Estimates for top-of-atmosphere, global-annual radiative forcing due to sea salt are - 1.51 and -5.03 W m-2 for low and high emission values, respectively (IPCC, 2001). Different sea spray flux formulations agree to within one order of magnitude (Andreas, 2002).
In the ARIA-2 project a tool has been developed for the estimation of regional aerosol emissions to reduce the uncertainties described above. In this part of the project observed aerosol optical depths (retrieved from ATSR-2) are used to optimise the emissions in the regional aerosol chemistry / transport model LOTOS (Van Loon et al., 2000), using Kalman filtering. In the AAQSD (Aerosol Air Quality Satellite Data ; Builtjes et al., 2001) project the LOTOS-model has been extended to contain an aerosol module. The Kalman Filter data assimilation scheme has been used for LOTOS in combination with observed AOD from ATSR for august 1997. In this way a complete AOD field was constructed, and first noise factors for the emissions used as input were derived (Builtjes et al. 2001).
By covering different regions of the globe, where different aerosols dominate, the regional data assimilation system has the potential to improve the estimates of emissions that are very uncertain up to now.
In this project the tool will be applied for Europe, where emissions are relatively well known. If a good performance of the system is obtained and the observations that are available for assimilation are of sufficient quality, the   system can be applied for a region with more uncertain emissions, such as Southeast Asia (INDOEX campaign), which is rapidly becoming a major source of pollution.

Around the start of the ARIA-2 project an agreement was signed between TNO and RIVM-MNP to combine the TNO LOTOS model and the RIVM EUROS model into one combined regional air quality/chemical transport model. As basic structure the LOTOS model was chosen, and comparisons were carried out to evaluate the different modules of the two models like dry deposition, chemical schemes etc. The new

combined LOTOS-EUROS model was tested to determine its performance against the system developed in a previous model intercomparison study (Van Loon et al, 2004). The new LOTOS-EUROS model was operational by 1-1-2005, and it was decided to use this new model also in the ARIA-2 project. The new model is described in Schaap et al. (2005a,b). We summarize the main features of the model below.

2.3.1 The LOTOS-EUROS modeling system

In this section we give an overview of the LOTOS-EUROS modelling system

Domain
The master domain of LOTOS-EUROS is bound at 35° and 70° North and 10° West and 60° East. The projection is normal longitude-latitude and the standard grid resolution is 0.50° longitude x 0.25° latitude, approximately 25x25 km. in this study we have used several domains within this master domain. The final results are calculated over a domain that covers Europe (up to 40° East) but excludes the largest part of European Russia   In the vertical there are three dynamic layers and an optional surface layer. The model extends in vertical direction 3.5 km above sea level. The lowest dynamic layer is the mixing layer, followed by two reservoir layers. The height of the mixing layer is part of the diagnostic meteorological input data. The heights of the reservoir layers are determined by the difference between the mixing layer height and 3.5 km. Both reservoir layers are equally thick with a minimum of 50m. In some cases when the mixing layer extends near or above 3500 m the top of the model exceeds the 3500 m according to the abovementioned description. Simulations were performed with the optional surface layer of a fixed depth of 25 m. Hence, this layer is always part of the dynamic mixing layer.
For output purposes the concentrations at measuring height (usually 3.6 m) are diagnosed by assuming that the flux is constant with height and equal to the deposition velocity times the concentration at height z.

Transport
The transport consists of advection in 3 dimensions, horizontal and vertical diffusion, and entrainment/detrainment. The advection is driven by meteorological fields (u,v) which are input every 3 hours. The vertical wind speed w is calculated by the model as a result of the divergence of the horizontal wind fields. The recently improved and highly-accurate, monotonic advection scheme developed by Walcek (2000) is used to solve the system. The number of steps within the advection scheme is chosen such that the courant restriction is fulfilled.
Entrainment is caused by the growth of the mixing layer during the day. Each hour the vertical structure of the model is adjusted to the new mixing layer depth. After the new structure is set the pollutant concentrations are redistributed using linear interpolation.
The horizontal diffusion is described with a horizontal eddy diffusion coefficient following the approach by Liu and Durran (1977). Vertical diffusion is described using the standard Kz-theory. Vertical exchange is calculated employing the new integral scheme by Yamartino et al. (2004).

Chemistry
The LOTOS-EUROS model contains two chemical mechanisms, the TNO CBM-IV scheme (Schaap et al., 2005a) and the CBM-IV by Adelman (1999). In this study we used the TNO CBM-IV scheme which is a modified version of the original CBM-IV (Whitten et al., 1980). The scheme includes 28 species and 66 reactions, including 12 photolytic reactions. Compared to the original scheme steady state approximations were used to reduce the number of reactions. In addition, reaction rates have been updated regularly. The mechanism was tested against the results of an intercomparison presented by Poppe et al. (1996) and found to be in good agreement with the results presented for the other mechanisms. Aerosol chemistry is represented using ISORROPIA (Nenes et al., 1999).

Dry and wet deposition
The dry deposition in LOTOS-EUROS is parameterised following the well known resistance approach. The deposition speed is described as the reciprocal sum of three resistances: the aerodynamic resistance, the viscous sub-layer resistance and the surface resistance. The aerodynamic resistance is dependent on atmospheric stability. The relevant stability parameters (u*, L and Kz) are calculated using standard similarity theory profiles. The viscous sub-layer resistance and the surface resistances for acidifying components and

particles are described following the EDACS system (Erisman et al., 1994).

Below cloud scavenging is described using simple scavenging coefficients for gases (Schaap et al., 2004) and following Simpson et al. (2003) for particles. In-cloud scavenging is neglected due to the limited information on clouds. Neglecting in-cloud scavenging results in too low wet deposition fluxes but has a very limited influence on ground level concentrations (see Schaap et al., 2004a).

Meteorological data

The LOTOS-EUROS system is presently driven by 3-hourly meteorological data. These include 3D fields for wind direction, wind speed, temperature, humidity and density, substantiated by 2-d gridded fields of mixing layer height, precipitation rates, cloud cover and several boundary layer and surface variables. The standard meteorological data for Europe are produced at the Free University of Berlin employing a diagnostic meteorological analysis system based on an optimum interpolation procedure on isentropic surfaces. The system utilizes all available synoptic surface and upper air data (Kerschbaumer and Reimer, 2003). Also, meteorological data obtained from ECMWF can be used to force the model.

Emissions

The anthropogenic emissions used in this study are a combination of the TNO emission database (Visschedijk and Denier van der Gon et al., 2005) and the CAFE baseline emissions for 2000. For each source category (Snap 1) and each country, we have scaled the country totals of the TNO emission database to those of the CAFE baseline emissions. Elemental carbon / Black Carbon (EC) emissions were derived from (and subtracted from) the primary PM2.5 (PPM2.5) emissions following Schaap et al. (2004b). Hence, we use the official emission totals as used within the LRTAP protocol but we benefit from the higher resolution of the TNO emission database (0.25x0.125 lon-lat). The annual emission totals are broken down to hourly emission estimates using time factors for the emissions strength variation over the months, days of the week and the hours of the day (Builtjes et al., 2003).

In LOTOS-EUROS biogenic isoprene emissions are calculated following Veldt (1991) using the actual meteorological data. In addition, sea salt emissions are parameterised following Monahan et al (1986) from the wind speed at ten meter height. Dust was neglected as it normally does not contribute a large fraction to the fine aerosol mass in Europe and, more importantly, because there are no reliable emission estimates and/or parameterisations

2.3.2   The Kalman filter around LOTOS-EUROS

Observations of aerosol optical depth (or any other component) consist of data that are irregularly distributed in space and time. Data assimilation allows to integrate measured data in a model calculation to obtain continuous fields in space and time. Data assimilation consists of making a best estimate of the state of the atmosphere on the basis of observations and a model prediction of the atmospheric state. Both components have associated errors. Data assimilation basicly defines a new atmospheric state by making a weighted average of the observed and modelled state in a statistically sound way. Hence, if a model value is more uncertain than an observed value, more weight will be put on the observation, and the assimilated value will tend to get closer to the observed value and vice versa.

In this study we use an ensemble Kalman filter (EnKF) (Evensen, 1997) to assimilate the AOD retrievals within LOTOS-EUROS. The uncertainties involved with the modelled and retrieved AOD values determine the weights that are put on the measured and calculated values. With an ensemble kalman filter there is no need to specify the model uncertainties beforehand as they are determined by the range of modelled states of the ensemble members. The ensemble is generated by adding noise to uncertain model parameters. Hence, the specification of the noise influences the weights and therewith results of the procedure. Below, we only give a brief technical description of the EnKF. For details we refer to Builtjes et al. (2001).

The first step in order to build the EnKF around LOTOS-EUROS is to embed the model and the available measurement in a stochastic environment:

$$x^{k+1} = f^k(x^k, w^k)$$

$$y^k \qquad = C^k x^k + v^k,$$

where the superscripts (k) denote the time level. The model state vector is denoted by x and the measurements by y. The function f denotes the non-linear model operator which apart from on the state vector acts on a white noise vector w with Gaussian distribution and diagonal covariance matrix Q. The measurement vector y is assumed be a linear combination of elements of the state vector and a random, uncorrelated Gaussian error v with (diagonal) covariance matrix R. The basic idea behind the ensemble filter is to express the probability function of the state in an ensemble of possible states $\{\xi_1,..., \xi_N\}$, and to approximate statistical moments with sample statistics:

$$\hat{x} \approx \frac{1}{N} \sum_{j=1}^{N} \xi_j$$

$$P \approx \frac{1}{N-1} \sum_{j=1}^{N} \left(\xi_j - \hat{x}\right)\left(\xi_j - \hat{x}\right)^T$$

where the pair ($\hat{x}$,P) (expectation and covariance matrix) describe the probability of the state vector x completely if x has a Gaussian distribution. Since we are dealing with strongly non-linear models, it cannot be expected that x really has a Gaussian distribution. We assume however that the distribution is at least close to Gaussian so that the bulk of the statistical properties is captured by the pair ($\hat{x}$,P). The filter algorithm consists of three stages:

Initialisation:
each ensemble member is set to the initial state:

$$\xi_j = x^0$$

Forecast:
each ensemble member is propagated in time by the model, where the noise input w^k is drawn from a random generator with covariance Q;

$$\xi_j^f = f(\xi_j, w^k)$$

Analysis:
given an (arbitrary) gain matrix K, each ensemble member is updated according to:

$$\xi_j^a = \xi_j^f + K(y + v - H^T \xi_j^f)$$

where v_j represents a measurement error, drawn from a random generator with zero mean and covariance R. The gain matrix K is given by the optimal gain matrix from the original Kalman Filter. In the original filter the Kalman gain was obtained by matrix multiplications in which the covariance matrix P is involved. Fortunately, the use of this matrix can be avoided, since this matrix is too large to store into memory. Instead, a square root S (such that $P=SS^T$) can be used. From the definition of P it can be seen that the columns s_i of such a square root can be defined by

$$s_i = \frac{1}{\sqrt{N-1}}\left(\xi_i - \hat{x}\right)$$
.

Note that the sample mean $\hat{x}$ and the matrix S completely define the ensemble and vice versa; it is therefore not necessary to store both S and the ensemble.

The analysis of the measurements y_j (entries of the vector y) can now be performed by the following sequential procedure (dropping the time index):

$$h_j = S_{j-1}^T c_j^T$$

$$a_j = \left(h_j^T h_j + r_{jj}\right)^{-1}$$

$$b_j = \left(1 + \sqrt{a_j r_{jj}}\right)^{-1}$$

$$k_j = a_j S_{j-1} h_j$$

$$S_j = S_{j-1} - b_j k_j h_j^T$$

$$x_j = x_{j-1} + h_j \left(y_j - c_j x_{j-1}\right)$$

The index j is the iteration index. The starting values for the procedure are $S_0 = S_f^{k+1}$ and $x_0 = x_f^{k+1}$. After the analysis of all the measurements the final values for the state vector and (square root of) the covariance matrix have been obtained: $S^{k+1} = S_m$ and $x^{k+1} = x_m$. For a detailed description we refer to van Loon et al. (2000) and Evensen (1997).

The forecast step is the most expensive part of the algorithm, since for each ensemble member the model has to be evaluated one time. Typical ensemble sizes range from 10-100. If the number of measurements is limited (in order of hundreds), the total computation time involved with the ensemble filter is proportional with the ensemble size.

Random noise
In the model implementation used in this study, the noise parameters are part of the model state. Hence they are estimated by the filter as well. Later on in this report, we will specify noise to several emission fields E_j. The noise parameters w_i can be interpreted as emission correction factors since the actual emission field E_j is estimated by the filter as

$$E_i \leftarrow E_j \,(1+w_i).$$

This approach has the disadvantage that there is no "memory" in the system: the w_i are uncorrelated in time; at a certain hour t the noise parameter may indicate an emission increase of 20% with respect to the original field, whereas it estimates a decrease of 20% at $t+1$. Such irregular behaviour can be prevented to a large extent by the use of coloured noise. However, in the present set-up we use the same noise factors for the 24 hour period between overpasses. Hence, the long period between the measurements warrants some correlation in time.

Spatially limiting influence of measurements
For two reasons correlations between elements in the state vector arise which are unlikely to be correlated. Firstly, spurious correlations arise, mainly because the sample size is finite. Secondly, undesired correlations arise due to the choice of the noise processes. The noise processes to be introduced in this study are all acting on emission fields of various emitted compounds causing "instantaneous" correlations throughout the domain. For example the ozone concentration at hour t somewhere in The Netherlands becomes correlated with the ozone concentration in, say, the south of France, because noise was added to the NO_x emission field at hour t-1. Although this is exactly what should happen when defining noise in this way, such correlations are not realistic and should be somehow ignored by the filter. The noise processes are chosen this way because it is infeasible to subdivide the emission fields into a number of subdomains on each of which a different noise parameter is acting. That would increase the dimension of the noise vector dramatically and hence the necessary ensemble size to capture the statistical properties.

One way to ignore unrealistic correlations over large distances is the use of a gain matrix which is only unequal to zero around the measurement sites. Such a gain matrix k may be formed using a covariance matrix which is an element wise product of the original sample covariance and a correlation function with local support. For a single scalar measurement, the resulting gain matrix is given by (omitting the subscripts):

$$k = I(\rho)Ph/(h^T Ph + r)$$

where $I(\rho)$ is a diagonal matrix; the diagonal elements are filled with a prescribed correlation between the corresponding grid cell and the grid cell of the measurement. Different choices for the values of ρ_i are possible. In this study we take

$$\rho_i = \exp(-0.5\ (r_i/L)^2) \qquad \text{for } r_i \leq 3.5\ L$$

and zero otherwise. r_i denotes the distance from the grid cell considered to the site of the analysed measurement and L denotes a length scale parameter.

2.4 AOD-DATA FROM ATSR-2

ATSR-2 satellite measurements of the radiation at the top of the atmosphere are input for the semi-operational ATSR aerosol retrieval algorithm, based on scientific algorithms (Robles González et al.,2000), that has been developed in the framework of the former ARIA-1 project for the INDOEX region.
For ARIA-2 the algorithm has been enhanced, modified and utilized to retrieve the AOD maps over Europe for the months March, May and August of the year 2000 from the available ATSR-2 data set. The data was delivered by ESA for the area confined by the latitudinal boundaries (20°N, 80°N) and the longitudinal boundaries (20°W, 40°E). Also retrievals for the INDOEX regions have been performed for the months of February and March of the year 1999 based on earlier data sets obtained from ESA. The ATSR-2 swath of 512 km allows for an overpass over each geolocation every three days, at 10:30 in the morning and for many overpasses AOD cannot be retrieved due to the presence of clouds. As a consequence, the data represent a snapshot of the situation during the overpass, and at best each snapshot is available once every third day. A further restriction is the solar zenith angle of maximum 81°, which puts a limit to the amount of available data for the Northern part of Europe, in particular in winter.

The retrieval method proceeds as follows according to the following retrieval schematics:
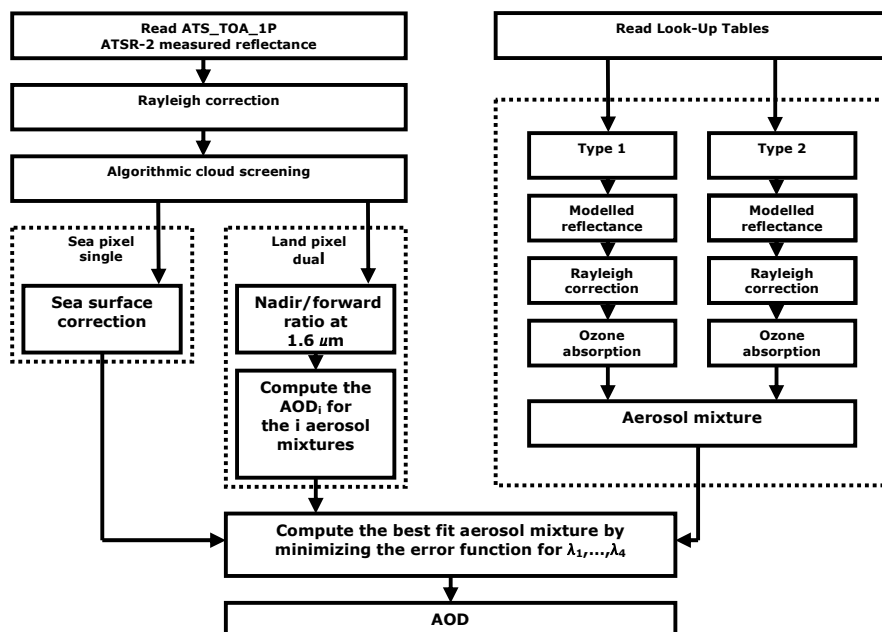
Figure 2.2 Retrieval scheme for aerosol optical depth from ATSR2 radiances.

The aerosol model used for Europe is an external mixture of anthropogenic aerosol (sulphate/nitrate water soluble, r_{eff} = 0.05 μm; Volz, 1972) and sea salt (r_{eff} = 1 μm; Shettle et al., 1979). A Mie scattering code and the Radiative Transfer Model DAK (Stammes (2001) are used for the generation of Look-up tables (LUT's). Cloud-free pixels are essential for a proper retrieval of aerosol properties; hence an automated cloud screening procedure with three tests for the presence of clouds is used based on cloud detection routines developed by Koelemeijer et al. (2001). Subsequently, corrections for ozone, surface contributions and atmospheric (Rayleigh) contributions are computed. Finally, the corrected TOA (Top of the Atmosphere) reflectance at the satellite sensor is compared with the modeled reflectances in iterative steps in order to select the right aerosol mixture. This procedure is based on a LUT approach. Measured and modeled reflectances are matched using an error minimization procedure to determine the most likely aerosol mixture and the AOD for the available ATSR-2 wavelengths (Robles González et al., 2000, and Robles González, 2003).

The aerosol mixtures used to create the Look-up tables for the INDOEX region consisted of sea salt particles and an 'effective' aerosol type that was derived from sun photometer measurements on the Maldives during the INDOEX campaign (Dubovik et al., 2002). The aerosol optical depths (AOD) that were retrieved showed good agreement with independent sun photometer data obtained during the INDOEX experiment (February and March, 1999), i.e. AOD values agreed within 0.05 at 656nm at a location on the Maldives. The AOD determined by the algorithm ranged from 0.4 over most over the continent to 0.1 in the Southern Hemispheric Indian Ocean. The aerosol mixing ratio's changed with fetch, i.e. the algorithm indicated the increasing sea salt contribution as the air mass was advected over the ocean.

For the data assimilation scheme daily AOD maps over Europe are produced for the 1 x 1 km^2 sensor resolution. The final AOD maps for the European scale are given as a product with a (default) resolution of 10x10 km^2 (roughly 0.1° x 0.1° over Europe) by means of an automated post-processing step, where the AOD values for the individual ATSR-2 pixels in each 10 x 10 km^2 area are averaged. For the assimilation of these data into the TM4 model this final resolution is still too high. The observations are therefore aggregated to so-called 'super observations', as described in section 2.2.

19

For the data assimilation scheme daily AOD maps over Europe are produced for the 1 x 1 km^2 sensor resolution. The final AOD maps for the European scale are given as a product with a (default) resolution of 10x10 km^2 (roughly 0.1° x 0.1° over Europe) by means of an automated post-processing step, where the AOD values for the individual ATSR-2 pixels in each 10 x 10 km^2 area are averaged.

Satellite retrieved AOD values are more reliable with an essential validation for proper use in assimilation schemes and other applications. Validation is performed by comparing the satellite retrieved AOD values with ground-based measurements from AERONET. The worldwide AERONET network has a huge quantity of sun photometers that measure the AOD in the atmospheric column from ground to sun with an accuracy between ±0.01 and ±0.015 (Eck et al., 1999). This accuracy is higher than the retrieval accuracy of the ATSR-2 retrievals, which is ±0.05 over land and ±0.03 over sea (Robles González, 2003). There are however a couple of restrictions that limit the amount of proper data for comparisons. In contrast to the distribution like measurements from space-based sensors are the discrete point like measurements of AERONET. This spatial resolution feature strongly restricts the amount of comparable data. Secondly, the number of satellite overpasses is limited to once every three days. It is noted that the sun photometer should be operational at the exact time of sensing for the geolocation of the sun photometer; which is not always the case. Furthermore, and this is a third restriction in the usable data set, is the cloudiness of the pixel at time of overpass. With cloud cover there is no aerosol retrieval from AATSR, like there is no measurement of the sun photometer either. Moreover, cloud screening algorithms differ for both sensing techniques and it sometimes occurs that one of two measurements is cloud-screened and the other is not. For Europe some seventeen sun photometers are used for comparing the ATSR-2 retrievals of the year 2000 dataset. For the INDOEX campaign back in 1999 a very sparse dataset was used for the validation, that is, two AERONET sites over land for the dual view retrieval and two sites on islands for the single view retrieval over water.

ATSR-2 retrieval results for Europe and INDOEX
For the assimilation scheme daily retrieved AOD values are used. These daily retrievals represent pieces of orbits and are uniquely retrieved. Because of the swath width of 512 km and the polar orbit of the ATSR-2 instrument, a global coverage is achieved every three days. This implies that every three days the same spot on Earth is exposed to the sensor. An orbit lasts approx. 100 minutes while the satellite revolves around the Earth in a sun-synchronous orbit, which implies that the location on Earth will be captured at the same time of the day subsequently. This (local) time is around 10:30 in the morning. For a domain the size of Europe one can see in Figure 2.3 that pieces of three orbits are captured. The requirement of cloud free pixels for a proper retrieval cause the limited amount of useful pixels over land, hence the fragmentation in the orbits.
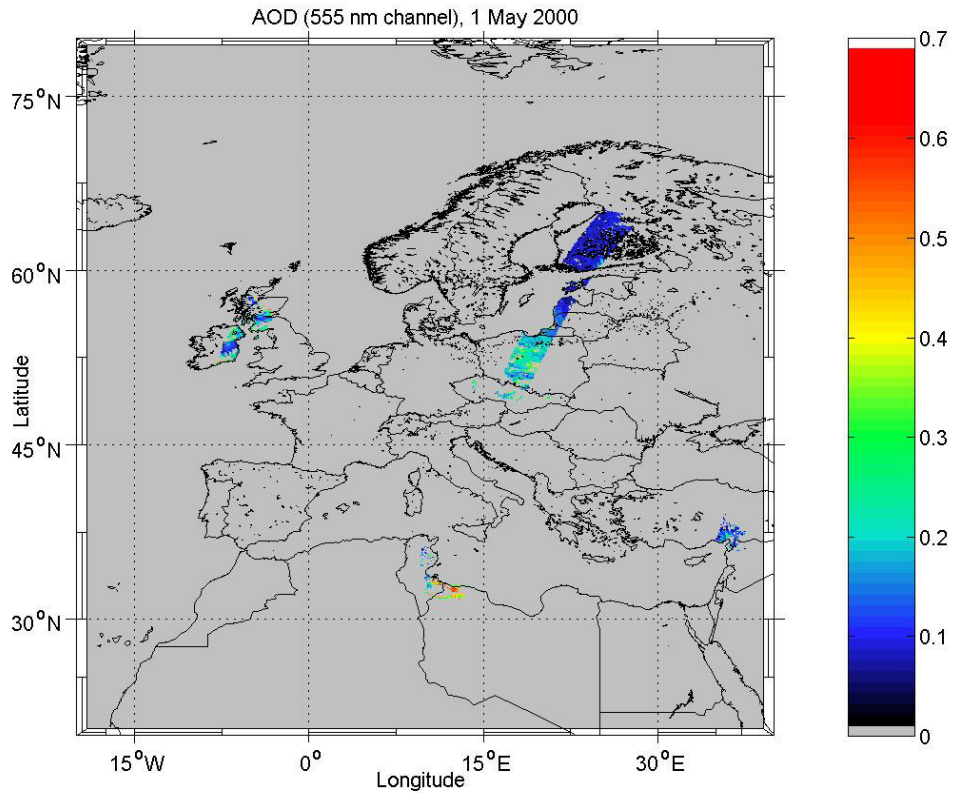
Figure 2.3: A daily retrieval for 1 May 2000 for the 0.55 µm channel. Three orbits can be distinguished despite the fragmented data set due to cloud screening.

By combining all daily retrievals for a certain month the average of the AOD values for each geolocation, that is for a granule of 10 x 10 km^2, is computed. Monthly averages show the trends of aerosol distributions in time. Figure 2.4 shows the targeted month of May 2000 and depicts the monthly average for the retrieved AOD for the 0.55 µm channel.

AOD (555 nm channel), May 2000
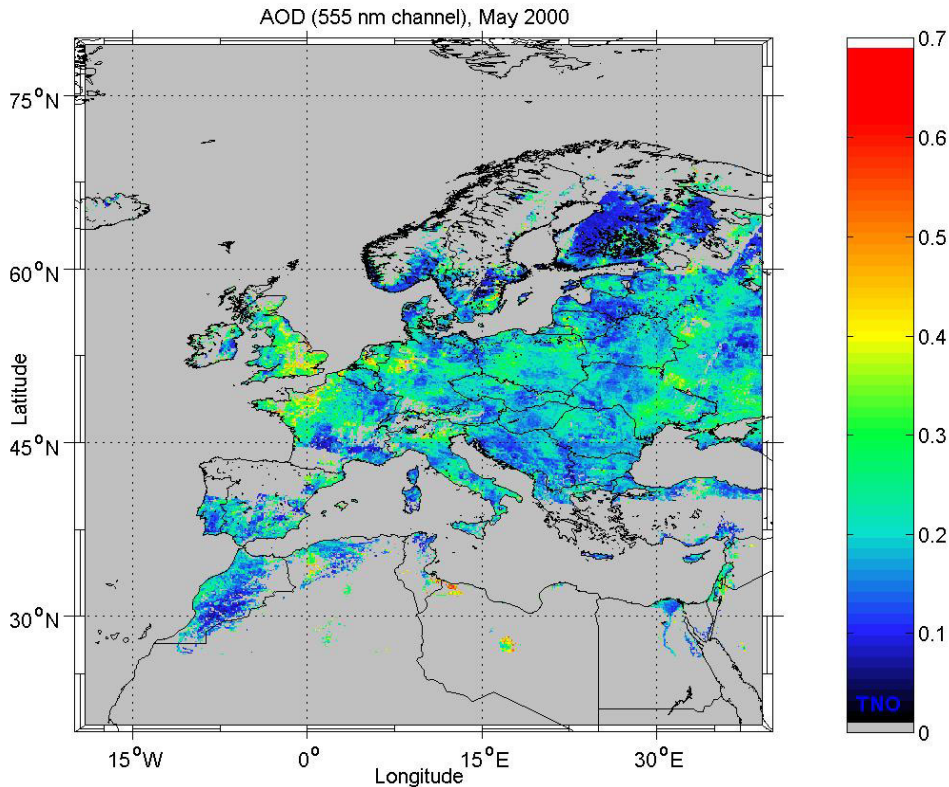
Figure 2.4: Monthly average of the AOD for the 0.55 µm channel for the month of May 2000.

Figures like Figure 2.4 show a huge amount of collected data in one image which is representative of the data set used. For certain regions over land one can see also that no data is processed at all. For example the north of Spain and most of Turkey lack any data for a large portion of the year 2000 data. The reason is not the cloud screening in the algorithm but an unrecoverable omission in the dataset that has been used. The north of Europe also shows very few useful data points. Here parts are screened due to the high reflection of snow (Norway and Sweden e.g.) and clouds. For winter times the solar zenith angle restricts a proper retrieval for higher latitudes, i.e. the scenes of 512 by 512 pixels are overall darker, which result in less accurate retrieval of AOD.

The results compare favourably with the ground based measurements from the sun photometers all over the region. The AOD from the daily retrievals can be used for the assimilation procedures. However, it is noted that the two aerosol types are not perfectly representative for every location of Europe. That is, Aerosol Optical Depth over France differs from AOD over Eastern Europe, not necessarily in the number of particles in the atmospheric column, the more in the scattering and/or absorption characteristics of the types used. In order to show the sparsity in the data set due to the restrictions mentioned above, an example is shown in Figure 2.5 for ATSR-2/AERONET comparisons for the three target months March, May and August for one specific AERONET site in Avignon, France. This station is one of the few sites that have data for the targeted months.
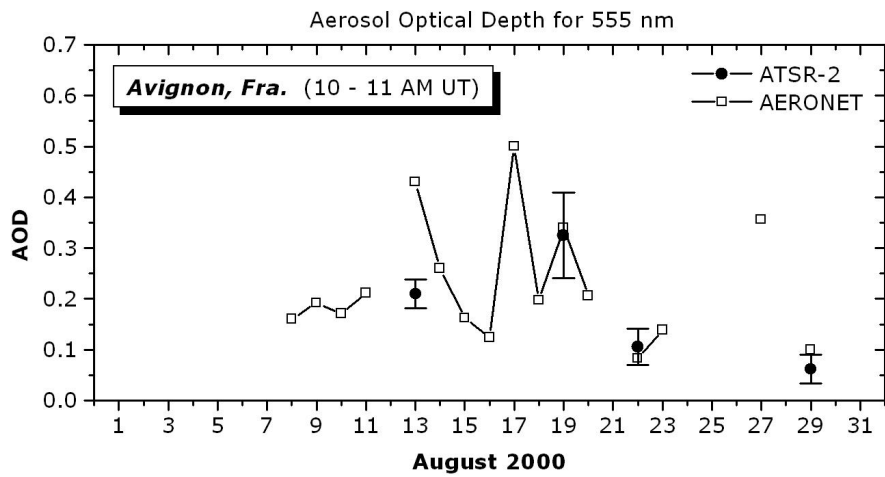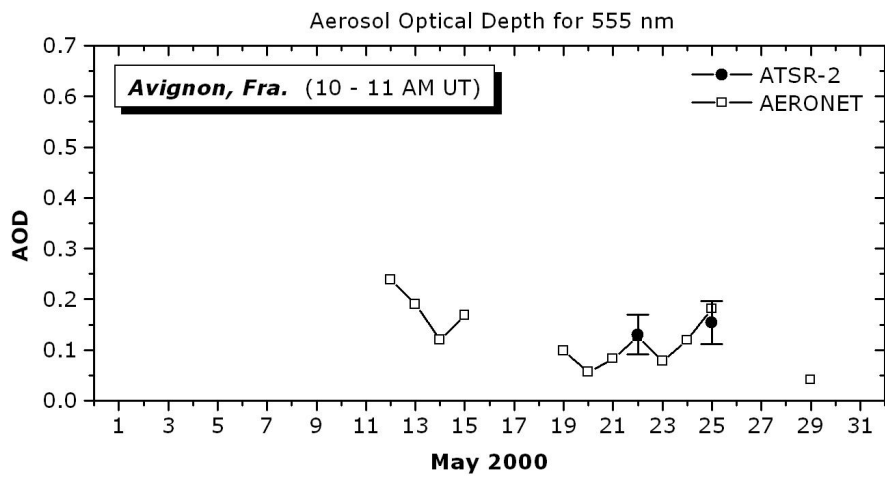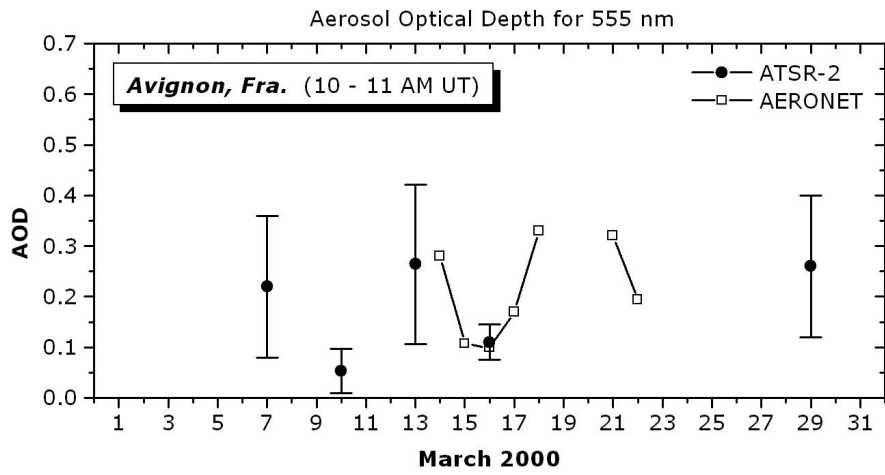
Figure 2.5: ATSR-2 vs. AERONET for all measurements in August for the Avignon (France) sun photometer site.

For INDOEX a daily retrieval example is shown in Figure 2.5. The three consecutive orbits for the date and time for the region are clearly recognized, better than the example for Europe in Figure 2.3.
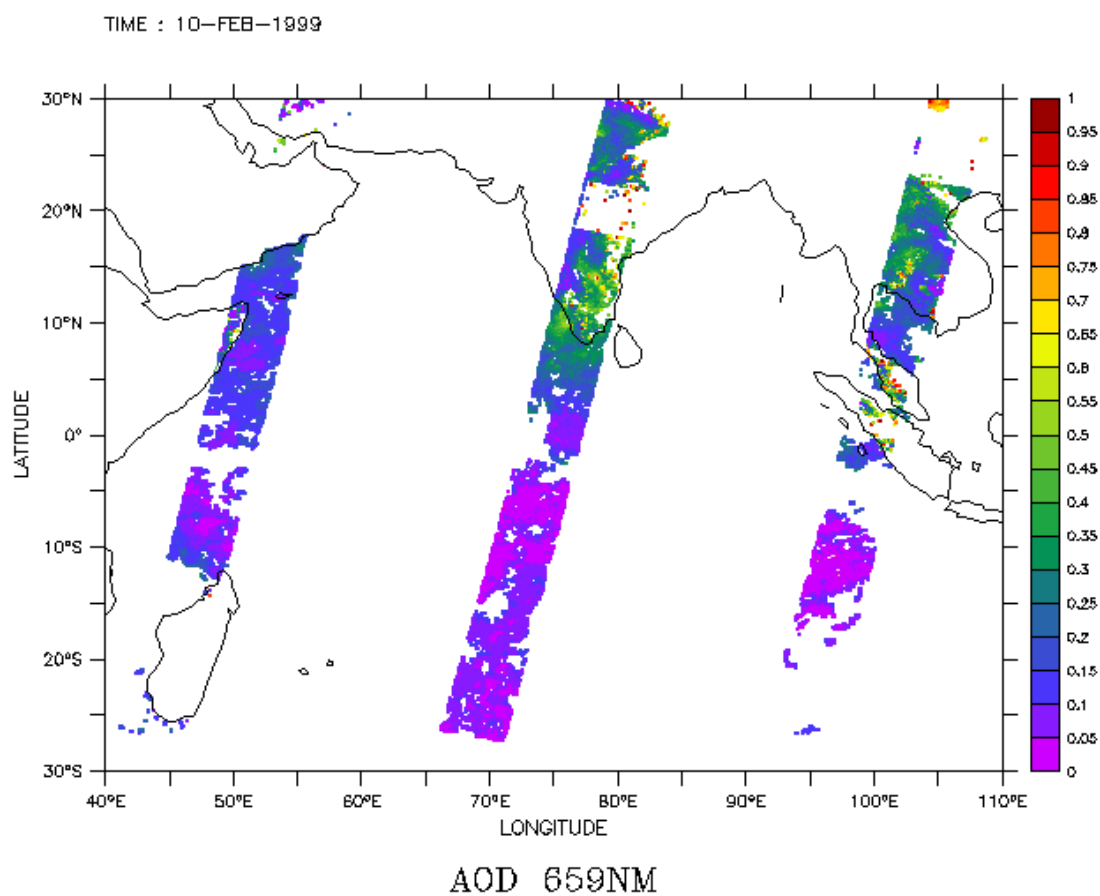
Figure 2.6: A daily retrieval for February 10, 1999.

The monthly mean composite map is shown in Figure 2.7. The retrieval results have been performed for the 0.67 μm channel for a pixel size of 10 by 10 km. High AOD values are most probably caused by anthropogenic sources (industry and fossil fuel burning).
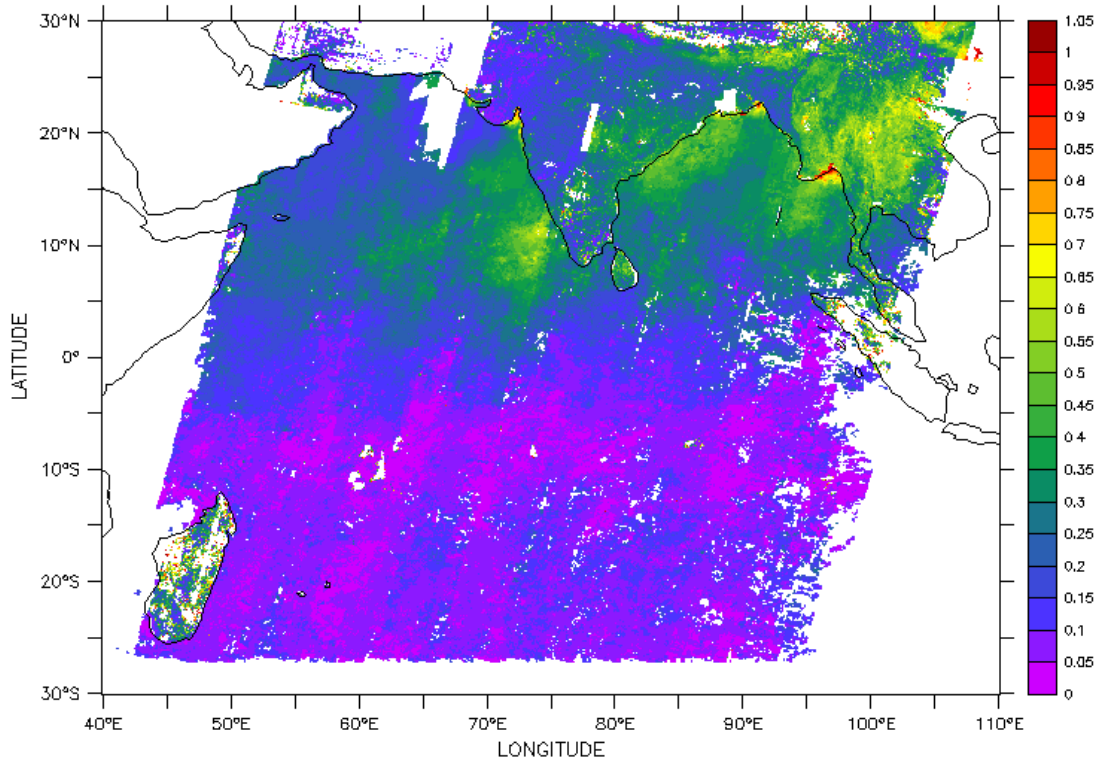
Figure 2.7: Monthly mean ADO for the months of February and March 1999 during INDOEX.

Validation results are given in Figure 2.8. The accuracy in this validation depends on only four AERONET comparisons on three days, that is, February 10, March 10 and March 26. Very few sun photometer stations where present during the INDOEX campaign.
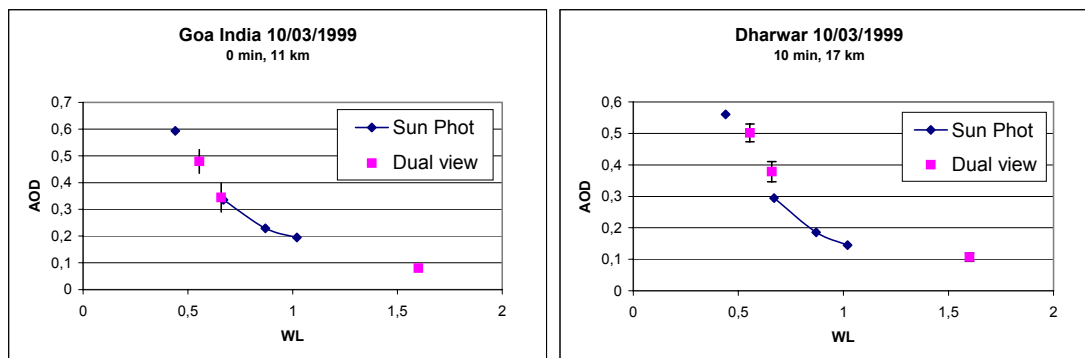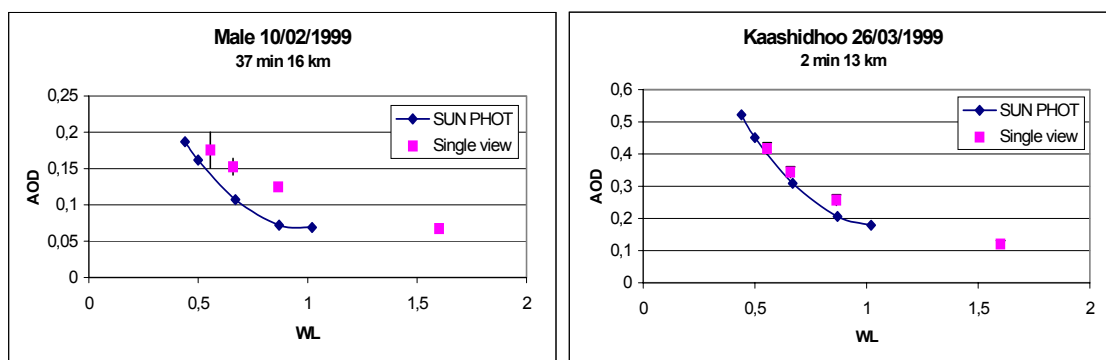
Figure 2.8: AOD versus wavelength for four stations in the INDOEX region.

2.5 AEROSOL SURFACE OBSERVATIONS

The modelled mass concentrations of secondary inorganic aerosol (SIA) components are compared with observations at rural stations in Europe. Observations of SIA and SO_2 used in this study are gathered from the EMEP (www.emep.int) database. Additional PM2.5 and/or aerosol composition data have been obtained for Melpitz (Germany) (G. Spindler, personal communication). Mountain stations were excluded from the analysis. The data for nitrate and ammonium were screened as the measurements of these compounds are prone to artefacts (Schaap et al., 2002; 2004b). Nitrate data obtained with cellulose filters were interpreted as total nitrate. Aerosol nitrate data from inert filters were used in this study, although we are aware that they are prone to losses at temperatures above about 20 °C. Total nitrate and ammonium data which were not obtained in a single measurement set-up were disregarded. As the coverage for nitrate and ammonium is low all stations were included in the analysis. Hence, the results for these components are biased to a few stations.

Statistical parameters
For the statistical parameters used to compare modelled (M) with observed (O) data we follow the definitions by van Loon et al. (2004). The comparison is based on pairs of modelled and measured data for a number of stations (S) with available data for 1995. The number of days is given by D, whereas d and s represent the day and station number, respectively.
The ratio of model results $M_{s,d}$ over observations $O_{s,d}$ is defined as:

$$Ratio = \frac{\sum\limits_{s=1}^{S} \sum\limits_{d=1}^{D} M_{s,d}}{\sum\limits_{s=1}^{S} \sum\limits_{d=1}^{D} O_{s,d}} = \frac{\overline{M}}{\overline{O}}$$

The residual is the sum of the absolute deviations of model results and results from observations:

26

$$\mathrm{Re}\,sidual = \frac{1}{S}\sum_{s=1}^{S}\frac{1}{D}\sum_{d=1}^{D}\left|M_{s,d} - O_{s,d}\right|$$

The root mean square error is defined as:

$$RMSE = \frac{1}{S}\sum_{s=1}^{S}\sqrt{\frac{1}{D}\sum_{d=1}^{D}\left(M_{s,d} - O_{s,d}\right)^{2}}$$

The normalized ratio of standard deviation (given in the tables as sigma) is

$$\sigma^{*} = \frac{1}{S}\sum_{1}^{S}\frac{\overline{O_{s}}}{\overline{M}_{s}} * \frac{\sigma_{s,M}}{\sigma_{s,O}}$$

with the standard deviation

$$\sigma_{s,O} = \sqrt{\frac{1}{D}\sum_{1}^{D}(O_{s,d} - \overline{O_{s}})}$$

and the observed mean at a station s

$$\overline{O}_{s} = \frac{1}{D}\sum_{1}^{D}O_{s,d}$$

and a similar definition for the modelled mean.
The average correlation coefficient rho is defined as

$$rho = \frac{1}{S}\sum_{s=1}^{S}rho_{s}$$

using the correlation in time at the individual stations

$$rho_{s} = \frac{\displaystyle\sum_{d=1}^{D}(O_{s,d} - \overline{O}_{s})(M_{s,d} - \overline{M}_{s})}{\sigma_{s,O} * \sigma_{s,M}}$$

A similar expression is used for the correlation in space, where D is replaced by S.

2.6   SYNTHESIS

A schematic representation of the assimilation system as used in ARIA-2 is depicted in figure 2.1. The regional LOTOS-EUROS model including the assimilation is run for certain periods and regions to obtain aerosol mass distribution and PM2.5, and as a tool to assess emissions. Updated regional emission strengths can subsequently be used in the global system. The global and regional model can provide valuable information about the distribution of aerosols (profiles and aerosol types) which may improve the initial assumptions required by the aerosol retrieval algorithm. The combined use of transport modelling and aerosol retrieval potentially yields aerosol products that are superior to current products that use climatological information in the retrieval. However, since the retrieval itself was not part of this ARIA-2 project, the coupling of retrieval with chemistry/transport model data was not implemented.

A more accurate assessment of the global climate forcing caused by aerosols is possible when the assimilation system developed in this project yields improved aerosol distribution. Examples of the new product, the assimilated aerosol distribution, will also be derived in this last phase. Other products of the project are a prototype version of the aerosol assimilation and retrieval system, as well as a tool to estimate regional aerosol emissions and PM2.5.

In the course of the project consultation of the anticipated users of the new aerosol products has been carried out. This final report contains a list of requirements for the operational implementation as a service element for e.g. SCIAMACHY.

3 RESULTS

3.1 INTRODUCTION

The implementation of the global assimilation system into version 3 of TM (TM3) was made during the first phase of ARIA (ARIA-1). We concluded from the results of the first phase that additional aerosol types needed to be implemented in the TM3 model in order to properly describe the aerosol optical depth during the Indian Ocean Experiment (INDOEX). We also suggested that the emission of aerosol was underestimated due to the rapid industrialization that takes place in the INDOEX region, which was not completely taken into account by the model sources.

In this chapter we describe the results of the second phase, using an updated version of the global model TM4 (section 3.2), an updated version of the assimilation scheme (section 3.4). The regional EUROS-LOTOS model was used to estimate aerosol sources, and fields of PM2.5 (section 3.5). The performance of both models without assimilation is evaluated by a comparison with surface aerosol observations (section 3.3).

3.2 DEVELOPMENTS OF THE GLOBAL MODEL TM4

The TM4 aerosol model has been updated during the second phase in ARIA with respect to aerosol emissions, secondary formation, aerosol sinks, and aerosol optics. The changes are specified below

Aerosol emissions and formation

A source for sea salt aerosol particles (Gong, 2003b) that is based on the source function given by Monahan et al. (1986) has been included in the model. This source function, which is a function of the wind speed at 10-meter height (U10), provides the number of particles emitted in a certain size range per unit time and per unit sea surface. In our model the series of physical transport processes on sea salt aerosol are most conveniently formulated in terms of the dry part of the aerosol particles. Therefore, we have translated the source function, which is valid at 80% relative humidity (Monahan et al., 1983), in a dry particle source function using the size dependence of sea salt aerosol as a function of relative humidity given by Gerber (1985). To solve the size distribution both in number and mass it is sufficient to use 12 log-equidistant sectional bins (Gong et al., 2003a). Our 12 bins cover the dry radius spectrum from 0.03 (m to 10.0 (m. Offline, we have calculated the mass emission [kg sea salt per second and per unit sea surface] in every bin for 1 m s-1 wind speed, from which the actual emission is obtained by multiplication with U103.41 (Monahan et. al., 1986). In the model, aerosol particles are assumed to be in a stable equilibrium size with respect to ambient relative humidity. The actual size of sea salt aerosol, which is used to calculate the below-cloud scavenging, is related to their dry size by the relationship of Gerber (1985).

Applying this model of the sea salt source, we find for the year 2000 a global total sea salt mass emission of 2,440 Tg for particles with dry radii between 0.03 and 10 (m. This value falls well within the range of estimates reported in the literature (1,000 to 3,000 Tg/yr, Erickson and Duce, 1988; 5,900 Tg/yr, Tegen et al., 1997) and can be compared to the current best estimate of 3,300 Tg/yr for sea salt particles with dry radii between 0.03 and 8 (m that is given in IPCC (2001). Super-micron (sub-micron) aerosol particles by definition have diameters larger (smaller) than 1(m. Super-micron (sub-micron) mass emissions add to 2,390 (48) Tg/yr, which agrees with the ranges of 1,000 to 6,000 (18 to 100) Tg/yr provided by IPCC (2001). In Figure 3.1 we show the seasonal variations of global and hemispheric monthly emissions in our model. The strong seasonal variations in both the northern and southern hemisphere agree with the findings of Gong et al. (2002). The monthly average sea salt concentration near the surface in March 2000 is given in figure 3.2.

Guelle et al., (2001) used the Monahan (1986) source function for sea salt to estimate a mean annual global mass-load of 0.5 and 10.6 Tg for submicron and supermicron (cut off at 4(m radius). Using the Gong-Monahan source, that mainly differs from the original Monahan source function for small particle size that make up only a small fraction from the total mass, we find for size ranges corresponding to Guelle et al. global mean loads of 0.5 and 6.1 Tg for submicron and supermicron aerosol, respectively. For the whole size range we find 9.8 Tg which can be compared to Guelle et al. (2001) who have 12.7 Tg.

For IPCC (2001) six models with prescribed sea salt sources were run to estimate global burdens. Using these estimates the average sea salt lifetime for the whole size range is 2.1 days (varying between 0.8 and 4.55 days). Our estimate of 2.16 days is in close agreement with these values.
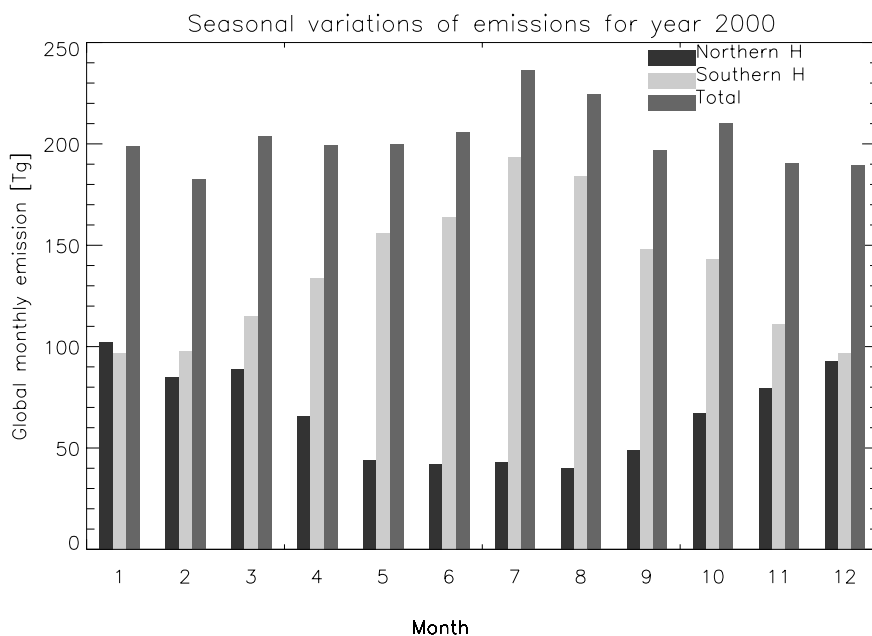
Figure 3.1. Simulated monthly variations of global and hemispheric emissions.
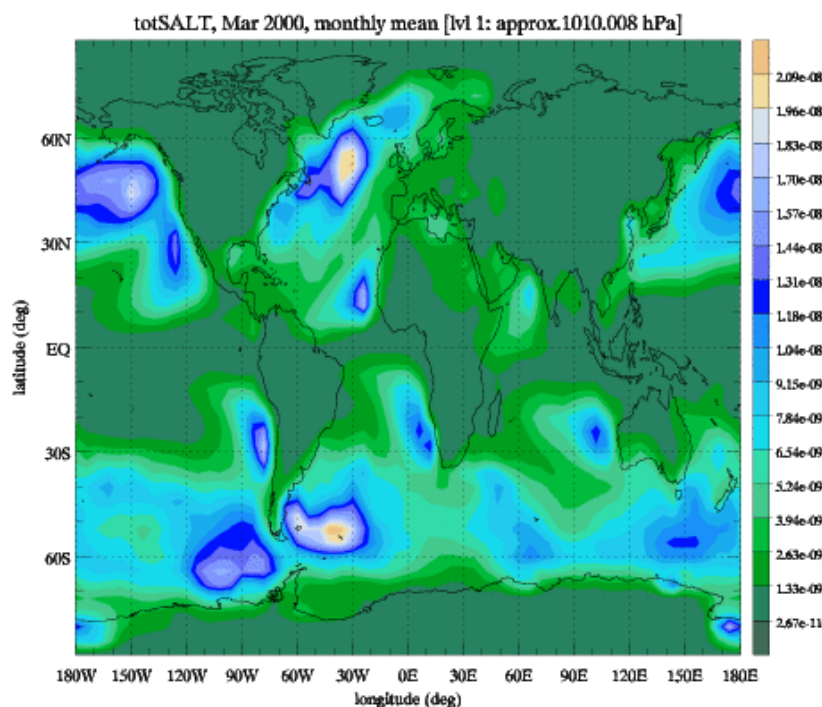
Figure 3.2. Total sea salt concentration (sum of all size bins) in the lowest TM4 model layer

Aerosol sinks

A size dependent parameterization for the removal of aerosol particles by falling rain droplets is developed in two steps. First the scavenging coefficients as a function of aerosol particle size and precipitation intensity is calculated, including the full interaction of rain droplet size distribution and aerosol particles. In a second step, we fit an analytical function through the pre-calculated values of the scavenging coefficient for every aerosol particle radius (1000 log-equidistant increments per order of magnitude increase in particle radius). A function of the form

$$\beta(P) = A_0 \left(e^{A_1 P^{A_2}} - 1 \right) \qquad (4)$$

fits the data quite well and yields a scavenging coefficient for every aerosol particle radius that is only a function of the precipitation intensity. Using the fit function instead of an explicit integration over the rain droplet spectrum (as is done in step 1), introduces errors much smaller than 1% except in a very small size region around 1 μm.

The simple three-parameter fit to calculate the scavenging coefficients is used in the global chemistry transport model TM4. For sea salt aerosol the importance of below-cloud scavenging relative to other removal mechanisms is investigated. After a full year run (year 2000), we find that below-cloud scavenging accounts for 12% of the total removal of super-micron aerosol. At mid-latitudes of both hemispheres the fractional contribution of below-cloud scavenging to the total removal of super-micron sea salt is about 30% with regional maxima exceeding 50%. Below-cloud scavenging reduces the global average super-micron aerosol lifetime from 2.47 to 2.16 days in our simulations. Despite large uncertainties in precipitation, relative humidity, and water uptake by aerosol particles, we conclude that below cloud scavenging is an important sink for super-micron sized sea salt aerosol particles that needs to be included in size-resolved aerosol models.

Aerosol optics

The model predicts aerosol mass whereas the quantity that is assimilated is aerosol optical depth. The optical depth τ in layer k is given by:

$$\tau(k) = g^{-1} \int_{p_k}^{p_{k+1}} \sum_i \chi_i q_i dp.$$

Here i is an index for aerosol species, χ_i is the extinction cross section per unit mass for specie i, [$m^2 kg^{-1}$], q_i is the aerosol mixing ratio [(kg aerosol)/(kg air)], and p_k is the pressure at the bottom of layer k. Total aerosol optical depth is given by the summation over all vertical layers. The extinction cross sections are significantly changed compared to the values used in the TM3 model that was used in the first phase of the ARIA project.

The cross section χ_i can be calculated for a known aerosol particle size distribution, water uptake by aerosols as a function of relative humidity, and mixing state of the different aerosol species. For computational efficiency this calculation is done offline. A dry log-normal size distribution and the appropriate water uptake are prescribed for all species. For relative humidity varying between 0% and 100%, we calculate the 'hydrated' size distribution, to which we can closely fit a new log-normal distribution. For hydrated particles we calculate the refractive index using an effective medium approximation. The extinction cross section is obtained from Mie calculations using the hydrated size distribution and the accompanying refractive index.

Optics of carbonaceous aerosols

Hydrophobic organic carbon (OC) and black carbon (BC) aerosols are fresh combustion products. The size of these particles depends on the combustion process and the fuel used. In remote regions, Clarke et al. (1997) measured the particle number size distributions after heating up the sample to 300 °C. They interpreted the remaining, refractory, number distributions as the distribution of cores on which volatile fine particle mass had condensed. If these cores exist of BC and OC then the refractory number distribution provides an estimate of the hydrophobic particle size distribution. Converting their size distribution to a log-normal distribution we find for the mean radius $r_g = 0.03$ and a geometric standard deviation $\sigma = 2.0$. For black

carbon we use for the real part of the refractive index $m_r = 1.75$ and the for the imaginary part $m_i = -4.4e^{-3}$ (Hess et al., 1998); for organic carbon we use $m_r = 1.75$ and $m_i = -4.4e^{-3}$ (Gelencsér, 2004; Liousse et al., 1996). Mie calculations yield $\chi_{BC} = 10.85$ m^2 g^{-1} and $\chi_{OC} = 3.61$ m^2 g^{-1}. These values are used by the model to calculate the contribution of carbonaceous aerosol to the total aerosol optical depth.

Optics of sulfate, ammonium, and nitrate aerosols
For the sulfate-ammonium-nitrate system, the dry log-normal size distribution is expressed by a geometric mean radius $r_g = 0.05$ and a geometric standard deviation $\sigma = 2.0$ (Jeuken et al., 2000, Kiehl et al., 2000). The water uptake of these inorganic aerosols, expressed as a function of relative humidity and particle size, is that of ammonium bi-sulfate (Gerber, 1985). The density of dry inorganic salts is 1760.3 kg m^{-3} and the real part of the refractive index (m_r) is 1.53 and the imaginary part of the refractive index (m_i) is $-6.0e^{-3}$ (Hess et al., 1998). For pure water these values are: $m_r = 1.333$ and $m_i = -1.96e^{-9}$. It is assumed that each particle consists of a homogeneous mixture of solutions and that the water, sulfate, nitrate, and ammonium masses are equally distributed over all particles of the aerosol. Therefore, a simple volume-weighted average of the individual refractive indices can be used to calculate the refractive index of the composite particles.

Optics of internal mixtures of carbonaceous and secondary inorganic aerosols
During the first phase of ARIA it was assumed that all aerosols were 'externally mixed', meaning that the aerosol mass of individual aerosol traces do not depend on the concentrations of other aerosol species. However aerosols in the atmosphere are nearly always internally mixed to some degree (Penner et al., 2001; Haywood and Boucher, 2000), i.e. most aerosol particles are made up of several chemical species. In the second phase of ARIA this was taken into account as follows:
Hydrophilic OC and BC are 'impure' carbonaceous particles that contain species other than the fresh combustion products hydrophobic OC and BC. These impurities mainly consist of sulfates, ammonium and nitrates, also denoted by secondary inorganic aerosols (SIAs). We assume here that the various carbonaceous and SIA species are homogeneously mixed within the composite particle. The so-called `effective medium approximation` from Chylek et al. (1996, 2000) is used to determine the optical properties of heterogeneous particles. A simple volume-weighted average of the individual refractive indices is used (Lesins et al., 2002).
In our calculations the distribution of the hydrophilic OC and BC composite particles is described by a log-normal size distribution with a geometric mean radius $r_g = 0.05$ and a geometric standard deviation $\sigma = 2.0$. The volume fraction of OC and BC in all the individual particles of the distribution is given by the fractional contribution of the OC and BC volume, occupied by a log-normal distribution with $r_g = 0.02$ and $\sigma = 2.0$, to the total volume of the composite particle distribution. The remainder of the volume is occupied by SIAs. The fractional contributions of the various SIAs to the impure part of the composite hydrophilic carbonaceous particles are determined by the EQSAM model (Metzger et al., 2002a). If insufficient SIA is available, which sometimes occurs for carbonaceous rich regions over warm land surfaces, the amount of OC and BC in the composite particles is stepwise increased. The water uptake of hydrophilic OC and BC is supposed to be similar to that of urban aerosol (Gerber, 1985). The mass extinction cross sections per unit dry mass for relative humidities varying between 0-100% are obtained by fit functions given in Henzing (2006).

Optics of sea salt aerosols
For sea salt aerosol the mass extinction cross section χ_{salt} is needed as a function of relative humidity for each of the twelve size bins. The cross sections are obtained using the polynomial fit functions derived by Henzing (2006). The Mie calculations that were used to derive the optical parameters are based on a density of dry sea salt of 2170 kg m^{-3} and $m_r = 1.50$ and $m_i = -1.00 e^{-8}$ (Shettle and Fenn, 1979). The water uptake of sea salt is taken from Gerber (1985).

3.3 EVALUATION OF THE GLOBAL AND REGIONAL MODEL WITHOUT ASSIMILATION

The models TM4 and LOTOS-EUROS are used to estimate the three dimensional distribution of different aerosol types. The two different assimilation schemes constrain the aerosol distribution such that it becomes more consistent with the observed aerosol optical depths. The mixture of aerosol types as well as the vertical distribution is mainly determined by the model, since the observed optical depth that is assimilated does not carry any height information or information on the aerosol types that are present. Therefore the models should

be able to reasonably reproduce the distribution of the aerosol types that contribute most to the optical depth. The results of the models have been compared to ground based measurements of aerosol composition. In practice, only the secondary inorganic components are measured on a regular basis. The results of the validation is summarized in statistical way in Table 3.1. The statistical parameters represent averages over all stations. Hence, they give an overview but a lot of detail is missed. For this reason we have included the scatter plots for visual inspection as well (figure 3.3). Note that emissions used are the same in both TM4 and LOTOS-EUROS, and all comparisons are done with concentrations near the surface.

On average, TM4 and LOTOS-EUROS (LE) show a bias for sulphate. TM4 overestimates the average concentration by 20-25%, whereas LOTOS-EUROS underestimates by the same percentage. In Figure 3.4 we compare the measured and modelled sulphate concentrations as function of location in Europe. In general the models are able to reproduce the spatial variability of the time-averaged concentrations at the stations, and thus the general features of the aerosol distribution over Europe. Some regional differentiation can be made from this analysis. For instance, LOTOS-EUROS underestimates sulphate at German locations. Both models underestimate sulphate in Spain. The reason for this is not known. However, the corresponding ammonium measurements indicate that sulphate is not present as ammonium sulphate, the modelled quantity, which makes a proper comparison of observations and model values difficult.

For SO2 the comparison is less favourable. TM4 overestimates the sulphur dioxide concentrations severely, whereas LOTOS-EUROS overestimates concentrations by 50%. Significantly higher emissions of SO2 are used by TM4 which explains at least partly the differences between both models (see also section 3.6). In LOTOS-EUROS the conversion of SO2 to sulphate was diagnosed to be too slow (Schaap et al., 2005b), which may also be the case for TM4. The long atmospheric life time of sulphur dioxide in the models may also be caused by underestimating wet and dry deposition. The overestimation of surface SO2 concentrations may also be caused by underestimated vertical transport yielding too high concentrations near the surface. This is however not confirmed by other chemical species.

The average correlation coefficient is very similar in both models. LOTOS-EUROS generally shows lower absolute residues and RMSEs, although the average concentrations in LOTOS-EUROS are not always closer to the measured values compared to TM4. Further, the modeled variability in LOTOS-EUROS is closer to the measurements (expressed by the sigma ratio) except for total ammonium.

Although the number of stations is too low to draw firm conclusions, we can conclude that both models show the largest uncertainty for nitrate. This is explained by the complex formation process of nitrate and its dependence on ammonia and sulphate.
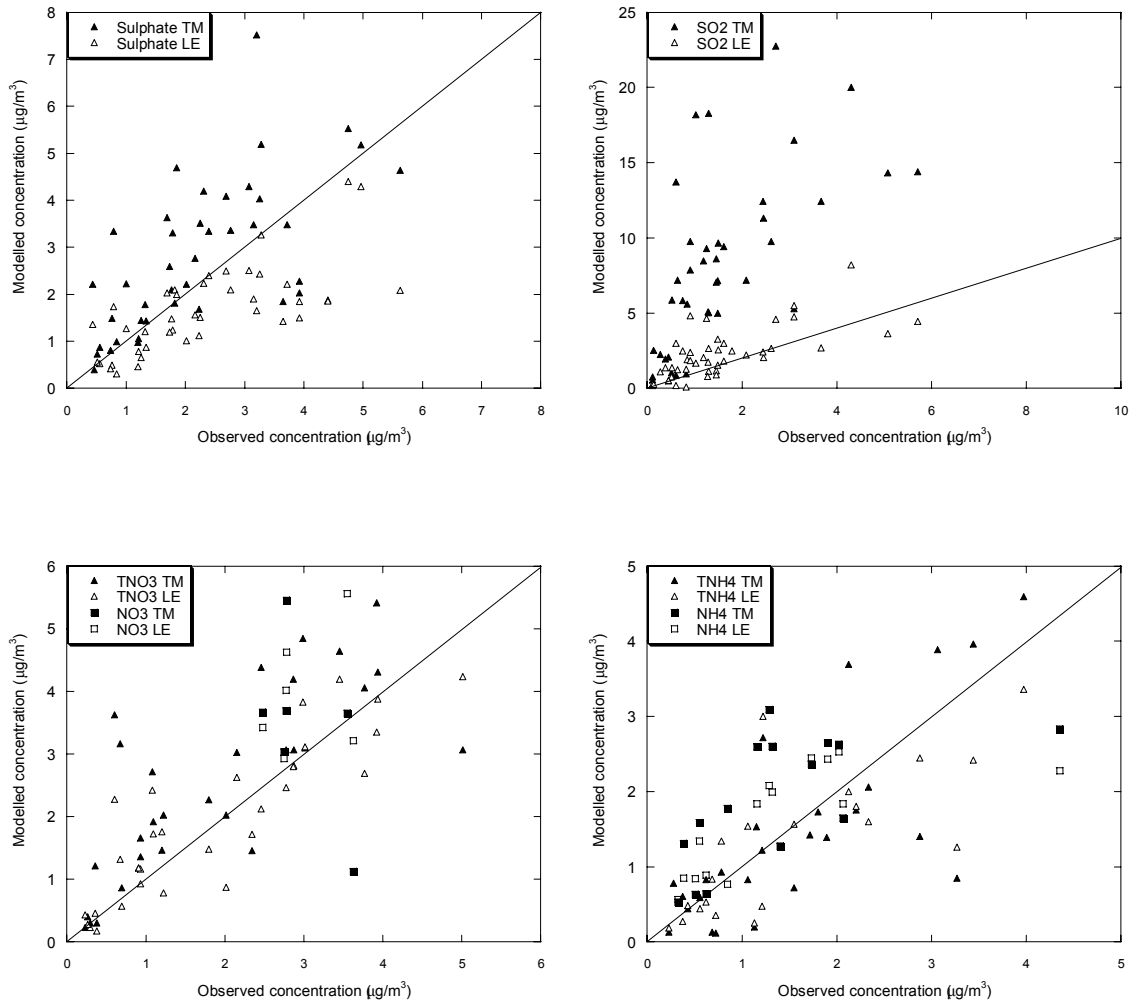
Figure 3.3. Comparison between measured and modelled annual average concentrations for SO2, SO4, NO3, NH4, TNO3 (=NO3+HNO3) and TNH4 (=NH4+NH3)

34
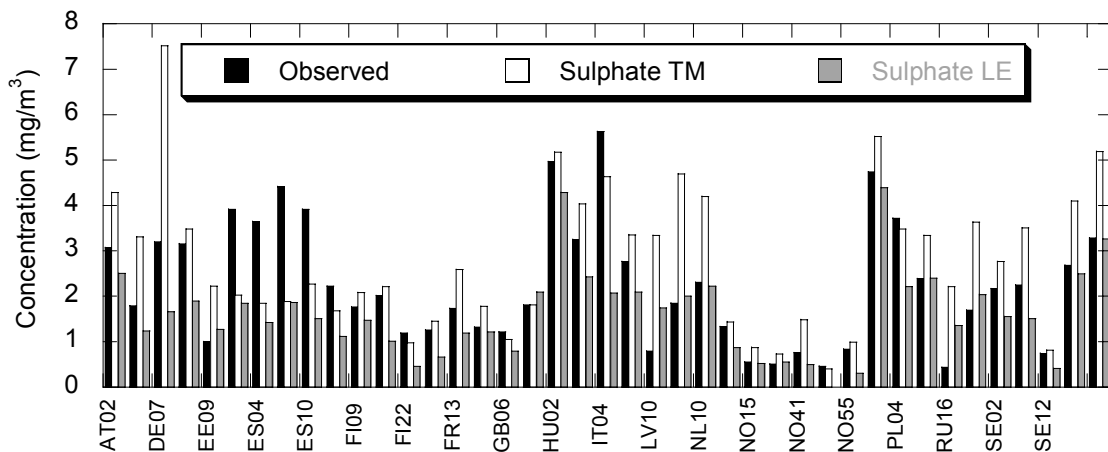
Figure 3.4 Observed and modeled sulphate concentrations near the surface, at 20 background EMEP locations in Europe (average over the year 2000). Note that station codes on the x-axis are in alphabetical order, and that only every second station is labeled. All stations are specified in table 3.2

	observed mean	modelled mean	residue	RMSE	correlation	sigma ratio	Spatial correlation
SO4 (41)							
TM4	2.26	2.79	1.53	2.13	0.52	1.30	0.62
LE	2.21	1.61	1.18	1.68	0.54	0.84	0.72
NO3(6)							
TM4	3.00	3.44	2.54	3.77	0.45	1.65	-0.56
LE	2.98	3.96	2.25	3.05	0.45	1.36	0.34
NH4(15)							
TM4	1.37	1.88	1.09	1.58	0.50	1.43	0.62
LE	1.36	1.60	0.87	1.22	0.54	1.07	0.71
SO2(45)							
TM4	1.57	9.03	7.57	8.92	0.38	4.26	0.46
LE	1.54	2.22	1.39	1.91	0.42	1.05	0.68
TNO3(31)							
TM4	2.07	2.58	1.53	2.37	0.40	1.40	0.81
LE	2.09	2.08	1.29	2.01	0.41	1.01	0.89
TNH4(26)							
TM4	1.50	1.45	0.92	1.34	0.45	0.88	0.76
LE	1.54	1.31	0.91	1.33	0.40	0.63	0.76

Table 3.1Statistics of model results and observations. Notes: The definition of the statistical quantities is given in section 2.5. The small difference of observed mean values for TM4 and LE are caused by the fact that 31 December is left out for LE. Between brackets are the number of stations.

```
Code Station name        Country         (Lat,lon,altitude)
AT02 Illmitz             Austria         (47°46'N, 16°46'E, 117)
CH02 Payerne             Switserland     (46°49'N,  6°57'E, 510)
DE07 Neuglobsow          Germany         (53°10'N, 13°2 'E, 62)
DE09 Zingst              Germany         (54°26'N, 12°44'E, 1)
EE09 Lahema              Estinia         (59°30'N, 25°54'E, 32)
ES03 Roquetas            Espania         (40°49'N,  0°29'E, 44)
ES04 Logroño             Espania         (42°27'N, 02°21'W, 370)
ES08 Niembro             Espania         (43°26'N,  4°51'W, 134)
ES10 Cabo de Creus       Spain           (42°19'N, 03°19'W, 23)
ES11 Barcarrola          Espania         (38°28'N,  6°55'W, 393)
FI09 Utö                 Finland         (59°47'N, 21°23'E, 7)
FI17 Virolahti II        Finland         (60°31'N, 27°41'E, 4)
FI22 Oulanka             Finland         (66°19'N, 29°24'E, 310)
FI37 Ahtari II           Finland         (62°35'N, 24°11'E, 180)
FR13 Peyrusse Vieille    France          (43°37'N, 00°11'E, 236)
GB02 Eskdalemuir         United Kingdom  (55°18'N, 03°12'W, 243)
GB06 Lough Navar         United Kingdom  (54°26'N,  7°54'W, 126)
GB14 High Muffles        United Kingdom  (54°20'N,  0°48'W, 267)
HU02 K-puszta            Hungary         (46°58'N, 19°35'E, 125)
IT01 Montelibretti       Italy           (42° 6'N, 12°38'E, 48)
IT04 Ispra               Italy           (45°48'N,  8°38'E, 209)
LT15 Preila              Lithouania      (55°21'N, 21° 4'E, 5)
LV10 Rucava              Latvia          (56°13'N, 21°13'E, 18)
NL09 Kollumerwaard       The Netherlands (53°20'N,  6°16'E, 1)
NL10 Vreedepeel          The Netherlands (51°32'N,  5°51'E, 5)
NO01 Birkenes            Norway          (58°23'N,  8°15'E, 190)
NO15 Tustervatn          Norway          (65°50'N, 13°55'E, 439)
NO39 Kårvatn             Norway          (62°47'N,  8°53'E, 210)
NO41 Osen                Norway          (61°15'N, 11°47'E, 440)
NO42 Spitsbergen         Norway          (78°54'N, 11°53'E, 474)
NO55 Karasjok            Norway          (69°28'N, 25°13'E, 333)
PL02 Jarczew             Poland          (51°49'N, 21°59'E, 180)
PLO4 Leba                Poland          (54°45'N, 17°32'E, 2)
PL05 Diabla Gora         Poland          (54° 9'N, 22° 4'E, 157)
RU16 Shepeljovo          Russia          (59°58'N, 29°07'E, 4)
RU18 Danki               Russia          (54°54'N, 37°48'E, 150)
SE02 Rörvik              Sweden          (57°25'N, 11°56'E, 10)
SE11 Vavihill            Sweden          (56° 1'N, 13° 9'E, 175)
SE12 Aspvreten           Sweden          (58°48'N, 17°23'E, 20)
SI08 Iskrba              Slovenia        (45°34'N, 14°52'E, 520)
SK06 Starina             Slowakia        (49° 3'N, 22°16'E, 345)
```

Table 3.2 EMEP stations used for the model evaluation

3.4 RESULTS OF AEROSOL DATA ASSIMILATION IN THE GLOBAL MODEL TM4

The TM4 model is used to assimilate ATSR2 optical depths observed over Europe in 2000 (section 3.4.2) and over the Indian Ocean during the INDOEX measurement campaign in 1999 (section 3.4.3). In the next section we first derived expressions that are used for the observation and model error needed by the optimal interpolation assimilation scheme in TM.

3.4.1 Estimation of errors
In the first phase of ARIA it was simply assumed that the observational error and model error were the same and that the observational errors were uncorrelated in space and time. In ARIA-2 we derived expressions for the model and observation errors based independent observations.

Estimation of the observational error

The error in ATSR-2 retrievals is estimated from a comparison with independent aerosol optical depth observations that are made available by AERONET (AErosol RObotic NETwork, Holben et al., 1998). For this purpose the AERONET aerosol optical depth (AOD) at 550 nm is estimated from the AOD at measured wavelengths (440, 670, 870 and 1020 nm) using the provided Ångstrom exponent that is valid between 440 and 670 nm (or, when not available, the nearest two wavelengths). For the year 2000, all simultaneous ATSR-2 retrievals and AERONET observations of AOD are compared for the months March, May, and August. We use the mean aerosol optical depth of all individual ATSR-2 retrievals within an area of 0.1°(0.1° surrounding an AERONET site and we average the AERONET AOD from half an hour before to half an hour after the satellite overpass. This yields 46 simultaneous observations in the selected period. The average aerosol optical depth for this data set is 0.21 both for the AERONET and ATSR-2. Comparing the simultaneous observations and retrievals one-by-one we find for the variance of the distribution around the mean 0.025 ((= 0.16). Since the accuracy of the AERONET measurements is estimated to be between 0.01 and 0.015 (Eck et al., 1999), we assumed that the variance is caused by uncertainties in the retrievals only. By using 0.025 for the observational error variance, it is implicitly assumed that the retrieval errors are fully correlated within the area of the super observation.

Estimation of the TM4 model error

We estimate the uncertainty in the modeled aerosol optical depth from the comparison with AERONET AOD observations. This comparison is not straightforward since the AERONET point observation is not necessarily representative for the area covered by a model grid cell. The same problem is found when super-observations are compared to point observations. Assuming that the representation error of AERONET is equal for both super-observation and model result of the grid cell covering the same area, we can use the ATSR-2 data to estimate the representation error of the point observation and use this information in the error estimation of modeled AOD.

To estimate the representation error we first select the super-observation covering each simultaneous high-resolution ATSR-2 and AERONET observation pair. The difference between individual ATSR-2 and AERONET AOD is used 'correct' the corresponding super-observation, implicitly assuming that the same difference is found in all ATSR-2 pixels within the supper-observation. (In other words: it is assumed that the errors in individual high-resolution ATSR-2 retrievals are highly correlated within the area of the super-observation.)

The 'corrected' super-observations are subsequently compared to the AERONET optical depths. The result is given in figure 3.5, clearly showing that the ATSR-2 super-observations overestimate the AOD at low AERONET values and that the AOD is underestimated at high AERONET values. The explanation for this result is that the spatial averaging reduces extreme values of the point observations. The standard deviation around the mean optical depth is 0.12 for all individual high-resolution ATSR-2 observations, and only 0.089 for the super-observations, confirming this leveling down. Therefore we argue that the optical depth dependent difference between super-observation and AERONET is caused by a lack of representation. The representation error involved in the AERONET observations is given by:

(repre, AERONET = - 0.07 + 0.6(AOD(AERONET).

Finally we estimate the model error by comparing modeled and observed AERONET aerosol optical depths. By substracting the representation error from the AOD differences that are found, we get an estimation of the error in the modelled AOD, which can be represented by (TM4 = 0.07 + 0.2(AOD(TM4).
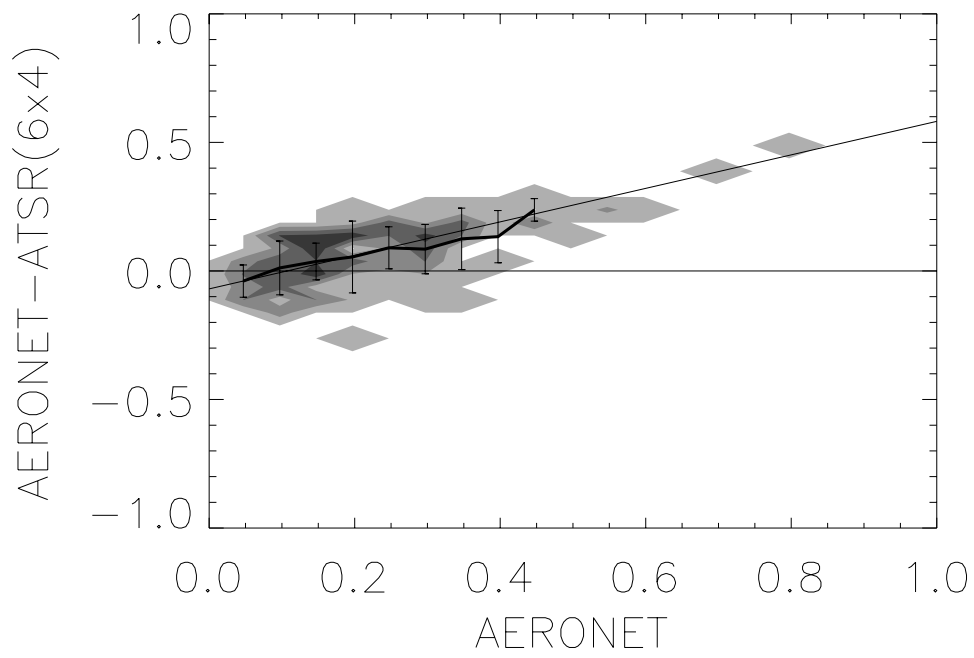
Figure 3.5. Difference between AERONET and corrected ATSR-2 super-observation of aerosol optical depth, as function of the AERONET AOD.

3.4.2   Aerosol optical depth over Europe

The TM4 model can provide an estimate of the aerosol optical depth on a global scale. Except for Saharan dust aerosols, which are episodically important only over the Mediterranean, all relevant aerosol species that contribute to the aerosol optical depth over Europe are included. Here, we select a large area including Europe (30W-48E; 30N-78N) to evaluate the models' capability to predict the aerosol optical depth.

The spatial distribution of the yearly average AOD for the year 2000 is shown in Fig 3.6. What catches the eye is the area with high aerosol optical depths over the eastern part of the domain. These yearly average high values are predominantly caused by high values in the winter period that last until March (Fig 3.6b). A possible explanation may be that aerosols are built up in a stable winter boundary layer from which escape is hampered due to the blocking inversion. This also happens over other parts of Europe but there depression activity more often washes out the aerosol. In spring and summer the highest aerosol optical depths occur over central Europe (Fig 3.6c and 3.6d), but these maxima are less pronounced.
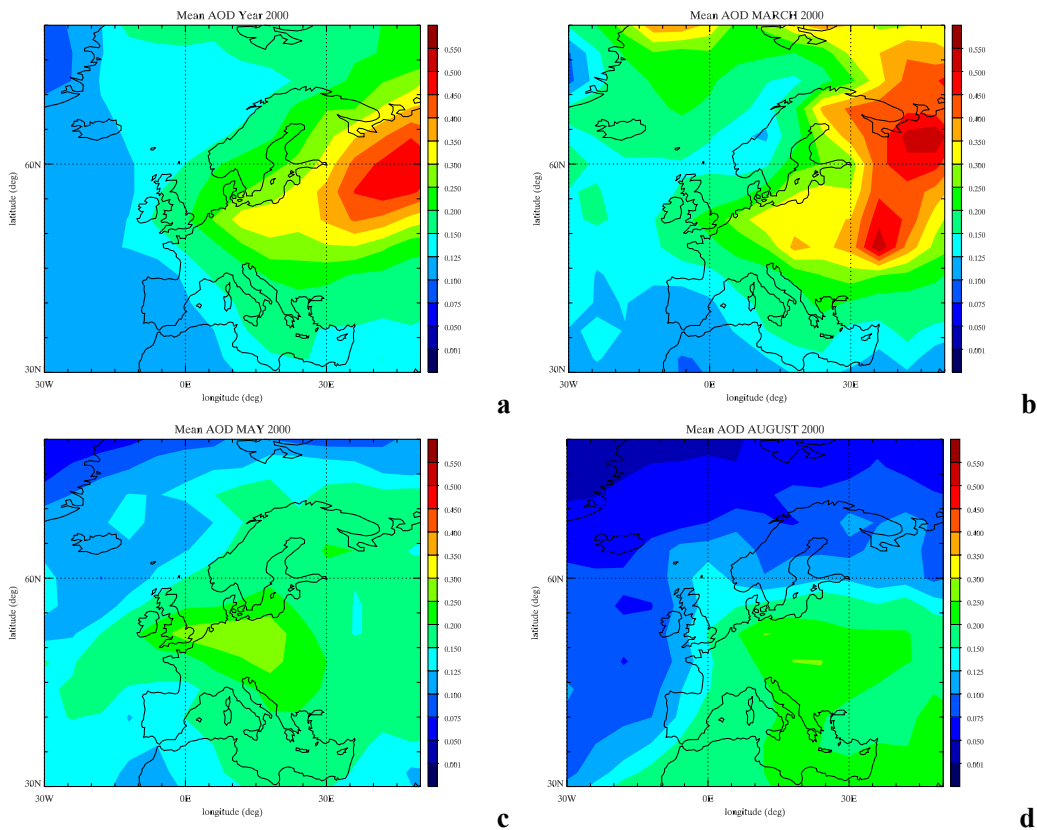
Fig 3.6*. Spatial distribution of the aerosol optical depth. (a) Yearly mean. (b) March. (c) May. (d) August.*

The partitioning of the aerosol optical depth over the various species is shown in Fig 3.7. For the yearly average, we find that sea salt and secondary inorganic aerosols are almost equally important over the Atlantic Ocean. The aerosol optical depth over the Norwegian Sea and the northern parts of Russia is dominated by secondary inorganic aerosols. The internal mixtures of carbonaceous and secondary inorganic aerosols are the main contributors to the aerosol optical depth over Central and Central-East Europe. The fractional contributions of the various species for individual months are not shown here but are briefly described below. For the month of March they do not substantially differ from the yearly average. In the month May, sea salt becomes less important even over the ocean, and the hydrophilic carbons become the dominant contributor to the aerosol optical depth except for the Iberian Peninsula and northern Africa where secondary inorganic aerosols contribute most to the AOD. The patterns for the month of August strongly resemble those of May.

The maximum in the contribution of secondary inorganic aerosols to the aerosol optical depth forms a bridge between two regions, one dominated by sea salt over the ocean and the other dominated by hydrophilic carbonaceous aerosols over land. For all months the contribution to the AOD of hydrophobic BC and OC is small everywhere except for central Europe where the contribution more than 5% and locally close to 20%.
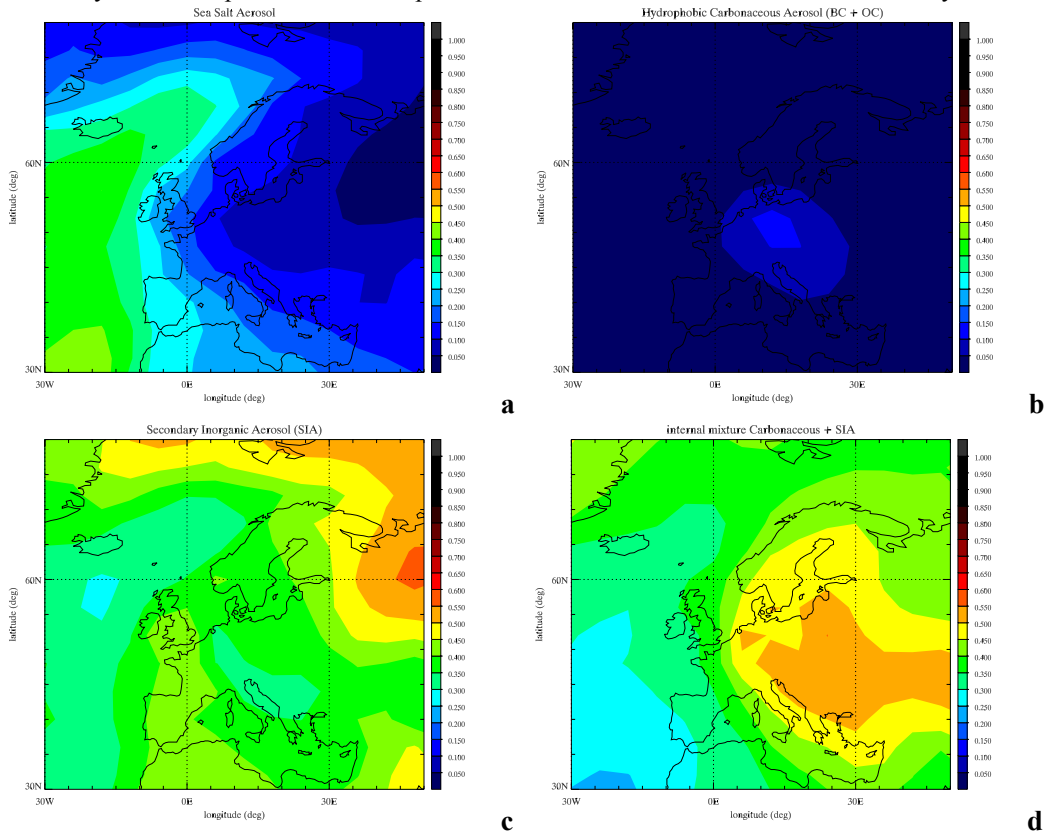
Figure 3.7. Spatial distribution of the fractional contribution of the various aerosol species to the total aerosol optical depth. (a) Sea salt (b) Hydrophobic black and organic carbon. (c) Secondary Inorganic aerosol salts. (d) Hydrophilic black and organic carbon.

In Fig. 3.8, the fractional contributions of the various species to the aerosol optical depth are given per month and spatially integrated over the selected domain. The contribution of hydrophobic BC and OC is smaller than 3% in all months, with the maximum contribution in (late) summer. The hydrophilic carbonaceous aerosols are the dominant contributors to the optical depth for a large part of the year. Only in winter the pure secondary inorganic aerosols dominate. The difference between the two contributors is largest in spring and summer. The occurrence of this yearly cycle cannot be explained by the emissions of aerosols and their precursor gases, but is most likely caused by the aerosol-gas partitioning of the secondary inorganic aerosols. In winter, lower temperatures prevail that cause a quicker condensation of the SIA precursor gases. This means that in winter compared to carbonaceous material relatively more SIA is available. In our model secondary inorganic aerosols are used to form the internal mixture, what is 'left over' is pure SIA. Note that only the contribution of this externally mixed SIA to the total optical depth is represented in figure 3.8. This explains the occurrence of this yearly cycle in the fractional contributions of the SIA and hydrophilic carbonaceous species, and the cycle might be expected to be independent of the absolute value of the aerosol optical depth. The sea salt contribution varies between a minimum value of about 6% in August to a maximum of 18% in March. The temporal variability in sea salt load and thus sea salt aerosol optical depth is source driven, whereas for the other species the load is mainly determined by the sinks. The peak in sea salt aerosol optical depth that occurs in March in 2000, as well as its maximum fractional contribution, can therefore in other years occur in other winter months, as the occurrence of storms shows substantial interannual variability. The maximum aerosol optical depths of the other species are caused by long fair

weather periods, which may occur in any season, although some high pressure systems have a preference, e.g. the Siberian winter High.
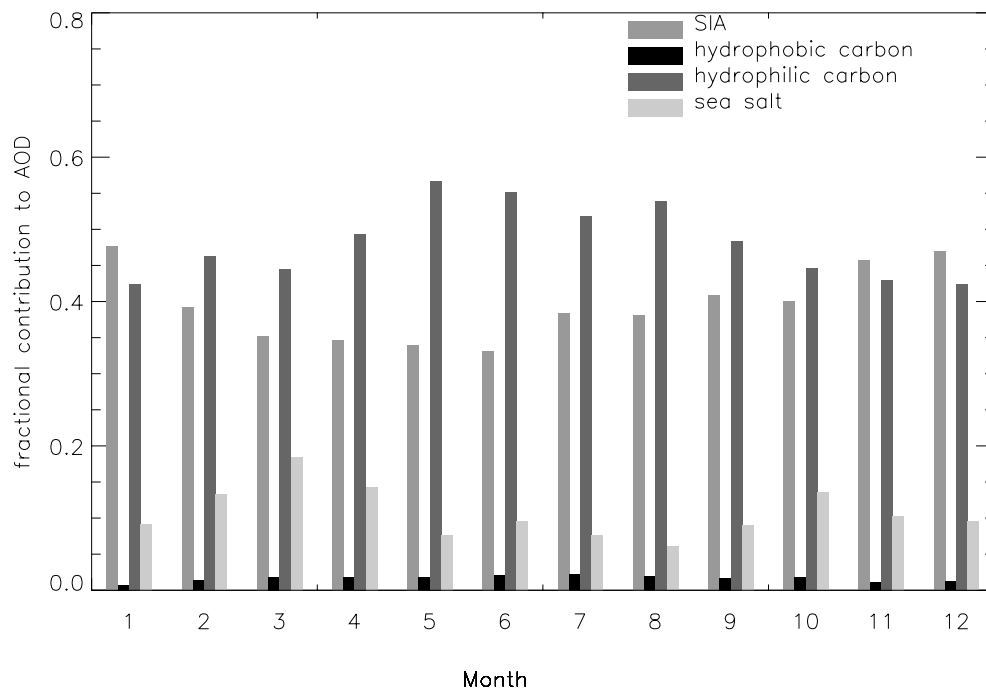
Figure 3.8 Yearly variation of the fractional contribution of the various aerosol species to the total aerosol optical depth.

Comparison to AERONET observations

We compare our modeled aerosol optical depths to ground based aerosol optical depth observations that are made available by AERONET (AErosol RObotic NETwork, Holben et al., 1998). For this purpose the AERONET aerosol optical depth at 550 nm is estimated from the AOD at measured wavelengths (440, 670, 870 and 1020 nm) using the provided Ångstrom exponent that is valid for the closest two enveloping wavelengths. For the year 2000, all simultaneous modeled aerosol optical depths and a selected set of AERONET observations of aerosol optical depth are compared. The selected stations are listed in Table 3.3.
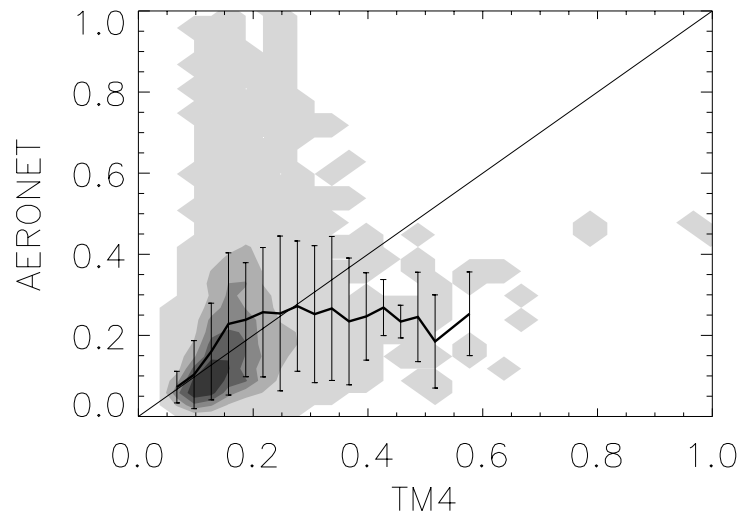
a
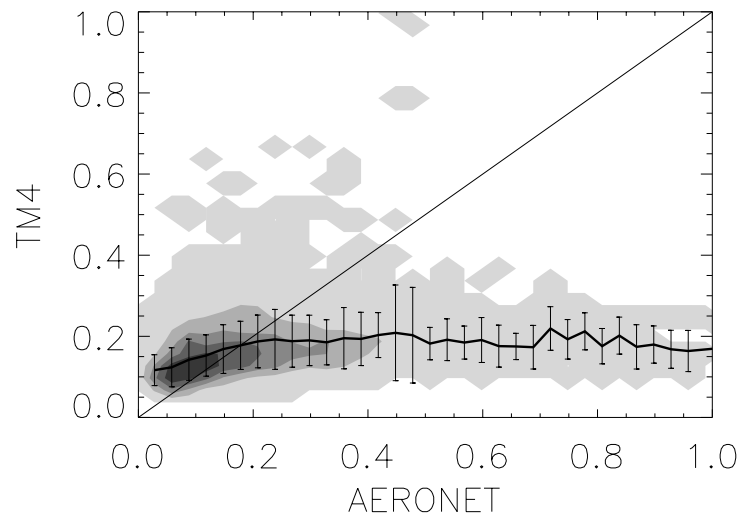
b

Figure 3.9. Density plots of simultaneous modeled (TM4) and observed (AERONET) aerosol optical depth. The space is divided in pixels of 0.03 by 0.03 in AOD, the darkest smoothed area contains the pixels with the highest data density and contains 20% of all TM4-AERONET pairs. From dark to light, the other colored areas contain 40, 60, 80, and 100 % of the data pairs, respectively. (a) The heavy black line indicates the average AERONET AOD for the TM4 AOD specified by the x-axis, the bars indicate the standard deviations of the distribution of AERONET observations around the mean. The thin straight black line indicates perfect agreement. (b) as in (a) but the roles of observations and modeled values have been swapped.

For the year 2000, the average modeled aerosol optical depth at all stations is 0.19 and the standard deviation of the distribution, ($\sigma_{dis.}$=0.13. If only the modeled values are used when AERONET observations are available, the average simulated aerosol optical depth reduces to 0.17 ($\sigma_{dis.}$=0.06); to be compared to the AERONET average AOD of 0.20 ($\sigma_{dis.}$=0.15) (see also table 3.4). The model thus clearly underestimates the aerosol optical depth. When different periods are selected, this underestimation is found to be a persistent. To explain it, we individually compare all simultaneous modeled and observed aerosol optical depths. In Fig. 3.9, the AERONET AOD values together with the simultaneous modeled AOD values are given as a function of the modeled values. From this figure we conclude that the persistent underestimation of the mean AOD is not caused by a systematic underestimation of all modeled values. Rather, high modeled AOD values are not supported by high observed AOD values and the other way around, and at the same time high observed AOD values are not accompanied by high modeled values. The same figure but with the role of modeled and measured aerosol optical depths interchanged (Fig 3.9b), more clearly characterizes the reason for the underestimation of the modeled aerosol optical depths. As the average modeled aerosol optical depth is lower than the observed AOD, high observed aerosol optical depths that are not accompanied by modeled high values is decisive for the lower modeled mean AOD.

Station	Latitude °N	Longitude °E
Avignon	43.9	4.9
Creteil	48.8	2.4
Gotland	57.9	19.0
Hamburg	53.6	10.0
Helgoland	54.2	7.9
Ispra	45.8	8.6
Lampedusa	35.5	12.6
Lille	50.6	3.1
Modena	44.6	10.9
Moldova	47.0	28.8
Palaiseau	48.7	2.2
Paris	48.9	2.3
Toulouse	43.6	1.4
Venise	45.3	12.5

Table 3.3. European AERONET stations selected for the comparison to TM4 model results.

From figures 3.9, it might be anticipated that the correlation between observed and modeled aerosol optical depths is not very high. Indeed, the correlation for the individual stations is sometimes acceptable, but mostly weak and sometimes there seems to be no correlation at all (Table 3.5).

	Period	Mean AOD	$\sigma_{dis.}$	N
TM4	2000	0.165	0.065	7505
	MMA	0.170	0.058	2726
	March	0.162	0.051	501
	May	0.182	0.070	912
	August	0.163	0.048	1313
AERONET	2000	0.199	0.154	7505
	MMA	0.216	0.141	2726
	March	0.211	0.160	501
	May	0.211	0.146	912
	August	0.223	0.128	1313

Table 3.4. Average modeled (TM4) and measured (AERONET) aerosol optical depth for various temporal selections of the data. The standard deviation of the distribution (square root of the variance), (dis. and the number of AOD values that contributed to the calculations N are also provided. The TM4 data shown only contains the modeled values when AERONET observations are available.

Station	YEAR 2000		MMA		March		May		August	
	Cor.	N	Cor.	N	Cor.	N	Cor.	N	Cor.	N
Avignon	0.47	1260	0.46	346	0.40	58	0.30	142	0.60	146
Creteil	0.40	349	0.68	136		0		0	0.68	136
Gotland	0.45	161	0.54	88	0.73	14	0.58	74		0
Hamburg	0.34	282	0.29	81		0		0	0.29	81
Helgoland	0.44	163	0.54	104		0		0	0.54	104
Ispra	0.47	1117	0.42	386	0.64	123	0.53	94	0.04	169
Lampedusa	0.38	546	0.16	205		0		0	0.16	205
Lille	0.31	418	0.24	124	0.65	6	-0.18	27	0.57	91
Modena	0.49	35	0.49	35		0	0.49	35		0
Moldova	0.40	696	0.58	304	0.76	33	0.53	271		0
Palaiseau	0.42	555	0.52	252	-0.07	51	0.58	69	0.63	132
Paris	0.45	23	-1.00	2		0		0	-1.00	2
Toulouse	0.31	253	0.44	93	0.44	93		0		0
Venise	0.20	1647	0.07	570	0.14	123	0.08	200	-0.17	247

Table 3.5. Correlation between time series of modeled (TM4) and measured (AERONET) aerosol optical depth. MMA stands for March + May + August, Cor. Stands for linear Pearson correlation, N is the number of pairs used for the comparison.

Sensitivity study - Water vapor redistribution
The relative humidity used in this study directly comes from the ECMWF meteorological fields. The relative humidity in every TM4 grid cell is therefore constant throughout the cell. This is not realistic. Most grid cells contain both cloudy and cloud free fractions. The cloudy part of the grid cell should be saturated. In a sensitivity run we have redistributed the water vapor in our model cells such that the cloudy fraction has a relative humidity of 100%. The remaining water vapor is uniformly distributed over the rest of the grid cell but we tentatively assume that the relative humidity can not drop below 30% by this redistribution. Effectively this water vapor redistribution or relative humidity scaling lowers the relative humidity of the cloud free fraction for which the aerosol optical depth is calculated. This reduction in relative humidity reduces the monthly mean aerosol optical thickness for the whole European domain for March 2000 from 0.21 to 0.18. We find that the effect of the reduction of relative humidity is especially strong over the oceans. Maxima in aerosol optical depth dominated by sea salt, that are related to strong depression activity, are effectively lowered and are sometimes damped out completely. The largest aerosol optical depths, which are related to extreme water uptake and not necessarily to high aerosol mass loads, are also strongly affected. The reason for this is that the extinction cross section per unit mass increases rapidly with increasing relative humidity. The aerosol optical depth in large fair-weather regions associated with high pressure systems, is not affected much. If TM4 aerosol optical thicknesses are selected with simultaneous AERONET observations the monthly mean aerosol optical thickness is also reduced but the reduction is modest and does not show up in de rounded value that remains 0.16. The correlation between the time series of AERONET observations and modeled aerosol optical depth does not change significantly.

3.4.3   Aerosol optical depth over the INDOEX region

In the first phase of ARIA the Indian Ocean Experiment (INDOEX) was selected to test the assimilation system. INDOEX (Ramanathan et al, 2002) was undertaken in February and March 1999 with the objective to determine the pollution outflow from India over the Indian Ocean, and to assess its radiative impact. The chemical and optical properties of the aerosols were studied by performing a large number of in-situ observations both on the ground and during aircraft flights. In addition satellite and ground-based remote sensing instruments made nearly continuous measurements. The vast amount of data that was collected during the intensive field phase contains valuable information that can be used to evaluate all parts of the assimilation system: the retrieval, the chemistry/transport model and the assimilation procedure.

The TM4 model was run for one month, February 1999, with ECMWF meteorological analyses. All model

settings and assimilation parameters were the same as what is used for Europe (section 3.4.2).

Figure 3.10 and 3.11 give the optical depth distribution of the model without and without assimilation, the ATSR2 super observations and the change of AOD during the time step in which the data are assimilated. The impact of the observational data is an increase of AOD. The 'footprint' of the observations for these days can be seen in the AOD in panel d in both figures, and is in most grid cells positive.

Figure 3.12 shows surface observations, ATSR observations and the TM4 model with and without assimilation for the Maldives in the Indian Ocean. It is clear that the optical depths from the free running model are too low, which is partly compensated by the assimilation of observations. Nevertheless, also the ATSR data are low compared to the sunphotometer data in Kaashidhoo and Male. The main sources of aerosol are located on the Indian mainland, several hundred kilometers upwind from the measurement site. However, the instantaneous surface observations still show significant variations which may be caused by sea salt emission events or variations in relative humidity (e.g. by fluctuating boundary layer heights).

The contribution of the different aerosol types that make up the optical depth is depicted in figure 3.13. Sea salt is the larges contributor, but carbon and sulphate aerosols, transported mainly from India, also contribute significantly. The composition of the aerosol mixture seems fairly constant in time.

At certain times, when observations are available near the measurement site, the assimilation causes sudden increases of optical depths, proportional to the original contribution of each species. Since the mixture is of a relatively constant composition, it is difficult to derive from this figure which type of aerosol is causing the discrepancy between observation and model.
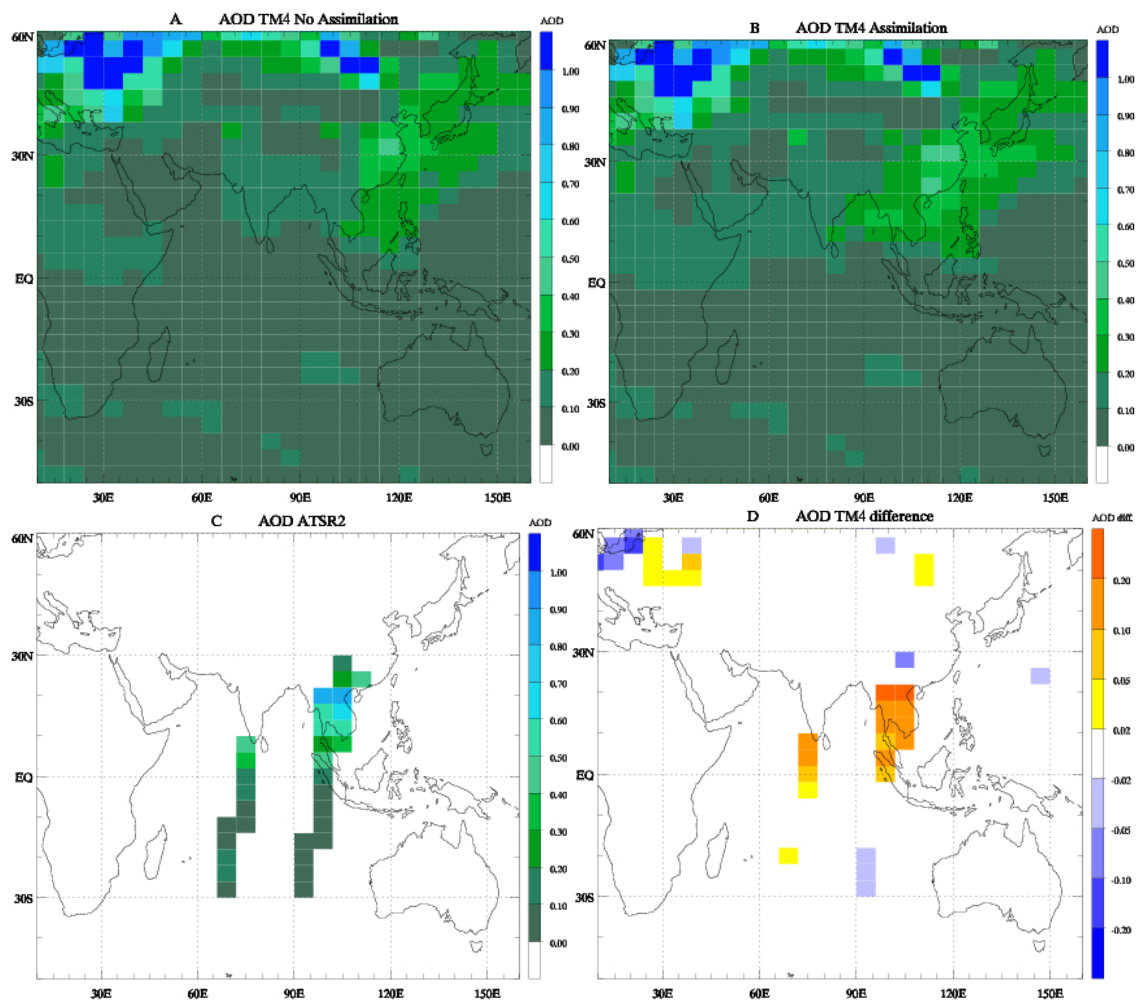
Figure 3.10 Aerosol optical depths over the INDOEX area: Model run without assimilation (A); model run with assimilation (B); and the AOD-change in one hour model integration (D) which includes the assimilation of the ATSR2 observations shown in (C).
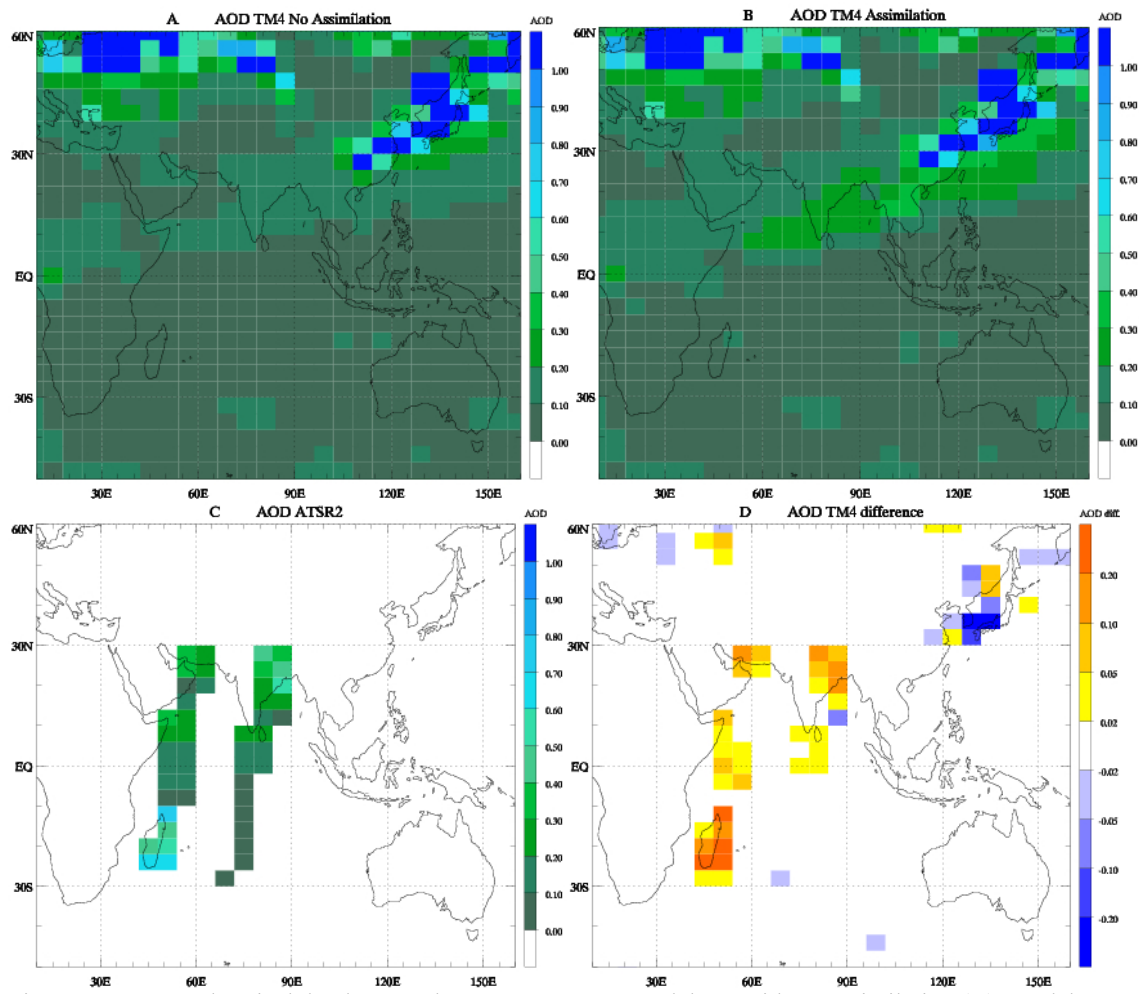
Figure 3.11 Aerosol optical depths over the INDOEX area: Model run without assimilation (A); model run with assimilation (B); and the AOD-change in one hour model integration (D) which includes the assimilation of the ATSR2 observations shown in (C).
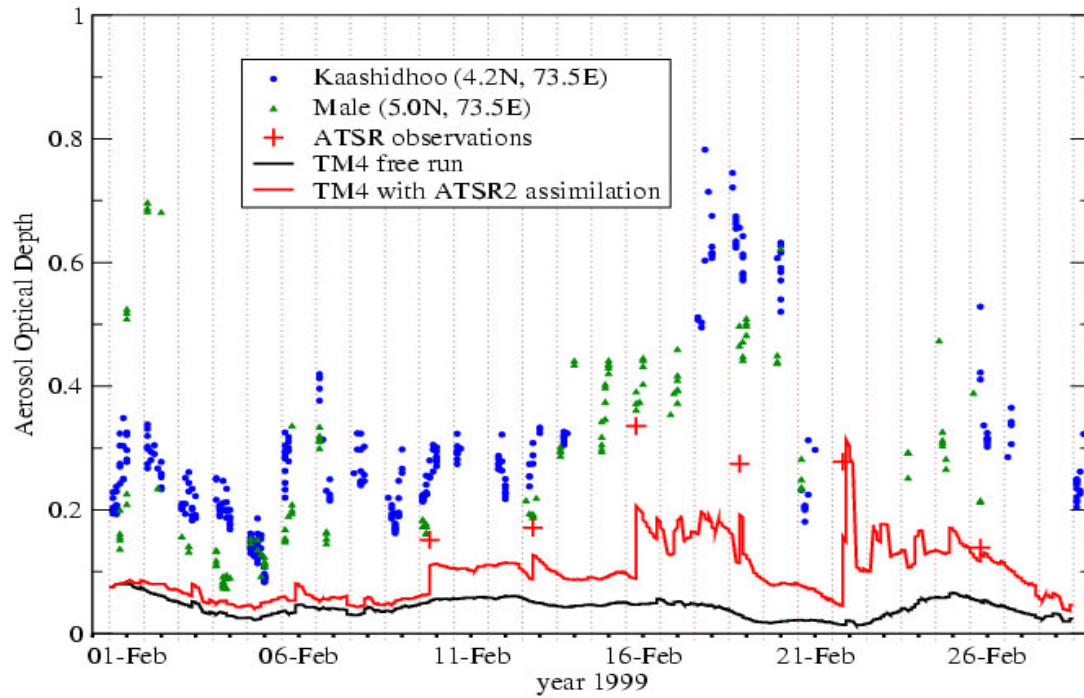
Figure 3.12 Time evolution of the aerosol optical depth observed at two surface stations on the Maldives (500nm), from the ATSR2 satellite instrument (555nm) and from the TM4 model (550nm) with and without assimilation. (Both surface stations are located in the same model grid cell.)
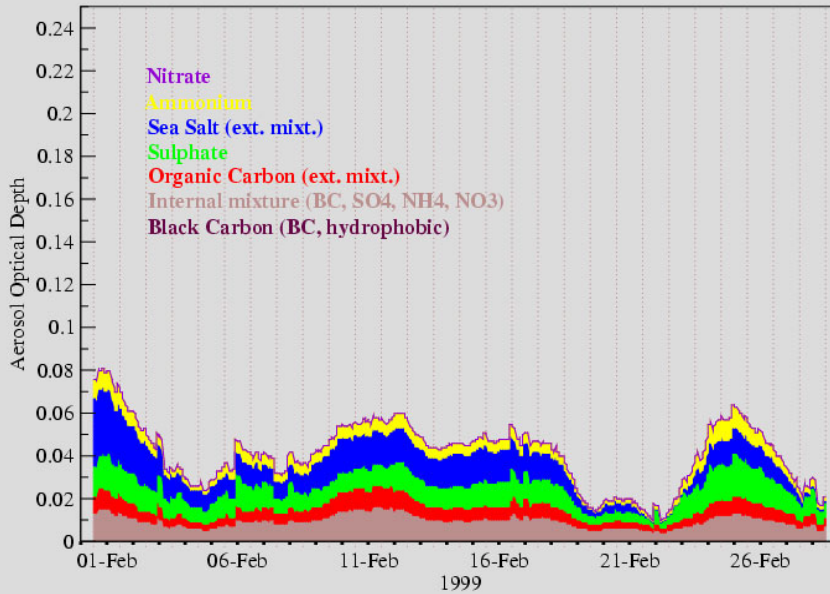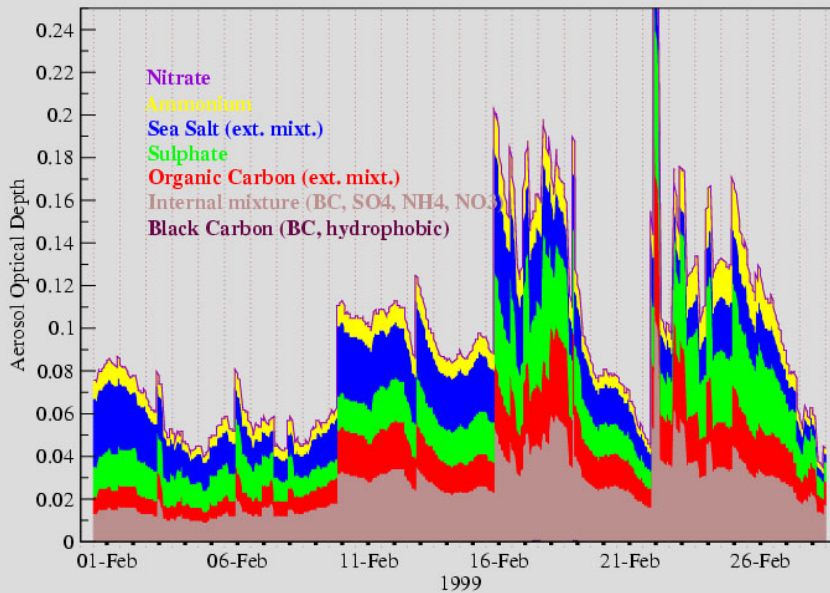
Figur 3.13 Contribution of different aerosol types to the total AOD in Male (Maldives) during INDOEX obtained from the TM4 model without assimilation.

3.5 RESULTS OF AEROSOL DATA ASSIMILATION IN THE REGIONAL MODEL LOTOS-EUROS

This section describes the results of the LOTOS-EUROS regional model. In section 3.5.1 the assimilation experiments are described. In section 3.5.2 the results over Europe are presented including validation with AERONET observations. PM2.5 and emission estimates over Europe are given in sections 3.5.3 and 3.5.4 respectively.

3.5.1   The ensemble Kalman filter

In this study we used an ensemble Kalman filter to assimilate the AOD retrievals within LOTOS-EUROS. The uncertainties involved with the modelled and retrieved AOD values determine the weights that are put on the measured and calculated values. With a kalman filter there is no need to specify the model uncertainties as they are determined by the range of modelled states of the ensemble members. Hence, the specification of the noise influences the weights and therewith results of the procedure. Here we only used ensemble of 15 ensemble members. Random noise was added to the emissions of NOx, SOx, VOC, NH3 and particles. The noise factors were kept constant between analyses. The satellite overpass takes place around noon every day. In the model the analysis is performed at 12:00 hours GMT and all ensemble members have disturbed but constant emissions for the 24 hours in between overpasses. At noon, the AOD is calculated for the grid cells for which observations are available and the state and ensemble members are updated in the analysis step.
We have performed assimilation simulations for two cases. In the first case we have calculated the mean and the standard deviation of the retrieved AOD for each grid cell of the model. The standard deviation was used to specify the uncertainty in the measurement (=the mean). The consequence was that the standard deviation ranges between about 20 and 80% of the mean. Hence, the retrievals are relatively uncertain. In the second case we have used a fixed small standard deviation (0.03) to mimic a high accurate in the measurements.

3.5.2   Aerosol optical depth over Europe

In the upper panel of Fig. 3.15 we show the retrieved AOD values for the 9th of May, 2000. There are two swaths over Europe, one over the north west of Europe and one over Russia. The swath over north western Europe shows large area of valid AOD data. On the other hand, the swath over Russia shows a strange pattern with generally low AOD, except for isolated cells. These cells are suspected to be influenced by cloud occurrence. The modelled AOD for the simulation without assimilation (left) and with assimilation (right) are shown in the middle panels. As shown above, the modelled AOD underestimates the retrieved values. Assimilation affects the calculated AOD in these regions with a continuous AOD fields. For the 9th the assimilation results in enhanced AOD over the Netherlands, Belgium and Germany. As shown in the lower panels of Fig 3.15 the absolute residue is lowered considerably in this area. In regions with no continuous observations the assimilation scheme is not able to lower the discrepancy between the model and observation. Both experiments give the same patterns.
In Figure 3.16a,b we show the assimilated AOD fields for the 23rd of May for both experiments. At this day high AOD values are retrieved over central Europe. Again, the model without assimilation underestimates the retrieved AOD hugely. Both assimilation experiments are able to reproduce the high values over Germany and Poland. Experiment 2 has the lowest error on the measurements and the model state is forced to be closer to the retrieved values than experiment 1. In Fig 3.17a we illustrate the whole fields before and after assimilation for the 23rd. The assimilation yields smooth fields without a marked signature of the satellite swath. Also, previous analyses influence the calculated AOD that enters an analysis step (Fig 3.17b)
In Figure 3.18a we summarize the influence of the assimilation for the whole period. In this figure the average retrieved AOD is compared to the modelled and assimilated ones. Hence, we present averages for the swaths of the satellite. Experiment 1 reduces the gap between the model and the retrieved values by about 40% on average. Experiment 2 is able to reduce the gap by about 70 % or even more. Visual inspection of the assimilated fields learned that the assimilation is not effective near the edge of the domain. We illustrate this for the 21st in Fig 3.19. The assimilation is successful over central Europe but over Scandinavia the assimilation scheme is not able to reduce the residues between model and retrieval. Hence, we also summarize the influence of the assimilation scheme for central Europe (the area bound by lon = -5° to 30°

and lat = 45° to 57°; Fig 3.18b). Over the central part of the domain experiment 2 shows a very promising performance with only a slight tendency to underestimate the retrieved AOD fields. Using uncertain AOD values (exp 1) also yields an improvement when focusing on this sub-domain.
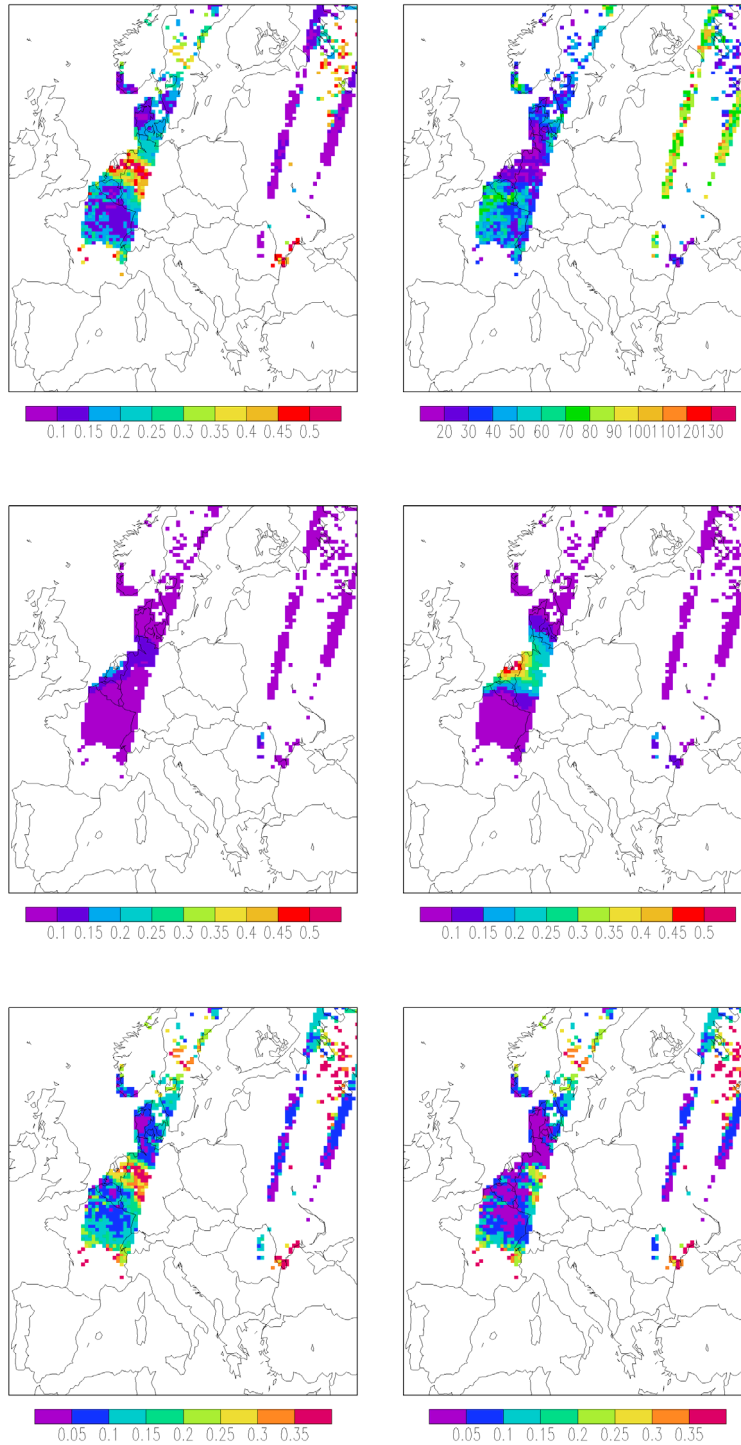
Figure 3.15 AOD assimilation results for May 9th, 2000. The upper left panel shows the retrieved AOD value. The corresponding relative standard deviation (%) is shown in the upper right panel. The middle left panel shows the modeled AOD values (without any assimilation) whereas the middle right panel shows the AOD in the assimilation experiment. The lower left and right panels show the residues for the model run and the assimlation experiment, respectively.
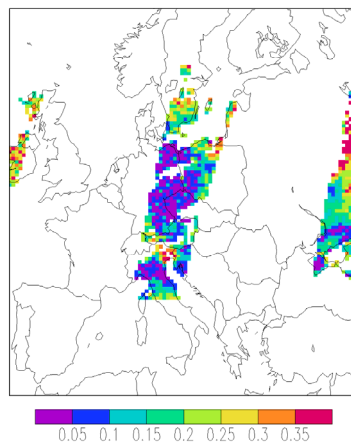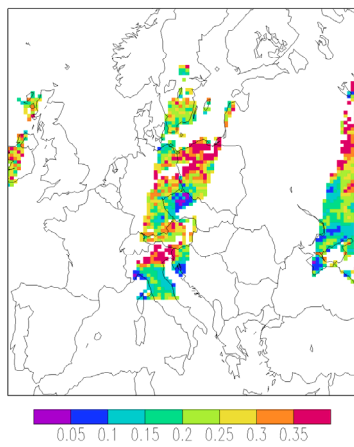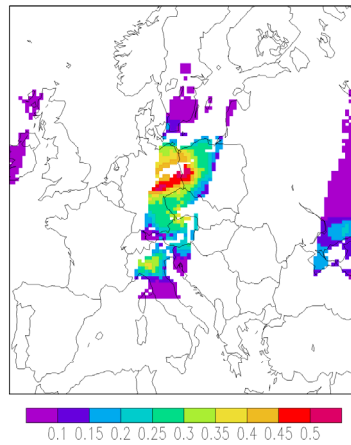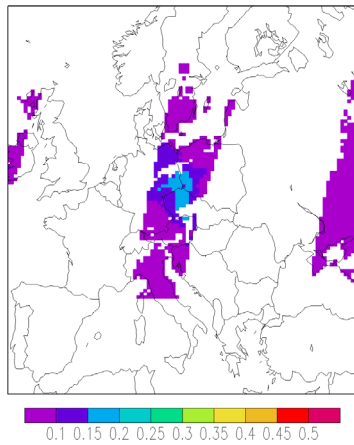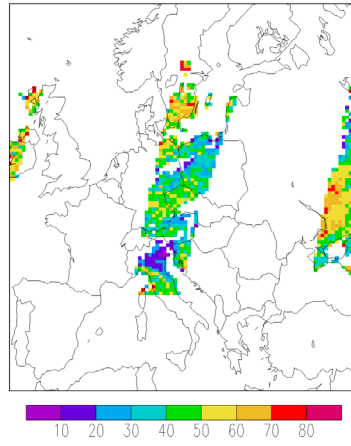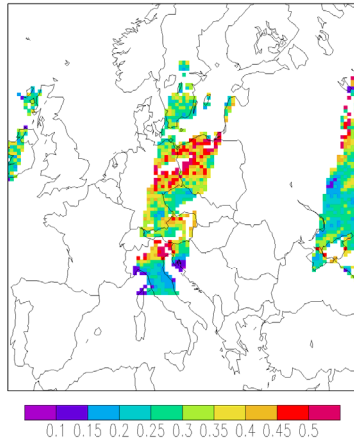
a

23 5 2000
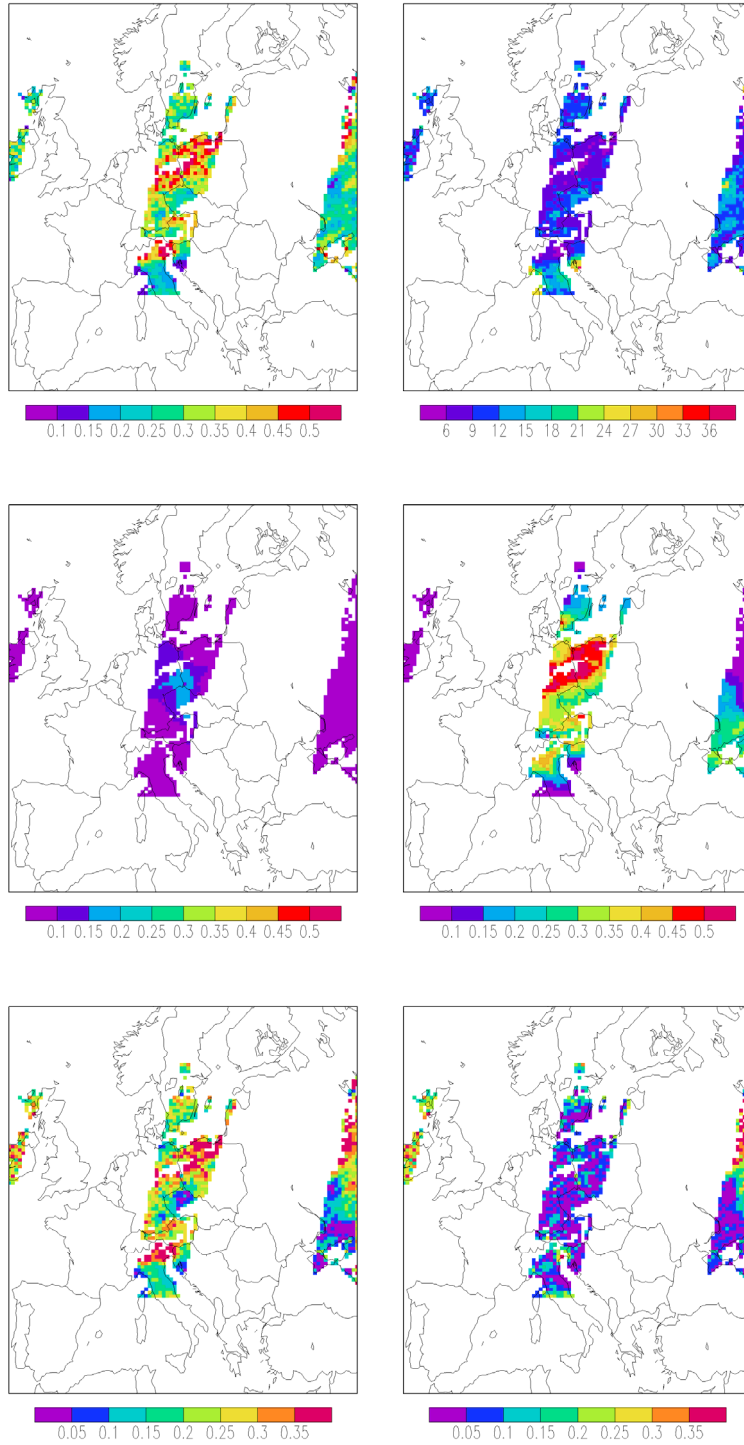
b

Figure 3.16a,b AOD assimilation results for May 23rd, 2000 for experiment 1 (a) and 2 (b). Panels defined as for Fig. 3.15.
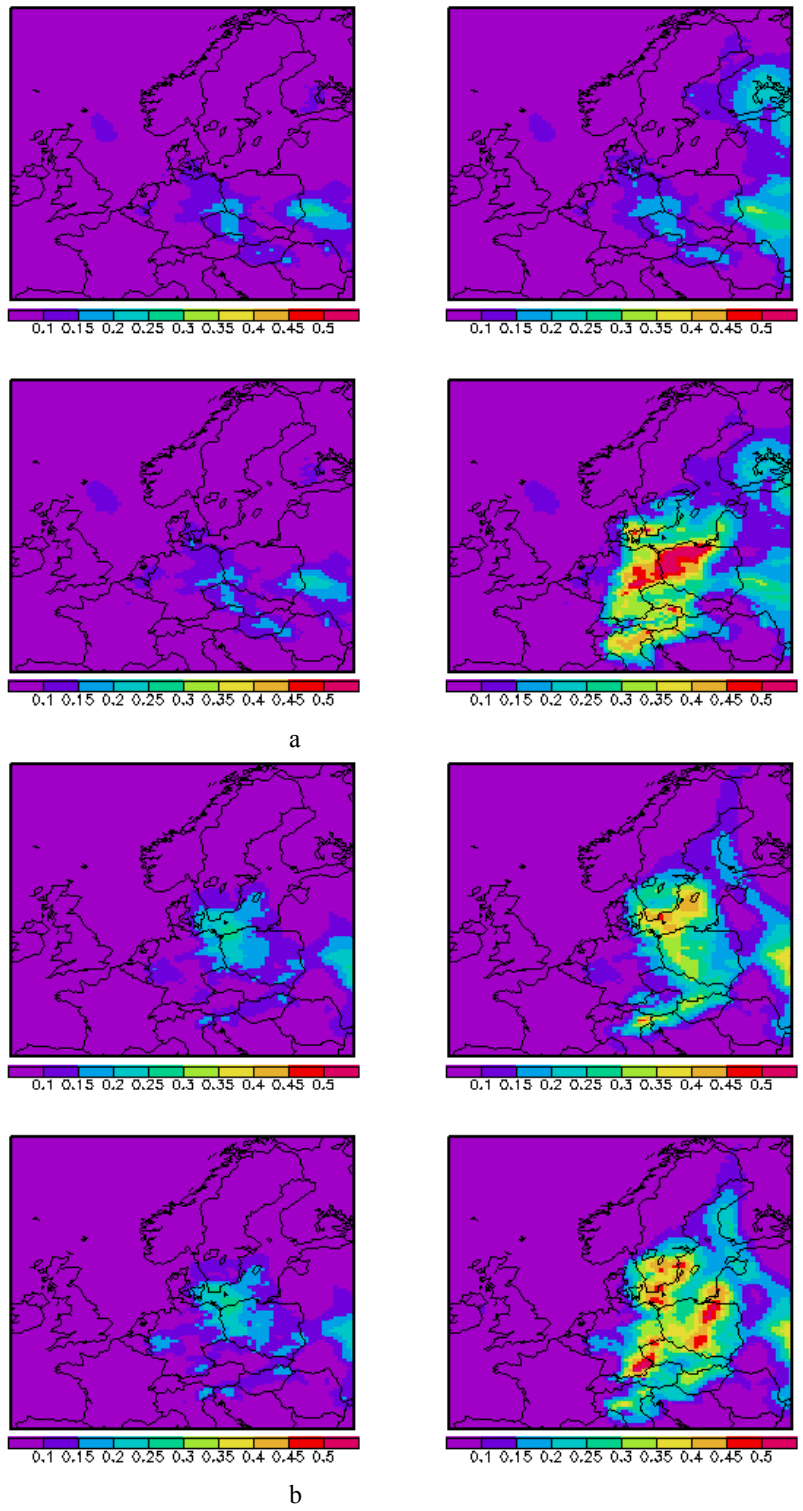
Fig 3.17 Field before (upper) and after assimilation (lower) for the model (left) and the assimilation experiment 2 (right) for the 23rd (a) and 20th (b)
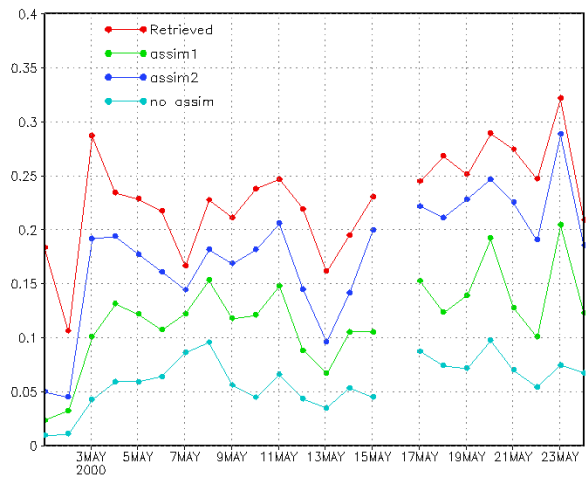
a)
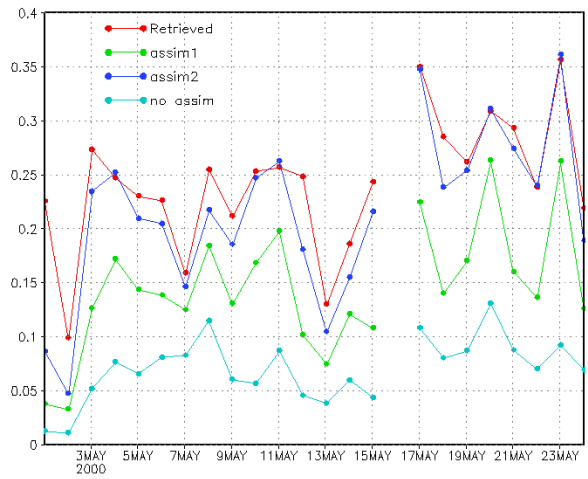
b)

Fig 3.18 Comparison of the average retrieved AOD compared to the corresponding average for the modelling experiments for the whole domain (a) and the area bound by lon = -5,30 and lat = 45,57(b)

21 5 2000
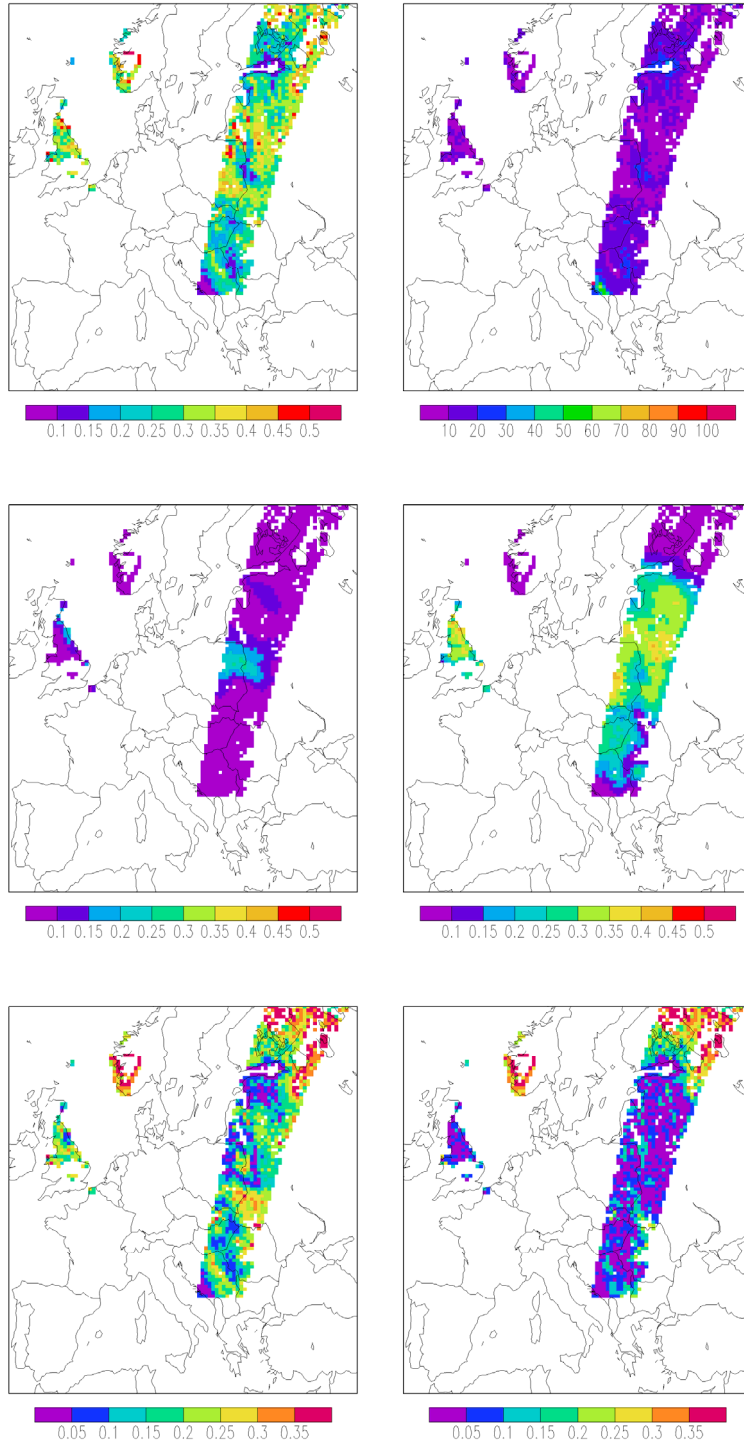
Figure 3.19 AOD assimilation results for May 21st, 2000 (exp2)

Validation with AERONET data

For May, 2000, only a few AERONET stations were operational. In this section we present a comparison of modelled and assimilated AOD data for four stations, see Figure 3.20. The comparison confirms that without assimilation the model (black) underestimates AOD. Assimilation improves the comparison significantly, although it can be seen that many events are missed due to the low availability of satellite retrievals to assimilate. For instance, around Avignon we can identify only 3 periods where assimilation AOD has affected the simulated AOD. Examples for a improved correspondence due the assimilation are found for all stations, e,g around hour 140 in Palaisseau, hour 450 in Avignon and hour 250 and 390 in Gotland.

The accuracy estimates in experiment 1 and 2 have a large influence. In general, the accurate AOD assumption yields better agreement with the AERONET AOD. The standard deviation in the retrieval in exp. 1 is often so large that the improvements are usually small. However, it should be noted that this is not always the case, e.g. around hour 290 in Palaisseau. In that particular case the satellite retrieval and the ground based data are not in agreement with each other. Hence, we speculate that the assimilated data may be affected by cloud contamination in the retrieval.

The comparison shows that a better time resolution (more overpasses in time) and a good estimate of the accuracy of an AOD value would be beneficial for the assimilation experiments.

59
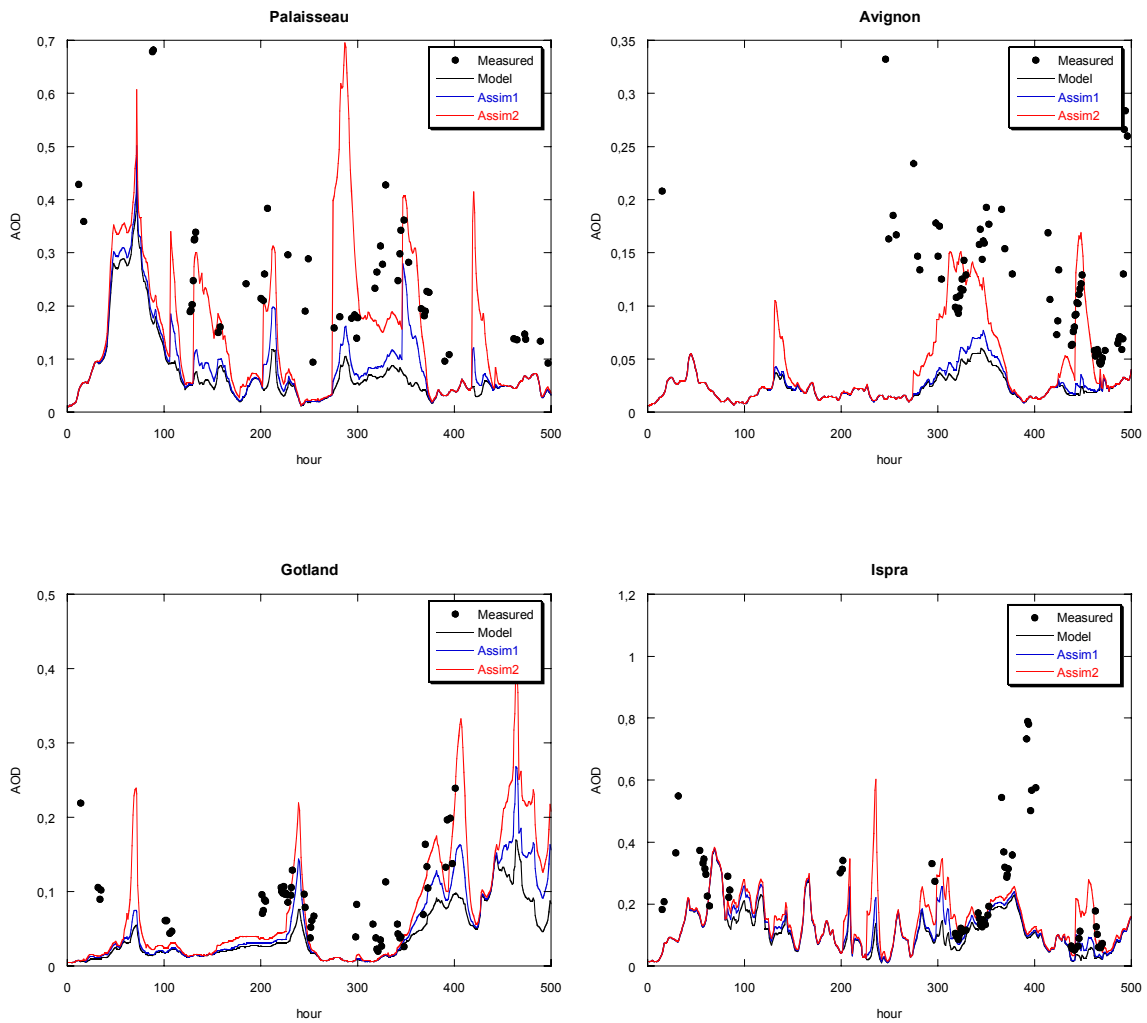
Figure 3.20 Comparison of modeled and assimilated AOD time series at four AERONET stations. The first 500 hours of May, 2000 are shown

3.5.3   PM2.5 over Europe

The assimilation system adjusts the model state and therewith the aerosol concentrations. In Figure 3.21 and 3.22 we illustrate the consequences of the AOD assimilation for PM2.5 in central Europe. The fields are averages for a three week period from May 5 to 25, 2000.

As the retrieved AOD data are underestimated by the model aerosol concentrations are increased by the system. The average increase in fine aerosol mass is depicted in the lower left panel of Figures 3.21 and 3.22 for experiment 1 and 2, respectively. For experiment 1 the increase ranges between 0.5-1 in remote areas and 3 $\mu g/m^3$ or more in polluted areas, e.g. Benelux and central Europe. Relatively, the system increases the PM2.5 mass by 20 to 50 % over continental Europe. Over remote areas the relative increase is even higher due to the low concentrations there. Experiment 2 yields twice the increase in PM2.5 levels compared to experiment 1 due to the larger increase in the assimilated AOD values.

Unfortunately, there are no PM2.5 measurements available for this period to compare with.
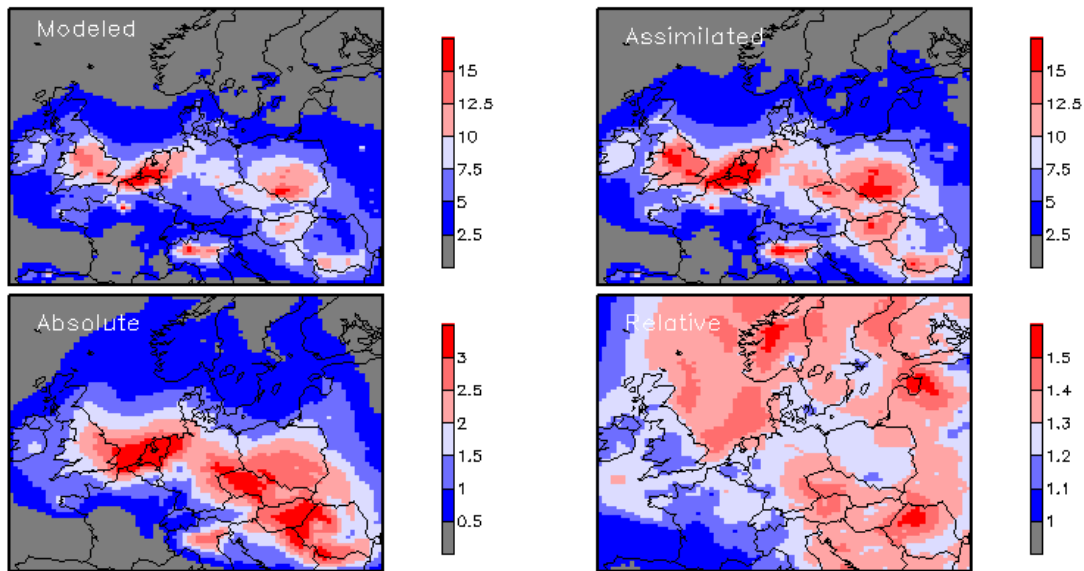
Figure 3.21 Modelled and assimilated PM2.5 fields as well as the absolute and relative differences between these fields for experiment 1.
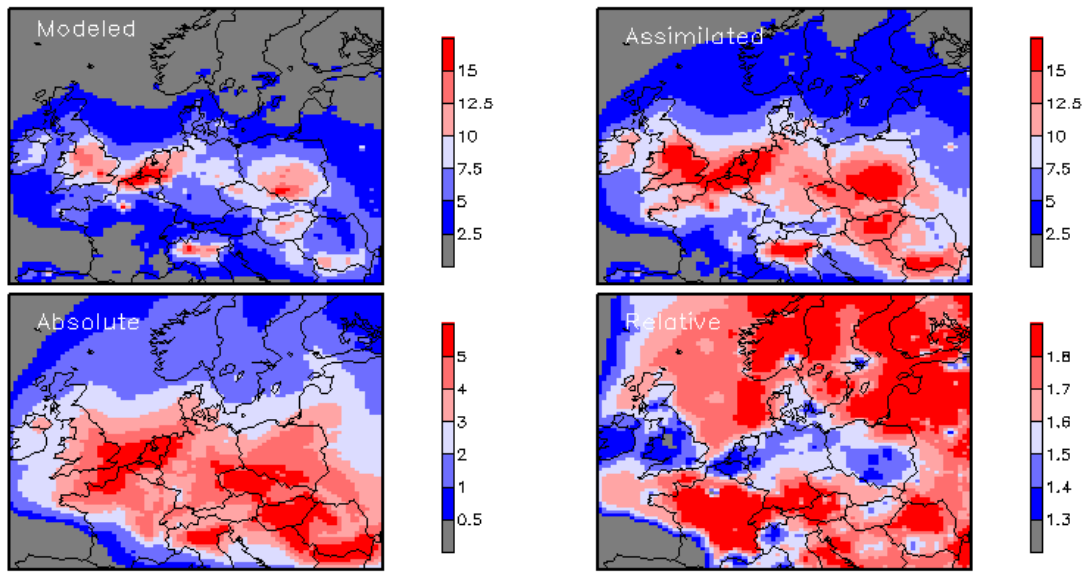
Figure 3.22 Modelled and assimilated PM2.5 fields as well as the absolute and relative differences between these fields for experiment 2.

3.5.4 Estimation of European emission

In Figure 3.23 we show the emissions adjustments as a result of the assimilation procedure. Almost all component show large areas where emissions are increased by 50-100 %. These large emission changes (and associated PM2.5 concentration changes) are a consequence of the large underestimation of the AOD data by the model. The amplitude of the change is not realistic as NOx and SOx emissions over Europe are thought to be associated with an uncertainty of at maximum about 35%. We discuss the cause of these unrealistic emission changes in section 3.6
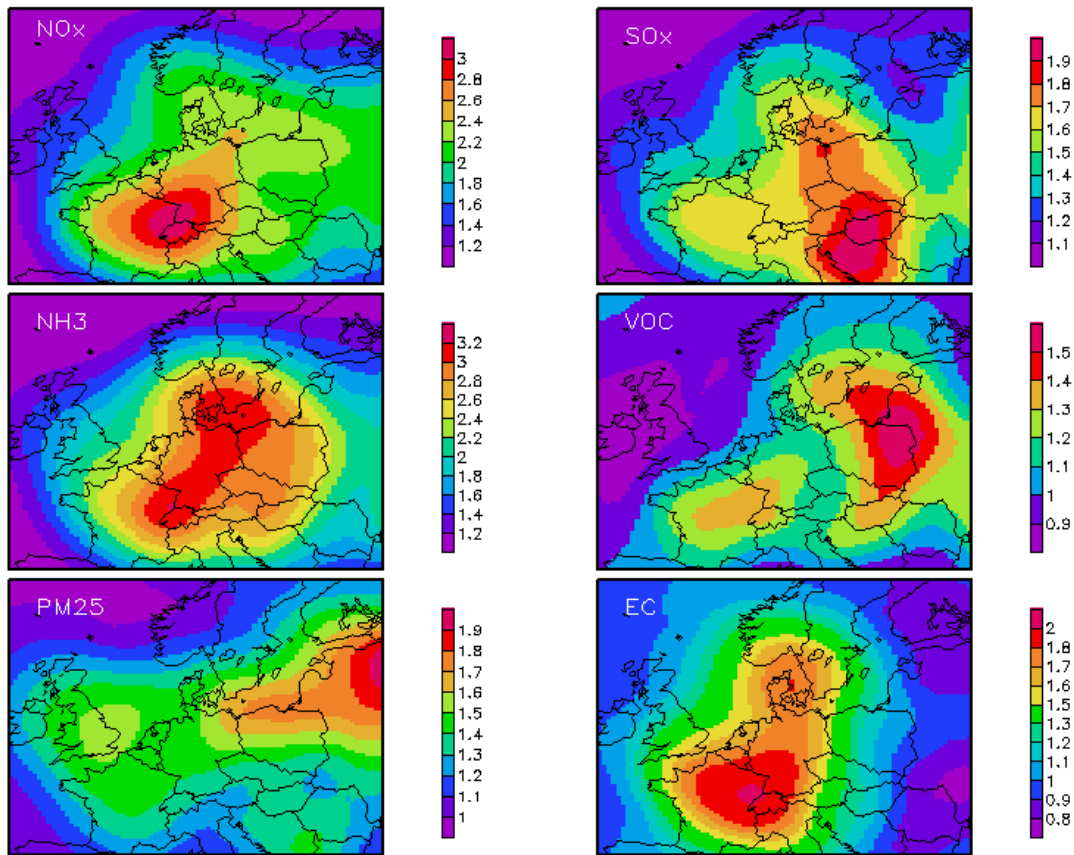
Figure 3.23 Fractional scale factors for emissions as derived by the assimilation system for exp 1. A factor of 1 means no change.

3.6 GLOBAL MODEL RESULTS WITH MODIFIED REGIONAL EMISSIONS

As has been described above, the LOTOS-EUROS model system with ensemble Kalman Filtering is operational. Assimilation over Europe using observed AOD values however results in highly unrealistic emission adaptation. As a consequence, the current system does not enable to produce improved emission estimates over Europe, an area with relatively good and reliable emission data. The purpose was, in case the system would have worked properly over Europe, to use the system over the INDOEX area, an region with highly uncertain emissions.

The input data needed to apply LOTOS-EUROS for the INDOEX area have been created: meteorology, land use and land cover and emissions from GEIA. However, because the same emission results as for Europe would have been obtained: i.e. a large increase in emissions, it has been decided not to perform such model runs for INDOEX. The danger would be, in case these model runs should be presented, that the calculated increase in emissions would be taken as possibly realistic because of the expectation that current GEIA emissions in that area are underestimated. The resulting increase in emissions might be correct/right, but for the wrong reasons, most likely.

However, in order to assess what the impact of improved emissions on the model results would be, a sensitivity study with the global model TM4 is performed with other sources of SO2, NO2, NH3, and carbonaceous aerosols. It is noted that the emission inventories used initially in this study are partly outdated. Effective clean air policies have led to significant reductions of some of the polluting species. For Europe

TNO recently updated the most relevant sources of aerosols and their precursor gases. We will use these updated sources to study the effect of emission source strengths on the aerosol optical depth. To do so, we replaced the old European emissions for the region 34N-66N and 6W-48E by the new TNO emissions. Total mass emissions of the gases SO_2, NO_2, NH_3 and the carbonaceous aerosol species BC and OC are 63, 36, 20, 59, and 28 % lower in the TNO inventory than in the previously used inventories. The reduction in emissions, reduce the monthly mean aerosol optical thickness for the whole European domain for March 2000 from 0.21 to 0.16. If TM4 aerosol optical thicknesses are selected with simultaneous AERONET observations the monthly mean aerosol optical thickness reduces from 0.16 to 0.13. This reduction is unwanted as it further increases the discrepancy between TM4 and AERONET aerosol optical depth. However, if it is true that the updated sources are better, it would mean that the earlier estimates of the aerosol optical thickness is reasonably right for the wrong reason. Moreover, the correlation between the time series of AERONET observations and new modeled aerosol optical depths is worse than for the older emissions. Only for 2 (Venise and Moldova) of the 7 AERONET stations that provide data this month, the correlation is improved, for the others the correlation is worse.

4 DISCUSSION

We have presented a study to the assimilation of aerosol optical depth over Europe and over the INDOEX region as retrieved by ATSR2. We have shown that the data assimilation technique can be applied to improve the distribution of aerosols, AOD and PM2.5. It was found that after the assimilation of satellite observations the agreement with independent surface observations of AOD improved. However, a number of unresolved issues prevent up to now the successful application of the system to obtain reliable estimates of aerosol mass, PM2.5 or aerosol emissions, using ATSR-2 data as input. These issues are discussed below.

Models:
One of the main results of this study is the large underestimation of the retrieved AOD data by the models (both TM4 and LOTOS-EUROS) without assimilation. Such a systematic underestimation can be explained by a number of factors including issues related to modelling and the optical properties of aerosols. From a modelling point of view some underestimation can be expected since not all existing aerosol types are in the models (although some additional aerosol types have been implemented during this project), and several sources are not very well known, e.g. fugitive dust, secondary formation of carbonaceous aerosols, and biomass burning sources. For the INDOEX simulation with TM4, emissions may have been underestimated due to the rapid development of the region. Previous evaluation of model results has shown that the concentrations of elemental and organic carbon are underestimated by a factor 2 (Schaap et al., 2004). Hence, the total fine aerosol concentration is underestimated and should cause an underestimate of AOD. For the LOTOS-EUROS model the vertical extend is only 3.5 km, which also contributes to the underestimation of the AOD, as it is estimated that about 10 % of the aerosol is found above the model domain (Banic etal., 1996; ten Brink et al., 2001).
The calculation of the AOD from the aerosol components was also identified to be a mayor source of uncertainty. We used a parameterisation developed as part of this project by Henzing (2006). The choice of the optical parameters and water uptake properties may cause substantial differences in the effective extinction coefficient. For example, using the AOD computation method from Robles-gonzalez et al. (2003) in combination with extinction coefficients for carbonaceous aerosols from Tegen et al. (1997) yields 50 % higher AOD values than the method used in this study. Moreover, the hydration process, and thus the particle size distribution depends non-linearly on the relative humidity, a quantity that is very variable both in time and space. For perfectly simulated aerosol mass concentrations, the homogeneous distribution of water vapor within a grid cell thus leads to systematic under prediction of aerosol optical depths. This effect becomes increasingly important for increasing relative humidity. The redistribution of humidity into the cloudy part and the clear part of the grid cell makes the agreement with observations (that are necessarily made in clear conditions) worse, as is shown in this study.

Observations:
Also, the retrieved AOD values may be biased in a systematic way. It is well known that AOD values above surfaces with a high albedo are very uncertain and difficult to detect. In this respect clouds are most important. Undetected cloud contamination yields an unknown overestimate of AOD. Furthermore, AOD values over shallow waters and over regions covered with snow are usually biased high. Consequently, shorelines and the large mountain ranges are often seen on AOD maps.
For the retrievals assumptions are made on the aerosol mixture that contributes to the AOD. The retrieval algorithm necessarily assumes that the total AOD is determined by a combination of only two types of aerosol, i.e. anthropogenic and sea salt aerosol. When other types dominate (e.g. dust, soot or internally mixtures) this may introduce errors in the retrievals.

Assimilation:
For the assimilation of observational data to produce reliable products two requirements need to be fulfilled: 1- results of the free running model as well as the observations need to reasonably agree with reality, and -2- some information must be available about the errors involved in both model and observations. The second point is illustrated by the two experiments done with LOTOS-EUROS described in this study indicating the influence of the uncertainty estimates in both the observations and model calculations. We have used an upper and lower limit for the uncertainty associated with AOD retrievals. With highly accurate AOD data the LOTOS-EUROS system is able to reproduce the AOD fields that are assimilated accurately. On the other hand, the simulation with the standard deviation that also represents the spatial variability was only able to

64

close the gap by 50% on average. Therefore, validation of satellite products, representation error and cloud contamination need to be addressed carefully. Further, the low temporal resolution of the ATSR retrievals (1 every three days if not cloudy) hampers the assimilation of AOD and needs to be improved by using several satellite products.

Error estimates were also made for the TM4 model as part of this study, by comparing model output and ATSR2 retrievals with independent surface observations from AERONET. After correcting for the representation difference (point observations versus gridcel average), the model AOD error was estimated to be $0.07+0.2 \times AOD_{TM4}$. The observational error was estimated to be 0.16.

We estimate that only a (small) part of the systematic difference between the modelled and retrieved AOD values is due to the uncertainties in the emissions that are input to the model. However, the LOTOS-EUROS system uses these emissions to close the complete gap between measured and observed data. Hence, the estimated emission changes do not yield realistic values, although after assimilation the AOD's are in better agreement with independent surface observations. The high corrections indicate that we need to improve the modelling of the total aerosol mass and the calculation of aerosol optical depth from the aerosol components. Since the assimilation of ATSR2 into TM4 also effectively acts as a source of aerosols (especially in the INDOEX simulation), we conclude that this model also needs improvements before a successful application of the system.

Besides these issues, the assimilation of AOD is an underdetermined problem. The systems have one property to assimilate (AOD) but several variables to estimate (the (precursor) emissions of the components in LOTOS-EUROS; the concentration distribution of several aerosol components in TM4). In our study with LOTOS-EUROS the optical properties are a function of BC fraction, total aerosol mass and RH. Thus, it does not matter if the system uses sulphate or nitrate concentrations to close the gap between measured and modelled AOD. This means that when the AOD calculation including water uptake would be accurate, the fine aerosol mass but not its composition could be estimated quite accurately. In our experiments with the TM4 model, a basic (but possibly wrong) assumption is made that all components need to be adjusted proportionally. More information characterizing the aerosol, in addition to the AOD, is lacking. We conclude that we may learn more by introducing additional surface observations of secondary inorganic aerosols and PM2.5 into the system, in combination with an integrated quantity like AOD. Using these data the number of variables can be reduced (e.g. by assimilating sulphate concentrations prior to assimilating AOD) which enables to peel off the information included in the AOD data.

5   CONCLUSIONS

We have shown that the data assimilation technique can be successfully applied to assimilate aerosol optical depth fields over Europe and INDOEX. Both models, LOTOS-EUROS and TM4, are adjusted towards the retrieved AOD values as a result of the assimilation. Experiments with the LOTOS-EUROS system revealed a close resemblance with retrieved AOD when it is assumed that the retrieval is very accurate. Unfortunately this is not the status of the present day AOD data, e.g. due to cloud contamination. Assimilation of observational data into the TM4 model effectively acts as a source of aerosols, and improves the agreement with independent surface observations of AOD. After the introduction of size resolved sea salt aerosol in TM4 it is shown that significant part of the AOD over the Atlantic Ocean and in the INDOEX region is determined by this type of aerosol.

Surface concentrations of NH4, NO3 and SO4 are reasonably represented by both models. Surface SO2 concentrations are overestimated by both models, but most severely by TM4. The free running models both systematically underestimate the AOD values. The systematic deviations are probably caused by one or more of the following factors:

- The calculation of the AOD from the aerosol concentrations is very uncertain
- The model does not represent all aerosol components
- Some emission sources might be underestimated
- Sinks of aerosols, e.g. wash-out, rain-out, or dry deposition, are overestimated
- Hydration of aerosols is underestimated

As a consequence of the large systematic deviation the assimilation scheme induces a large and unrealistic change in the emissions in LOTOS-EUROS and strong discontinuities in the distribution of aerosols in space and time in TM4.

An improvement is foreseen when the models are constrained by ground based measurements of (several) aerosol components. This avoids the introduction of additional errors due to the uncertain optical parameters and uncertain humidity effects on aerosol size distribution, which makes the AOD assimilation less effective. Since aerosols and humidity are both very variable parameters of the atmosphere, increasing the spatial resolution may also improve the agreement with observations. Finally a more accurate assessment of model and observational errors may help to find the optimal combination of model and observational data.

6   Outlook to operational use - cost / benefit analyses

Since long-term exposure to PM is particularly damaging to human health and reduces life expectancy, reducing long-term PM concentrations and exposure is a priority. This would also bring important financial savings. In Germany, the estimated annual monetary benefit from decreased population mortality attributed to PM is €13-34 billion, and savings on the costs of diseases attributed to PM account for €6 billion (WHO, 2005). When these numbers are scaled to the size of the population of the Netherlands the corresponding figures are €3-7 billion and €1 billion per year, respectively. A significant amount of money is also involved in reducing the exposure to PM by emission reductions. The Dutch government just recently increased the budget to improve air quality by €100 million mainly to reduce the traffic emission of PM. Infrastructural changes to reduce the future exposure of the population will also cost a significant amount of money.
Policy makers will have to decide on the measures to comply with the EU legislation and to serve public health. These decisions have to be based on reliable information. Moreover, the EU requires that the general public is warned in the case of air pollution episodes.
The operation implementation of the regional and global assimilation system will contribute to the monitoring and forecasting of the concentration of fine particulates to which the population is exposed. The information will be complimentary to the in-situ point measurements of the air quality measurement networks, by providing forecasts and a full spatial coverage. The costs (of which 50% is covered by NIVR) to execute ARIA-1 and ARIA-2 were 160 k€ and 272 k€ respectively. The estimated cost of embedding the OI assimilation scheme in an operational air quality forecast service is 150 k€, involving increased resolution of

the TM model and only some minor model improvements. To maintain the service after implementation involves an estimated 70k€ per year.

In the future further ahead, AOD observations might come from Geo-stationary satellites, which will substantially increase the amount of available AOD data, from once per 3 days to every 30 minutes. It is expected that the assimilation of these data, which may be complemented with ground based measurements of aerosols, results in better estimations of emissions and aerosol concentrations. Furthermore, to improve the operational forecasts a sustained effort is required to improve the model representations of aerosols.

List of papers and presentations based ARIA-2 results

Henzing, J.S., Aerosol Modelling, PhD thesis Eindhoven Technical University, 2006.(ISBN-13: 978-90-386-2431-0)
Henzing, J.S, D.J.L. Olivié, and P.F.J. van Velthoven, ACPD, acpd-2005-0381, 2005
Henzing, J.S., P.F.J. van Velthoven, and G.H.L. Verver, Global atmospheric aerosol modelling and data assimilation, presented at the National Aerosol Symposium, De Bilt, The Netherlands, June 10, 2005.
Schaap, M., R. Timmermans, F. Sauter, M. Roemer, G. J. M. Velders, G. Boersen, J. P. Beck, P.J.H. Builtjes (2005b), The LOTOS-EUROS model: description, validation and latest developments, Int. J. Environmental. Pollution, in press
Schaap, M., Loon, van, M., Builtjes, P. (2004), Aerosol modelling with the comprehensive LOTOS model: towards a data assimilation system for aerosols, paper presented at the NATO Advance Research Workshop, Borovetz, Bulgaria, 8-12 May, 2004.
Schaap, M., de Leeuw, G., Henzing, B., Builtjes, P. (2006), Assimilation of aerosol optical depth over Europe in a regional chemistry transport model, paper to be presented at the International Aerosol Conference, St Paul, Minesota, USA, September 110-15, 2006.

Acknowledgements

We also gratefully acknowledge the guidance provided by the ARIA Advisory Group, consisting of Dr. R. Koelemijer, Dr. G. Velders, Dr. H. ten Brink, and Dr. H. Slaper.

References
Adelman, Z.E. (1999) A re-evaluation of the Carbon Bond-IV photochemical mechanism. M.Sc. thesis, Department of Environmental Sciences and Engineering, School of Public Health, University of North Carolina, USA.
Builtjes, P.J.H. (1992) 'The LOTOS-Long Term Ozone Simulation-project Summary Rep.', *TNO Rep. TNO-MW-R92/240*.
Builtjes, P.J.H. et al.: Aerosol air quality satellite data. BRCS-Rep. USP-2, 4.1/AP-06 (2001).
Builtjes, P.J.H., van Loon, M., Schaap, M., Teeuwisse, S., Visschedijk, A.J.H., Bloos, J.P. (2003) 'Project on the modelling and verification of ozone reduction strategies: contribution of TNO-MEP', *TNO-report, MEP-R2003/166*, Apeldoorn, The Netherlands.
Beljaars, A. C. M. and P. Viterbo, Role of the boundary layer in a numerical weather prediction model, in *Clear and cloudy boundary layers*, edited by Holtslag, A. A. M. and P. G. Duynkerke, pp. 287-304, NH-publishers, 1999
Brink, H.M. ten, A. Hensen, A. Khlystov, R. van Dorland, A. Jeuken, P. van Velthoven, J. Lelieveld, A. van den Berg, D.P.J. Swart, J.B. Bergwerff, and A. Apituley: Aerosol: Cycle and Influence on the Radiation Balance. NOP-final report (2001) no. 410200064
Cachier, H.: Carbonaceous combustion particles. In: Atmospheric Particles, 295-348. Eds. R.M. Harrison, and R.E. Van Grieken, John Wiley, New York (1998).
Chylek, P., G. Lesins, G. Videen, J. G. D. Wong, R. G. Pinnick, D. Ngo, and J. D. Klett, Black carbon and absorption of solar radiation by clouds, *J. Geophys. Res.*, 101, 23365-23372, 1996
Chylek, P., G. Videen, W. Geldart, S. Dobbie, and W. Tso, Effective medium approximation for

heterogeneous particles, in light scattering by nonspherical particles, in *Theory, measurements, and geophysical applications*, edited by M. Mishchenko, pp. 273-308, Academic, San Diego, Calif., 2000

Clarke, A. D., T. Uehara, and J. W. Porter, Atmospheric nuclei and related aerosol fields over the Atlantic: clean subsiding air and continental pollution during ASTEX, *J. Geophys. Res.*, 102, 25281-25292, doi:10.1029/97JD01555, 1997

Collins, W.D., P.J. Rasch, B.E. Eaton, B.V. Khattatov, J-F. Lamarque and C.S. Zender: Simulating aerosols using a chemical transport model with assimilation of satellite aerosol retrievals: Methodology for INDOEX. J. Geophys. Res. 106, 7313-7336 (2001).

Cooke, W.F., C. Liousse, H. Cachier, and J. Feichter:: Construction of a 1x1 degree fossil fuel emission data set for carbonaceous aerosol and implementation and radiative impact in the ECHAM4-model. J. Geophys.Res. 104, 22,137-22,162 (1999).

Dentener, F., J. Feichter and A. Jeuken: Simulation of the transport of Rn222 using on-line and off-line global models at different horizontal resolutions: a detailed comparison with measurements. Tellus, 51B, 573-602 (1999).

Dubovik, O., B. N. Holben, T. F. Eck, A. Smirnov, Y. J. Kaufman, M. D. King, D. Tanre, and I. Slutsker: Variability of absorption and optical properties of key aerosol types observed in worldwide locations. J. Atmos. Sci. 59, 590-608 (2002).

Eck, T. F., B. N. Holben, J. S. Reid, O. Dubovik, A. Smirnov, N. T. O'Neill, I. Slutsker, and S. Kinne, Wavelength dependence of the optical depth of biomass burning, urban and desert dust aerosols, *J. Geophys. Res.*, 104(D24), 31333-31350, 1999

Erickson, D.J. III and R. A. Duce, On the global flux of atmospheric sea salt, J. Geophys. Res., 93, 14079-14088, 1988.

Erisman, J.W., van Pul, A., Wyers, P. (1994) 'Parametrization of surface-resistance for the quantification of atmospheric deposition of acidifying pollutants and ozone', *Atmos. Environ.*, Vol. 28, 2595-2607

Evensen, G.: Advanced data assimilation for strongly nonlinear dynamics. Monthly Weather Review 125, 1342-1354 (1997).

Gelencsér, A., Carbonaceous Aerosol, Springer, ISBN 1-4020-2886-5, Dordrecht, The Netherlands, 2004

Gerber, H. E., Relative-humidity parameterization of the Navy Aerosol Model (NAM), *NRL Report 8956*, Naval Research Laboratory, Washington, D.C., 1985

Gong S.L., L. A. Barrie, and M. Lazare, Canadian aerosol module (CAM): A size-segregated simulation of atmospheric aerosol processes for climate and air quality models 2. Global sea-salt aerosol and its budgets, *J. Geophys. Res.*, 107(D24), 4779, doi:10.1029/2001JD002004, 2002

Gong, S.L., et al., Canadian Aerosol Module: A size-segregated simulation of atmospheric aerosol processes for climate and air quality models, 1, Module development, *J. Geophys. Res.*, 108(D1), 4007, doi:10.1029/2001JD002002, 2003a

Gong, S.L., A parameterization of sea-salt aerosol source function for sub and super-micron particles, *Global Biogeochem. Cycles*, 17(4), 1097, doi:10.1029/ 2003GB002079, 2003b

Graaf, M., L.G. Tilstra, and P. Stammes: SCIAMACHY absorbing aerosol index: the scientific product compared to the operational product and TOMS data, in Envisat Calibration Review Proceedings, ESA Special publication SP-562, 2004.

Graaf, M., P. Stammes, O. Torres and R.B.A. Koelemeijer: Absorbing Aerosol Index: Sensitivity Analysis, application to GOME and comparison with TOMS, J. Geophys. Res., 110, D01201, doi:10.1029/2004JD005178, 2005.

Guelle, W., Y.J. Balkanski, J.E. Dibb, M. Schulz, and F. Dulac: Wet depositon in a global size-dependent aerosol transport model: 2. influence fo the scavenging scheme on ^{210}Pb vertical profiles, surface concentrations and deposition. J.Geophys. Res. 103, 11429-11445 (1997).

Guelle, W., M. Schulz, and Y. Balkanski, Influence of the source formulation on modeling the atmospheric global distribution of sea salt aerosol, *J. Geophys. Res.*, 106(D21), 27509-27524, 2001

Haywood, J.M., and O. Boucher: Estimates of the direct and indirect radiative forcing due to tropospheric aerosols: A Review. Rev. Geophys., 38,4, 513-543, 2000.

Henzing, J. S., D. J. L. Olivié and P. F. J. van Velthoven, A parametrization of size resolved below cloud scavenging of aerosols by rain, accepted for publication in *ACPD*, acpd-2005-0381, 2005

Heimann M.: The global atmospheric tracer model tm2: Technical Report 10, Deutches Klima Rechenzentrum, Modellbetreuungsgruppe, Hamburg (1995).

Hess M., P. Koepke and I. Schult: Optical properties of aerosols and clouds: The software package OPAC, Bull. Am. Meteor. Soc. 79, 831-844 (1998).

Holben B. N., T. F. Eck, I. Slutsker, D. Tanre, J. P. Buis, A. Setzer, E. Vermote, J. A. Reagan, Y. J. Kaufman, T. Nakajima, F. Lavenu, I. Jankowiak, and A. Smirnov: AERONET- A Federated Instrument Network and Data Archive for Aerosol Characterisation, Rem. Sens. of the Env. 66, 1-16 (1998).

Houweling, S., F. Dentener, and J. Lelieveld, The impact of non-methane hydrocarbon compounds on tropospheric photo-chemistry. J. Geophys. Res. 103, 10673 (1998).

Hsu, N. C, J.R. Herman, O. Torres; B.N. Holben, D. Tanre, T. F. Eck; A. Smirnov, B. Chatenet, and F. Lavenu.: Comparisons of the TOMS aerosol index with Sun-photometer aerosol optical thickness: Results and applications. J. Geophys. Res. 104, 6269-6280 (1999).

IPCC-TAR, Intergovernmental Panel on Climate Change Third Assesment Report, Contribution of working group I, "Climate Change 2001, The scientific basis" (2001).

Jeuken, A.B.M., H.J. Eskes, P.F.J. van Velthoven, and E.V. Holm: Assimilation of total ozone satellite measurements in a three-dimensional tracer transport model. J.Geophys.Res. 104, 5551-5563 (1999).

Jeuken, A.B.M.: Evaluation of chemistry and climate models using measurements and data assimilation. Ph.D. Thesis, Technical University of Eindhoven (2000).

Jeuken, A.B.M., J.P. Veefkind, F. Dentener, S. Metzger, and Robles Gonzalez: Simulation of the aerosol optical depth over Europe for August 1997, and a comparison with observations. J. Geophys. Res. 106, 28,295-28,311. (2001).

Kerschbaumer, A. and Reimer, E. (2003) 'Preparation of Meteorological input data for the RCG-model', *UBA-Rep. 299 43246,* Free Univ. Berlin Inst for Meteorology (in German).

Kiehl, J. T., T. L. Schneider, P.J. Rasch, M. C. Barth, and J. Wong, Radiative forcing due to sulfate aerosols from simulations with the National Center for Atmospheric Research Community Climate Model, Version 3, *J. Geophys. Res.*, 105, 1441-1457, 2000

Kiehl, J.T., T.L. Schneider, P.J. Rasch, and M.C. Barth: Radiative forcing due to sulfate aerosols from simulations with the National Center for Atmospheric Research Community Climate Model, version 3. J. Geophys. Res. 105, 1441-1457 (2002).

Koelemeijer, R.B.A., P. Stammes, J.W. Hovenier, and J.D. de Haan (2001), *A fast method for retrieval of cloud parameters using oxygen-A band measurements from the Global Ozone Measurement Instrument*, J. Geophys. Res., 106, pp. 3475-3490.

Leeuw, F.A.A.M. de, Rheineck Leyssius, H.J. van (1990), Modeling study of SOx and NOx during the januari 1985 smog episode. Water, Air and Soil Pollution, 51, 357-371

Lesins, G., P. Chylek, and U. Lohmann, A study of internal and external mixing scenarios and its effects on aerosol optical properties and direct radiative forcing, *J. Geophys. Res.*, 107, doi:10.1029/2001JD000973, 2002

Loon, M. van, Builtjes, P.J.H., Segers, A. (2000) 'Data assimilation of ozone in the atmospheric transport chemistry model LOTOS', *Env.Mod and Sotw.*, Vol. 15, pp.603-609.

Loon, M. van, Roemer, M. and Builtjes, P.J.H. (2004) 'Model intercomparison in the framework of the review of the Unified EMEP model', *TNO-Rep. R 2004/282*.

Liousse, C., J.E. Penner, C. Chuang, J.J. Walton, H. Eddleman, and H. Cachier: A global three-dimensional model study of carbonaceous aerosols. J. Geophys. Res. 101, 19411-19432 (1996).

Liu, M.K., and Durran, D., (1977), Development of a regional air pollution model and its application to the Northern Great Plains, US-EPA (EPA-908/1-77-001).

Novakov, T. and C.E. Corrigan: Cloud condensation nucleus activity of the organic component of biomass smoke particles. Geophys. Res. Lett. 23, 2141-2144 (1996).

Meijer, E.W., P.F.J. van Velthoven, A.M. Thompson, L. Pfister, H. Schlager, P. Schulte and H. Kelder: Model calculations of the impact of NOx from air traffic, lightning, and surface emissions, compared with measurements. J.Geophys.Res 105, 3833-3850 (2000).

Metzger, S., F. Dentener, S. Pandis, and J. Lelieveld, Gas/aerosol partitioning: 1. A computationally efficient model, *J. Geophys. Res.*, 107(D16), 4312, doi:10.1029/2001JD001102, 2002a

Metzger, S., F. Dentener, M. Krol, A. Jeuken, and J. Lelieveld, Gas/aerosol partitioning 2. Global modeling results, *J. Geophys. Res.*, 107(D16), 4313, doi:10.1029/2001JD001103, 2002b

Monahan, E. C., D. E. Spiel, and K. L. Davidson, Model of marine aerosol generation via whitecaps and wave disruption, in *Preprint Volume of 9th conference on aerospace and aeronautical meteorology*, American Meteorological Society, Boston, pp 147-152, 1983

Monahan, E. C., D. E. Spiel, and K. L. Davidson, A model of marine aerosol generation via whitecaps and wave disruption, in *Oceanic Whitecaps*, edited by E. C. Monahan and G. Mac Niocaill, pp 167-174, D. Reidel, Norwell, Mass., 1986

Nenes, A., Pilinis, C., and Pandis, S. N. (1999) 'Continued Development and Testing of a New Thermodynamic Aerosol Module for Urban and Regional Air Quality Models', Atmos. Env., Vol. 33 , pp.1553-1560.

Poppe, D., Andersson-Sköld, Y., Baart, A., Builtjes, P.J.H., Das, M., Fiedler, F., Hov, O., Kirchner, F., Kuhn, M., Makar, P.A., Milford, J.B., Roemer, M.G.M., Ruhnke, R., Simpson, D., Stockwell, W.R., Strand, A., Vogel, B., Vogel, H. (1996) 'Gas-phase reactions in atmospheric chemistry and transport models: a model intercomparison', Eurotrac report. ISS, Garmisch-Partenkirchen.

Ramanathan,V. , P.J.Crutzen, J. Lelieveld, A.P. Mitra, D. Althausen, J. Anderson, M.O. Andreae, W. Cantrell, G.R. Cass, C.E. Chung, A.D. Clarke, J.A. Coakley, W.D. Collins, W.C. Conant, F. Dulac, J. Heintzenberg, A.J. Heymsfield, B. Holben, S. Howell, J. Knudson, A. Jayaraman, J.T. Kiehl, T.N. Krishnamurti, D. Lubin,G. McFarquhar, T.Novakov, J.A. Ogren, I.A. Podgorny, K. Prather, K. Priestley, J.M. Prospero, P.K. Quinn, K. Rajeev, P. Rasch, S. Rupert, S. Sadourny, S.K. Satheesh, G.E. Shaw, P. Sheridan, and F.P.J. Valero: Indian Ocean Experiment: An integrated analysis of the climate forcing and effects of the great Indo-Asian haze. J. Geophys.Res 106, 28371-28398 (2001).

Rasch, P.J., H. Feichter, K. Law, N. Mahowald, J. Penner, D. Benkovitz, C. Genthon, C. Giannakopoulos, P. Kasibhatla, D. Koch, H. Levy, T. Maki, M. Prather, D.L. Roberts, G.-J. Roelofs, D. Stevenson, Z. Stockwell, S. Taguchi, M. Kritz, M. Chippperfield, D. Baldocchi, P. McMurry, L. Barry, Y. Balkansi, R. Chatfield, E. Kjellstrom, M. Lawrence, H.N. Lee, J. Lelieveld, K.J. Noone, J. Seinfeld, G. Stenchikov, S. Schwartz, C. Walcek, D. Williamson: A comparison of scavenging and deposition processes in global models. Results from the WCRP Cambridge workshop of 1995. Tellus 52, 1025-1056 (2000)

Rasch, P.J., W.D. Collins, and B.E. Eaton: Understanding the Indian Ocean Experiment (INDOEX) aerosol distributions with aerosol assimilation. J. Geophys. Res 106, 7337-7355 (2001)

Robles Gonzalez C., J. P. Veefkind, and G. de Leeuw: Aerosol optical depth over Europe in August 1997 derived from ATSR-2 data. Geophys. Res. Lett. 27, 955-958 (2000).

Robles-Gonzalez, C., J.P. Veefkind and G. de Leeuw: Mean aerosol optical depth over Europe in August 1997 derived from ATSR-2 data. Geophys. Res. Lett. 27, 955-959 (2000).

Robles-Gonzalez, C., G. de Leeuw, P.J.H. Builtjes, M. van Loon and M. Schaap: Interpretation of retrieved aerosol properties over Europe using a chemistry transport model. Submitted to J.Geophys.Res. (2001).

Robles González C. (2003), Retrieval of Aerosol Properties using ATSR-2 Observations and Their Interpretation., Ph. D Thesis, Utrecht University, Utrecht, The Netherlands.

Russell G.L., and J.A. Lerner: A finite difference scheme for the tracer transport equation. J. Appl. Meteorol. 20, 1483-1498 (1981).

Russell, P.B., P.V. Hobbs, and L.L. Stowe: Aerosol properties and radiative effects in the United States East Coast haze plume: An overview of the Tropospheric Aerosol Radiative Forcing Observational Experiment (TARFOX). J.Geophys.Res. 104, 2213-2222 (1999).

Schaap, M., van Loon, M., ten Brink, H.M., Dentener, F.D., Builtjes, P.J.H. (2004a) 'Secondary inorganic aerosol simulations for Europe with special attention to nitrate', Atmos. Phys. Chem., Vol. 4, pp.857-874

Schaap, M., Denier Van Der Gon, H.A.C., Dentener, F.J., Visschedijk, A.J.H., van Loon, M., Ten Brink, H.M., Putaud, J-P., Guillaume, B., Liousse, C. and Builtjes, P.J.H. (2004b) 'Anthropogenic Black Carbon and Fine Aerosol Distribution over Europe', J. Geophys. Res., Vol. 109, D18201, doi: 10.1029/2003JD004330.

Schaap, M., M. Roemer, F. Sauter, G. Boersen, R. Timmermans, P.J.H. Builtjes (2005a), LOTOS-EUROS Documentation, TNO report B&O 2005/297, TNO, Apeldoorn, the Netherlands.

Schaap, M., R. Timmermans, F. Sauter, M. Roemer, G. J. M. Velders, G. Boersen, J. P. Beck, P.J.H. Builtjes (2005b), The LOTOS-EUROS model: description, validation and latest developments, Int. J. Environmental. Pollution, in press

Seinfeld, J. H., and S.N. Pandis: Atmospheric chemistry and physics: from air pollution to Climate Change. John Wiley & Sons, Inc., New York (1998)

Shettle, E.P. and R.W. Fenn (1979), Models for the Aerosols of the Lower Atmosphere and the Effects of Humidity Variations on Their Optical Properties, AFGL-TR-79-0214 Environmental Research Papers, #676, published by the Air Force Geophysics Laboratory, Hanscom AFB, MA 01731.

Simpson, D., Fagerli, H., Jonson, J.E., Tsyro, S., Wind, P., and Tuovinen, J-P (2003) 'Transboundary Acidification, Eutrophication and Ground Level Ozone in Europe, Part 1: Unified EMEP Model Description', EMEP Report 1/2003, Norwegian Meteorological Institute, Oslo, Norway.

Sokolik I. N., O. B. Toon, R. W. Bergstrom: Modeling the radiative characteristics of airborne mineral aerosols at infrared wavelengths. J. Geophys. Res. 103, 8813-8826 (1998).

Stammes P., J. F. Bosma, and J. W. Hovenier: The adding method for multiple scattering calculations of polarised light. Astron. Astrophys. 225, 239-259 (1989).

Stammes, P. (2001), *Manual for the DAK program*, Royal Netherlands Meteorological Institute, De Bilt, The Netherlands

Tegen, I., P. Hollrig, M.Chin, I. Fung, D. Jacob, J. Penner, Contribution of different aerosol species to the global aerosol extinction optical thisckness: Estimates from model results. J. Geophys. Res. 102, 23,895-23,915 (1997).

United Nations: The United Nations energy statistics database (1991). Tech. Rep. Stat. Div., New York (1993).

Van Loon, M, M.G.M.Roemer, P.J.H.Builtjes : Model intercomparison in the framework of the review of the Unified EMEP model. TNO-Rep R2004/282 (2004).

Van Velthoven, P.F.J., P.J.H.Builtjes , M.Schaap. An assessment of the assimilation techniques presently available, as well as an assessment of the requirements for a fully functional aerosol assimilation system. DEADALUS Deliverable D2.1 (2004).

Veldt, C., (1989) The use of biogenic VOC-emissions, TNO report 89-306.

Verver, G.H.L., J.S. Henzing, G. De Leeuw, C. Robles Gonzalez, P.F.J. Van Velthoven: (2002). Aerosol Retrieval and Assimilation (ARIA), Final Report, NUSP-2, KNMI-publicatie: 200, 2002.

Visschedijk, A.J.H. and Denier van der Gon, H.A.C. (2005) 'Gridded European anthropogenic emission data for NOx, SOx, NMVOC, NH_3, CO, PPM10, PPM2.5 and CH_4 for the year 2000', TNO-Report B&O-A R 2005/106

Volz, F.E. (1972), *Infrared refractive index of atmosperic aerosol substances*, Applied Optics, 11, pp. 755-759.

Walcek, C.J. (2000) 'Minor flux adjustment near mixing ratio extremes for simplified yet highly accurate monotonic calculation of tracer advection', *J. Geophy. Res.*, Vol. 105, D7, pp.9335-9348.

Whitten, G., Hogo, H., Killus, J. (1980) 'The Carbon Bond Mechanism for photochemical smog', *Env. Sci. Techn.*, Vol. 14, pp.14690-14700.

Yamartino, R. J., Flemming, J. and Stern, R.M. (2004) 'Adaption of analytic diffusivity formulations to eulerian grid model layers finite thickness', *27th ITM on Air Pollution Modelling and its Application.* Banff, Canada, October 24-29, 2004.

The Advisary Group

Members:

Dr. H. Ten Brink, ECN
Dr. G. Velders, RIVM
Dr. R. Koelemijer, RIVM
Dr. H. Slaper, RIVM

7   Acronyms

ACE	Aerosol Characterisation experiment
ACTM	Aerosol Chemistry Transport Model
AOD	Aerosol Optical Depth
ARIA	Aerosol RetrIeval and Assimilation
ATSR	Along Track Scanning Radiometer
AVHRR	Advanced Very High Resolution Radiometer
CBM	Carbon Bond Mechanism
ECMWF	European Centre for Medium range Weather Forecasts
GOME	Global Ozone Monitoring Experiment
INDOEX	Indian Ocean Experiment
IPCC	Intergovernmental Panel on Climate Change
IR	Infra-Red
KCO	Kaashidhoo Climate Observatory (Maldives)
KNMI	Koninklijk Nederlands Meteorologisch Instituut
LUT	Look-Up Table
MISR	Multi-Angle Imaging SpectroRadiometer
MODIS	MOderate Resolution Imaging Spectrometer
NOP	Nationaal OnderzoeksProgramma luchtverontreiniging en klimaat
OMI	Ozone Monitoring Instrument
POLDER	Polarisation and Directionality of Earth Reflectances
SCIAMACHY	Scanning Imaging Absorption Spectrometer for Atmospheric Cartography
TAR	Third Assessment Report (of IPCC)
TARFOX	Tropospheric Aerosol Radiative Forcing Observational eXperiment
TNO-FEL	Fysisch Elektronisch Laboratorium
TNO-MEP	Milieu, Energie en Procesinnovatie
TOA	Top Of Atmosphere
TOMS	Total Ozone Mapping Spectrometer
TM3	Transport Model versie 3
UV	Ultraviolet
WCRP	World Climate Research Program